ABSTRACT


Title of Document: BIO-TEMPLATED SUBSTRATES FOR BIOSENSOR APPLICATIONS

**Angela Li-Hui Fu, Ph.D., 2013**

Directed By: Professor Peter Kofinas, Bioengineering

Nanopatterning of materials is of particular interest for applications in biosensors, microfluidics, and drug delivery devices. In biosensor applications there is a need for rapid, low cost, and durable system for detection. This dissertation aims to investigate methods to pattern nanostructured surfaces using virus particles as templates. The virus species used in these experiments is a cysteine modified tobacco mosaic virus. The first project utilized the lamellar microphase separation of a block copolymer to pattern the virus particles. Although microphase separation of the poly(styrene-*b*-2-vinylpyridine) (PS-P2VP) into lamellae was confirmed, specificity of the viruses to the gold doped block of the polymer could not be achieved. Single virus particles lay across multiple lamellae and aggregated in side-to-side and head-to-tail arrangements. The second project studied the effect of a surfactant on virus assembly onto a gold chip. The experiments included placing a gold chip in virus solutions with varying triton concentrations (0-0.15%), then plating the virus particles with a metal. Results showed that as the triton concentration in the virus solution increases, the virus density on the

surface decreases. The gold coated virus particles were applied to Surface Enhanced Raman Spectroscopy (SERS) detection in the final project. SERS is of interest for biosensor applications due to its rapid detection, low cost, portability, and label-free characteristics. In recent years, it has shown signal enhancement using gold, silver, and copper nanoparticles in solutions and on roughened surfaces. The gold plated virus surfaces were tested as SERS substrates using R6G dye as the analyte. An enhancement factor (EF) of $10^4$ was seen in these samples versus the non-SERS substrate. This corresponded to the sample with 0.05% triton in the virus solution which showed the most intersection points between the virus particles and the most uniform coverage of the viruses on the surface. This value is lower than that of previous studies; however, future work may be performed to optimize conditions to achieve the highest signal possible.

# BIO-TEMPLATED SUBSTRATES FOR BIOSENSOR APPLICATIONS

By

Angela Li-Hui Fu

Dissertation submitted to the Faculty of the Graduate School of the
University of Maryland, College Park, in partial fulfillment
of the requirements for the degree of
Doctor of Philosophy
2013

Advisory Committee:
Professor Peter Kofinas, Chair
Professor William E. Bentley
Professor Robert M. Briber
Professor James N. Culver
Professor Ian M. White

# Dedication

For Grandma & Grandpa Chen, and Nai Nai & Yieh Yieh Fu

I can’t wait to celebrate with you, Grandma! ☺

# Acknowledgements

I would like to express my appreciation to Dr. Peter Kofinas for his advice, guidance, and support during this research. He was always there to give me assistance and encourage me to do my best. I also want to thank the Department of Economics for their financial support for the past few years. It was a great experience working with all the staff there, especially Dorinda, Terry and Lizzie in the front office. A special thanks to my committee members Dr. Ian White, Dr. James Culver, Dr. Robert Briber, and Dr. William Bentley for their interest in my project and helpful suggestions. I owe Dr. White and his graduate student, Wei (Veemoon) Yu, many thanks for their expertise in SERS and Adam Brown his help with my virus templating studies. I am grateful to Dr. Briber, Dr. Isabel Lloyd, and Dr. Xin Zhang for attending my lab group meeting presentations to ask me questions and provide me with ideas to shape my project. A huge thanks to Robyn Rice in the copy center for helping me put together all my dissertation printouts and Tracy Chung for her help in keeping me on track for graduation!

I would like to acknowledge the Maryland Nanocenter, Dr. Wei-An Chiou, Dr. Li-Chung (Larry) Lai, and Che-Kuan (Ryan) Lin, who assisted me in obtaining all of the beautiful microscope pictures in this dissertation. They are really some of the greats in their field, and I would not have been able to complete my research without them.

Thanks also to members of the Kofinas Lab, especially my friends Dr. Linden Bolisay and Dr. Arthur von Wald Cresce for the training they provided in hydrogels, block copolymers, virus templating, the glove box, and graduate school survival. I've missed helping them procrastinate by working out at the gym, taking coffee breaks,

watching Maryland football games, and playing cricket in the street. A thank you to all of my other friends who have put up with me, especially Dr. George Engelmayr, Jr. and D. Quan. George has always been someone I could count on for his honesty since we met at University of Pittsburgh, and I consider him a great mentor who has really helped me deal with the harder times.

I would also like to extend a special thanks to my undergraduate advisors at the University of Pittsburgh, Dr. Harvey Borovetz, Dr. Mark Redfern, Dr. Michael Sacks, Dr. Marina Kameneva, and Dr. Anne Robertson, who guided me in my decisions and inspired me to be great (and also wrote all of my graduate school recommendation letters). Dr. B... this one's for you!

Finally, I would like to thank my parents, Ta-Wei and Hui-Ying Chen Fu for their support, and helping me become the greatest that I could be. Without them, I would not have been able to get so far. My sisters, Julia Fu Malalis and Jenna Fu, have always provided me with words of encouragement and helped me power through the tough times.

I give the most special thanks to my husband, David Khalil, for his love, encouragement, and continuous support in everything that I do. "WAYWARD"

FEAR THE TURTLE!

Table of Contents

List of Figures

# Chapter 1: Significance

Nanostructured biomaterials have been studied for applications in sectors such as biosensors, drug delivery, and microfluidic devices. The ability to spatially orient biomolecules at the nanoscale level allows for the development of functional materials that can be used with these devices. There is a need for faster, more durable, lower cost, label-free, and reagent-free methods for detection.

This research investigates the use of tobacco mosaic virus (TMV) particles as templates for biosensor applications. For this dissertation, we focused on three specific objectives towards better understanding of the nanopatterning of TMV on various structured surfaces. The first objective was the patterning of the cysteine-modified tobacco virus onto a gold doped block of a copolymer. The second objective was to study of the effect of surfactant addition at various concentrations on the assembly of the viruses onto a gold chip. These included control experiments with different wafer material as well as the variations in virus density were quantified by calculating the number of viruses in a certain area on the gold chip. The third objective tested these metal coated virus surfaces as substrates for surface enhanced Raman spectroscopy (SERS) activity.

Modified versions of TMV have also been used for developing nano-templated materials. Yi et al. assembled a TMV1cys modified virus template onto microfabricated electrodes [1]. Royston et al. utilized the same virus as a template in the fabrication of high surface area nickel and cobalt electrodes [2]. The templating of metals into a specific block of the copolymer can aid in the patterning of biological components. For

example, previous studies have templated nickel in a block copolymer of norbornene and norbornene dicarboxylic acid in order to test protein binding [3].

Patterned substrates can be applied to the molecular imprinting of materials. Molecularly imprinted polymers (MIPs) can mimic the function of some enzymes by creating cavities of a specific size and shape complementing that of the target molecule for recognition of bioactive compounds [4]. MIPs have high affinity and selectivity similar to natural receptors and possess stability superior to that of natural biomolecules. They can also be easily adapted to different applications, and are known to be resistant to chemically harsh environments [5]. The patterned surface can be used as a 2-dimensional stamping imprint for applications in biosensors.

Another application of these patterned substrates is surface enhanced Raman spectroscopy (SERS). Surfaces coated with silver, gold, and copper have shown increased intensity in the signals due to the electromagnetic interaction around the target molecules. Studies have also shown that the use of patterned nanostructures (creating surface roughness) produce a stronger signal [6]. There are several advantages to Raman Spectroscopy over current detection methods, such as the "fingerprinting" ability to produce distinct spectra from molecules similar in structure and function, elimination of expensive reagents and time-consuming sample preparation, and portability of Raman spectroscopy devices.

The findings from these experiments can have broad impacts on biosensor technology with applications in crop protection, homeland security, and disease prevention/detection. For example, in homeland security, this type of sensor could be taken into the field for TNT or anthrax detection and rapid detection of toxins in water

systems, pesticides in crops, or *e*-coli in food sources. The application of metal coated virus surfaces was expanded by using them for SERS testing. The hypothesis for these experiments is that there is a correlation between the densities of metal coated virus rods and the signal obtained with SERS.

# Chapter 2: Virus binding to block copolymers

## 2.1 Introduction

The assemblies of nanostructured systems may be used to pattern various biological components such as proteins, viruses, or bacteria [7]. Polymers are of particular interest for these applications due to their durability and ease of processing. Block copolymers, which are comprised of two or more chemically distinct polymer chains covalently linked together, are often useful in the synthesis of nanostructured materials due to their tendency to microphase separate into a variety of periodic nanostructures because of the thermodynamic incompatibility of the two blocks [8, 9]. The size and shape of these microstructures are dependent upon the volume fraction of the constituent polymers, block length, chemical nature of the blocks, and solvent type. Block copolymers have been previously used in experiments to pattern metals such as nickel and gold [3, 10, 11].

The templating of metals into a specific block of the copolymer can aid in the patterning of biological components. For example, previous studies have templated nickel in a block copolymer of norbornene and norbornene dicarboxylic acid in order to test protein binding [3]. Studies have also shown that Tobacco mosaic virus (TMV) templates engineered to encode unique cysteine residues (TMV1cys) are attracted to gold surfaces via gold-thiol interactions. The TMV1cys readily binds to the gold in an orientation perpendicular to the substrate when plated with metal nanoparticles [2, 12]. This is useful in applications requiring high surface area such as electrodes, sensors, and energy storage devices.

Block copolymers are long sequences of the same monomer unit, covalently bound to another chain of a different repeating unit. These segments are thermodynamically incompatible, which gives rise to a variety of microstructures in bulk and in solutions, a phenomenon known as microphase separation [8, 9]. The shape and size of the microstructures are dependent upon the volume fraction of the polymers, block length, chemical nature of the blocks, and solvent type. For example, if there are equal volume fractions of polymer A and B, then lamellae will be thermodynamically favorable. Some of the common equilibrium phases for block copolymers include spheres, cylinders, gyroid, and lamellae. Schematics of these are shown in Figure 2.1.

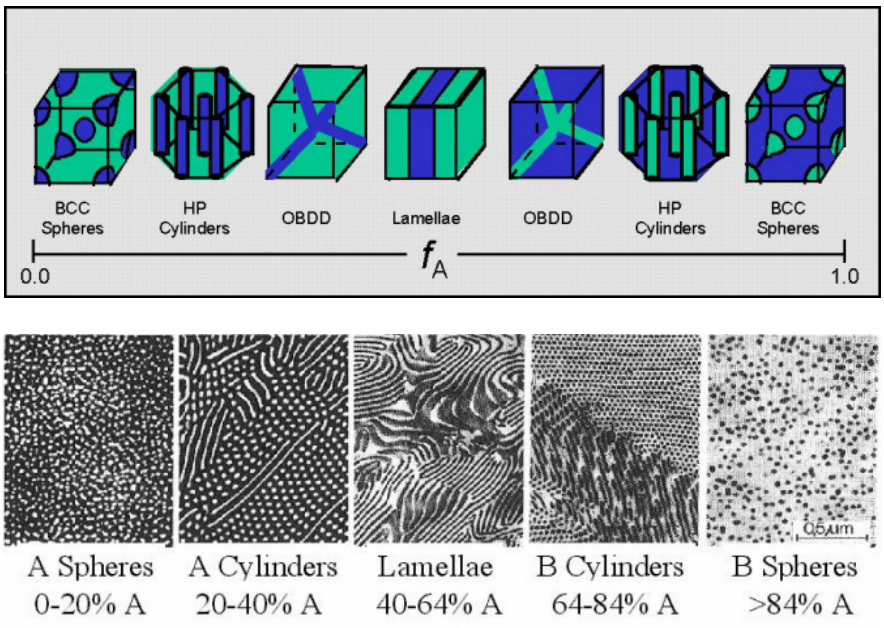


Figure 2.1: Representation of microdomains in block copolymers with respect to volume fraction [13].

The interfacial energy plays a crucial role in the microphase separation of block copolymer thin films. The preference of one phase to the substrate will drive the system to an alignment of the microdomains parallel to the film surface rather than perpendicular. The morphology of block copolymer thin films can be controlled by changing factors such as casting surface, solvent conditions, annealing time, or incorporation of nanoparticles in one of the blocks [14-22]. In the 1980s, Hashimoto studied the molecular weight, concentration and temperature dependence on lamellar size of polystyrene-b-polyisoprene block copolymers. This group found that the Bragg spacing D varies between 30 to 50 nm for volume fraction of the polymer in solution between 0.2 and 0.7. The effect of solvent on microphase separation has also been studied by Sotcker [18]. This group was able to induce a lamellar morphology in poly(styrene-*b*-methacrylate) (PS-*b*-PMMA) by evaporating the solvent over a period of one week. The slow evaporation allowed the chains to separate into lamellar periods perpendicular to the surface of the film. Lin et al. [16] have induced the perpendicular alignment of poly(styrene-*b*-ethylene oxide) cylindrical morphology by spin casting the polymer solution onto a surface of silicon oxide. Yokoyama et al. [20] have also observed this type of morphology using a poly(styrene-*b*-2-vinylpyridine) cast onto a silicon oxide substrate. A patterned surface can also assist in obtaining a desired morphology. Rockford et al. [17] used silicon oxide substrates striped with gold lines (width equal to block period) to induce a PS-*b*-PMMA lamellar morphology perpendicular to the film surfaces. Several groups have incorporated metal nanoclusters into the phases of block copolymers [23-26]. Cohen et al. used the carboxylic acid groups on block copolymers to bind to both PbS and ZnS nanoclusters. Bawendi et al.

employed CdSe semiconductor nanocrystals into polynorbornene-based block copolymers to gain surface-passivation and electron transport functionalities [26].

## 2.2 Virus Binding to Homopolymer

### 2.2.1 Project Objectives

The purpose of these experiments was to investigate the binding of tobacco viruses to certain polymers for biosensor applications using block copolymers in lamellar morphology. This was achieved by completing the following tasks:

1) Homopolymer binding to virus
2) Verifying lamellar structure of block copolymer

### 2.2.2 Virus Selection

One common and well-studied group of plant pathogens are the tobacco viruses, of which two are tobacco necrosis virus (TNV) and tobacco mosaic virus (TMV). TEM images showing the structure of these viruses are shown in Figure 2.2.

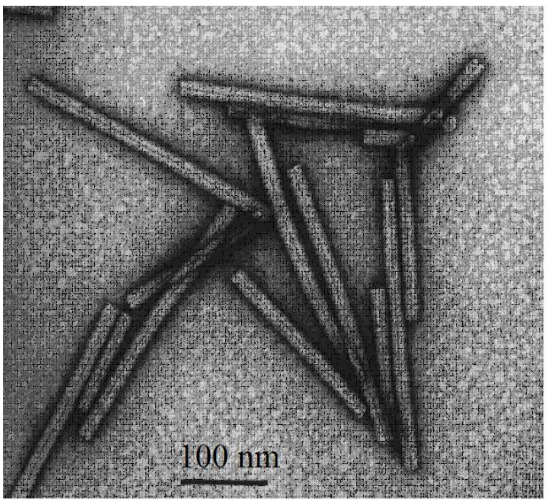


Tobacco Mosaic Virus

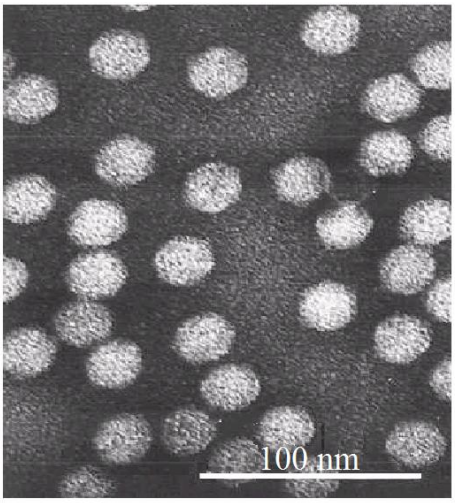


Tobacco Necrosis Virus

Figure 2.2: Transmission electron microscope images of tobacco viruses [27].

These viruses were chosen for the experiments due to their well-studied characteristics and ease of production in plants. The virions are also very physically and chemically stable, with the ability to be suspended in several polar solvents without substantial changes in their structural integrity. The structure of TNV has been studied in previous work [28]. When the virus particles infect plants, necrosis will occur in its leaves. TNV is non-enveloped, icosahedral shaped, and is 24 nm in diameter. The term non-enveloped refers to the absence of a lipid bilayer present on some viruses containing proteins coded for the viral genome and host genome. The virus is composed of a single 3.8 kb RNA strand inside a virus shell consisting of 180 protein subunits (each subunit containing 267-272 amino acid residues). TNV has an overall negative charge above its isoelectric point (pI), which occurs at pH = 4.5.

The TMV virus particle is shaped like a rigid rod with dimensions of 18 nm (D) x 300 nm (L). This is a non-enveloped virus which forms a mosaic-like pattern on infected

leaves. The virus is a supramolecular unit composed of one 5130 kb RNA strand surrounded by 2130 protein subunits (153 amino acids per subunit) arranged in a right hand helix. Many of the proteins translated from the viral RNA have been identified and studied [29]. The pI of TMV is pH= 3.5, and it is stable at pH values from 2-10 and temperatures up to 60°C [30].

The TMV coat protein can aggregate into different forms depending on the pH and ionic strength of the solution (see Figure 2.3). The 4S trimer/pentamer/monomer structure and 20S aggregates exist in equilibrium at pH 7 and temperature of 20C, and they both contribute to virion assembly. The 20S bilayer disk has 17 coat protein molecules in each layer and formation of these disks is important for initiation of virus assembly.

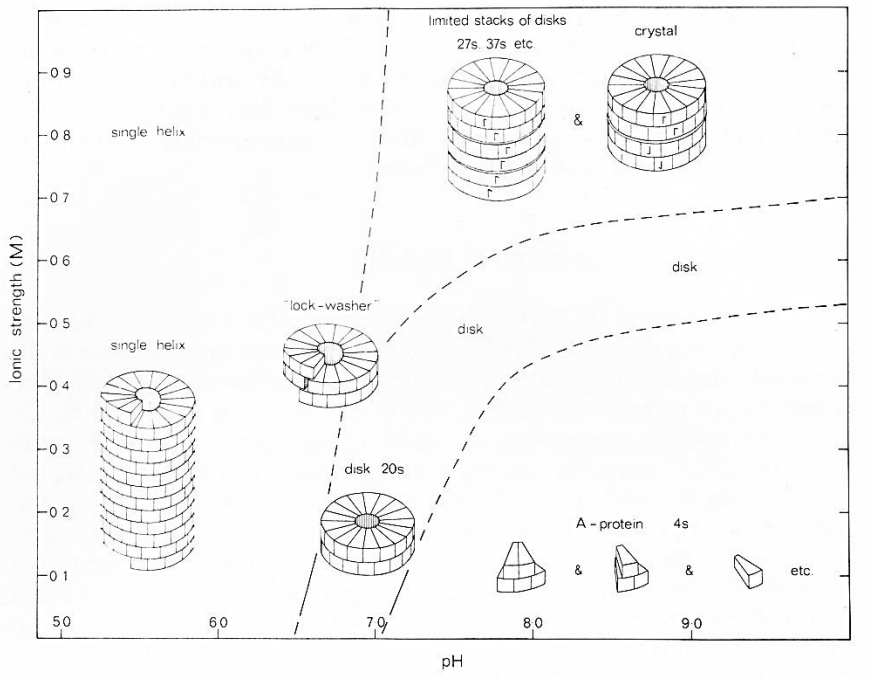


Figure 2.3: Diagram showing the polymorphic aggregates of TMV protein [31].

### 2.2.3 Polymer Selection

The aim of this project was to align the viruses in a pattern on the polymer film surface. An oriented pattern would arise when all the virus rods are confined to a single block copolymer domain. To create this pattern, the virus must be able to bind to one block of the copolymer while repelling the other. It would not bind to the second block because it did not contain the functional groups needed for binding to the virus. Since the viruses maintain a negative charge above their isoelectric point, it was essential to choose a polymer block with positively charged monomer units. The polymer must also be soluble in aqueous solutions due to the nature of virus solubility. The block copolymers chosen for this system were poly(ethylene oxide-*b*-2-vinylpyridine) (PEO-P2VP) and poly(ethylene oxide-*b*-4-vinylpyridine) (PEO-P4VP)). The chemical structures of the homopolymers can be seen in Figure 2.4.

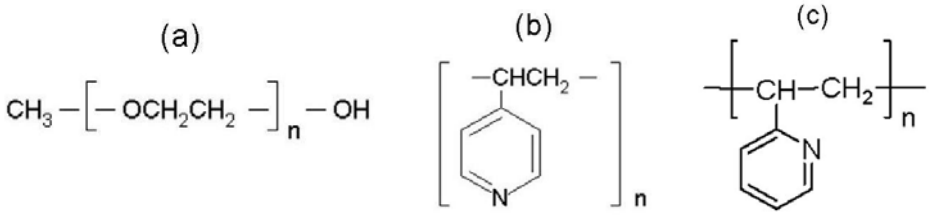


Figure 2.4: Chemical structure of (a) poly(ethylene glycol), (b) poly(4-vinyl pyridine), and (c) poly(2-vinyl pyridine)

P4VP and P2VP, which are normally hydrophobic, will dissolve in aqueous solutions upon protonation of the amine groups (Figure 2.5) at pH levels below 6 [32, 33]. Protonation also provides those polymers with a positively charged amine which will bind to the virus above pH 3.5.

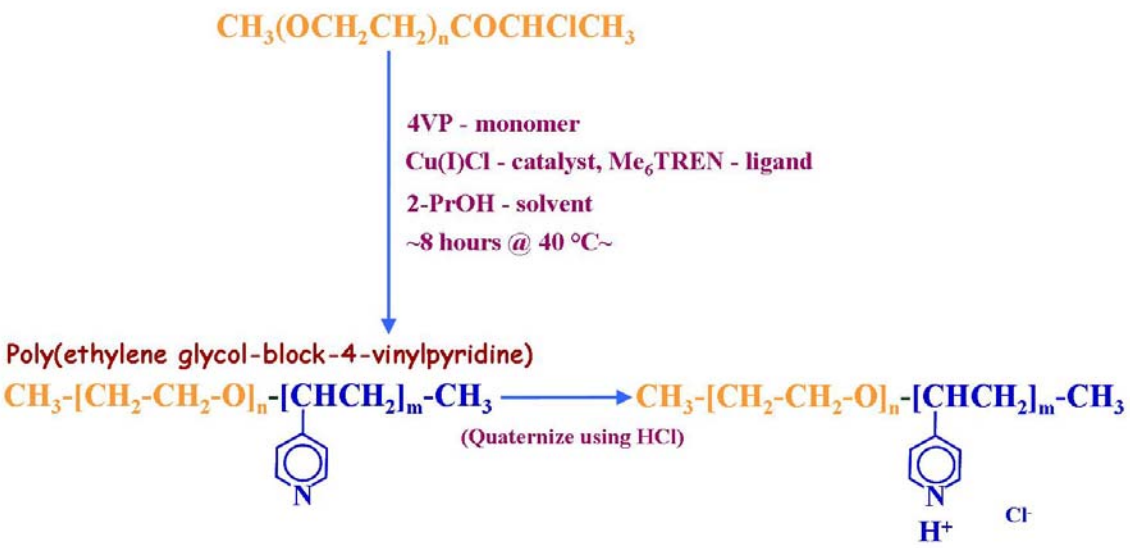


Figure 2.5: Procedure for protonation of amine groups of P4VP and P2VP polymers

### 2.2.4 Research Design and Methods

Virus Harvesting

Both TMV and TNV are stable and easily purified from infected plant tissue. They were purified using a method modified from Gooding and Hebert [34]. *Nicotiana tobacium* served as a differential host for TMV and TNV. Defined mosaic patterns appear on the tobacco leaves within 3-4 days after inoculation with TMV. A *N. tobacium* plant was mechanically infected with TMV by rubbing a 10 *m*L of 1 *mg/m*L virus solution onto two leaves on the second level from the top of the plant after spraying the leaves with carboranium. TNV infection showed defined necrotic lesions on the plant leaves approximately 5-7 days after inoculation. For the necrosis virus, the tobacco plants were infected in a similar manner as TMV, except all the leaves must be sprayed with carboranium and rubbed with the virus solution rather than just two. After the virus

infection spread throughout the plant, the leaves could be harvested and stored at -80 °C until purification.

To obtain purified virus, a blender was used to grind 0.5 kg of the harvested leaves into a slurry. The mixture was passed through cheesecloth and placed in an even number of 250 mL plastic centrifuge bottles. Total number of bottles depended on yield of filtered mixture. Chloroform was added to the bottles (20% of final volume) and shaken by hand for 20 minutes to extract organic debris, which formed a two-phase solution. The bottles were then spun in a centrifuge for 10 minutes at 5,000 rpm and 4 °C. The aqueous layer (top) was filtered through two Kim wipes placed in a funnel into a 1 L graduated cylinder. The solution was then poured into a 1 L beaker with potassium chloride (1.5% w/v of total volume) and polyethylene glycol (Mw 8000, 6% w/v of total volume), and mixed at 4 °C for one hour to precipitate the virus particles. The resulting solution was poured into centrifuge bottles and spun to pellet the virus for 10 minutes at 10,000 rpm. The supernatant was discarded and the pellet suspended overnight in ultrapure water. The virus solution was then placed in centrifuge tubes containing 10-40% sucrose gradient and centrifuged at 22,000 rpm for 2 hours at 4 °C. A white band of liquid showed the virus location and was collected, placed in centrifuge tubes, and spun at 30,000 rpm for 2 hours at 4 °C. The supernatant was discarded and the virus pellet dissolved overnight in 0.5 mL of water, then stored at -10 °C until use. Concentration of the virus solution was determined by UV-Vis spectroscopy using a Beckman DU-65 Spectrophotometer and the equation below:

$$Concentration\ of\ Virus = \frac{[OD_{260} - (OD_{325} \times 2.44)] \times dilution\ factor}{3}$$

Where OD is the optical density of the virus solution measured by the spectrophotometer and the dilution factor is the final volume being tested divided by the amount of the original dissolved sample that was added. Since the Beckman spectrometer requires 1 mL samples, the solution is diluted 100-fold prior to the measurements (using 10 μL of the sample).

Homopolymer binding to virus

These experiments were performed to show evidence of virus interaction with only one block of the PEO-P2VP copolymer. Film samples approximately 200 nm thick of each homopolymer (poly(ethylene oxide) (PEO), poly(4-vinylpyridine) (P4VP), and poly(2-vinylpyridine) (P2VP)) were placed on silicon monoxide-coated copper support grids (01830, Ted Pella, CA). A 5 $\mu$L drop of 1 *mg/m*L polymer solution in water was allowed to dry on the grid. A drop of 0.1 *mg/m*L virus solution was then placed on the grids and left for 2 minutes. Next, the solution was removed by placing a small piece of filter paper next to the drop, the grids dried, and washed in a 1% TWEEN 20 detergent solution to remove any particles with nonspecific binding. This involved placing the grid in the TWEEN solution for one minute and rinsing with a 10 $\mu$L drop of water. Negative staining was performed by placing 5 $\mu$L of 1% phosphotungstic acid (PTA) solution on the grid for 30 seconds, then wicking the remaining liquid away with a small piece of filter paper. Transmission electron microscopy (TEM) was performed to determine virus presence.

Block Copolymer Morphology

Studies were performed to determine the morphology of the PS-P4VP block copolymer. A 1 *mg/m*L solution of the block copolymer in chloroform was applied to a glass slide cover slip and allowed to dry overnight. Atomic force microscopy (AFM) was performed using contact mode.

### 2.2.5 Results and Discussion

As seen in Figure 2.6, the negatively stained TNV viruses remained bound to the P4VP polymer grids (a) after the TWEEN wash, but were not visible on the PEO grids (b). This indicates an interaction between the virus and the P4VP polymer other than non-specific binding. The P4VP film showed aggregates of virus due to the electrostatic interaction between the functional groups on the surface of the virus and the film. There were dark areas on the PEO film that could be due to PTA residue after staining; however no negatively stained distinct spherical shapes could be detected.

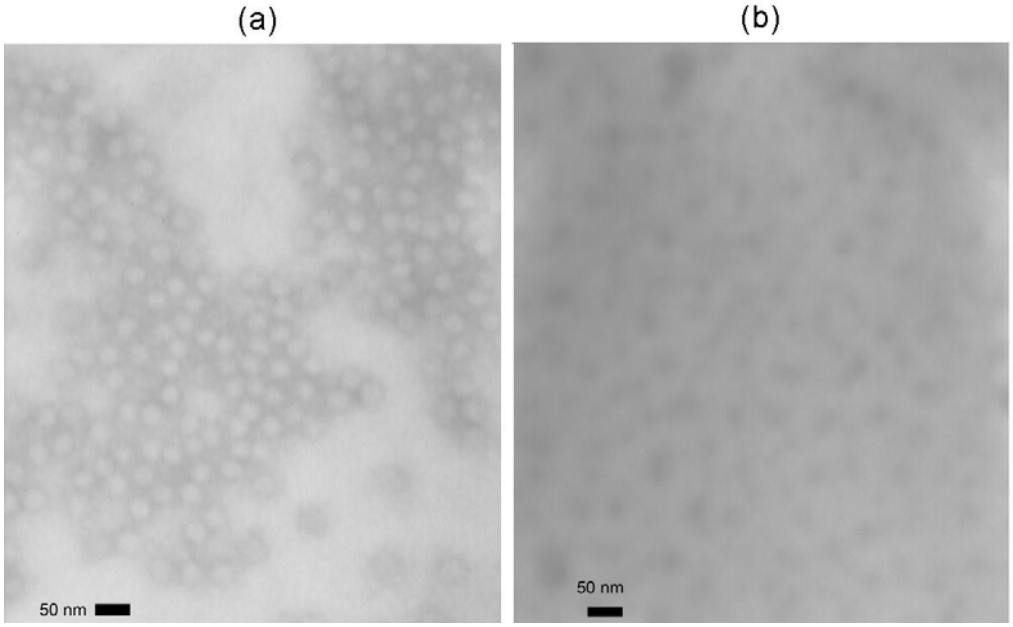


Figure 2.6: TEM images of TNV on (a) P4VP and (b) PEO homopolymer films

The AFM results showed a distinct lamellar microphase separated morphology (Figure 2.7a). This lamellar microstructure has also been shown in previous TEM work by Cresce et. al. Figure 2.6b shows a microtomed sample of the PS-P4VP block copolymer cast from tetrahydrofuran as seen in TEM [10].

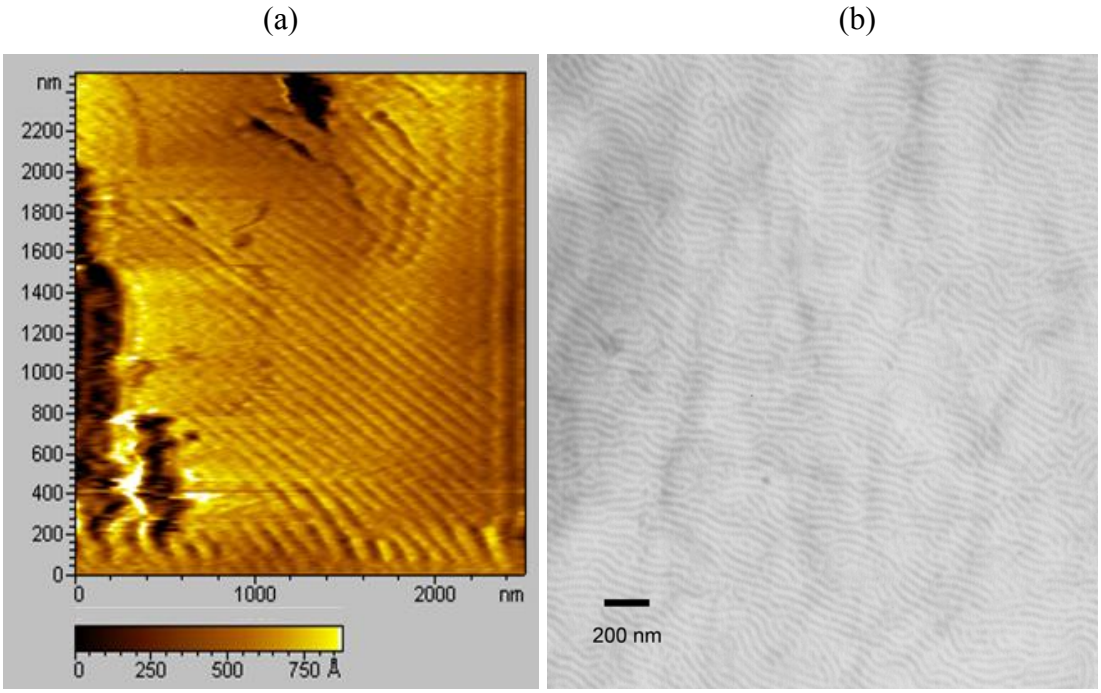


Figure 2.7: (a) AFM and (b) TEM images of PEO-P4VP block copolymer films

## 2.3 Cysteine Modified Tobacco Mosaic Virus Patterning

### 2.3.1 Project Objectives

The purpose of these experiments was to investigate the binding of a tobacco virus genetically modified with a cysteine residue to a gold doped block copolymer. This was achieved by completing the following tasks:

1) Develop lamellar structured block copolymer with one block doped with gold nanoparticles
2) Study the self-assembly of cysteine modified tobacco mosaic viruses to the gold doped block of the copolymer
3) Study the self-assembly of wildtype TMV to gold surfaces to validate the importance of the cysteine residue for the previous experiments (See Chapter 4)

### 2.3.2 Virus Selection

Modified versions of TMV have also been used for developing nano-templated materials. Yi et al. assembled a TMV1cys modified virus template onto microfabricated electrodes [1]. Royston et al. utilized the same virus as a template in the fabrication of high surface area nickel and cobalt electrodes [2].

The virus was modified by encoding an additional cysteine residue at the amino terminus of each of the virus coat proteins. This was created by inserting a TGT codon in the third amino acid position within the open reading frame of the full-length TMV infectious clone. This virus was chosen due to its affinity for binding to gold surfaces. It is hypothesized that the favorable attachment of the modified virus is perpendicular to the substrate, due to the cysteine residue locations being recessed within the virus structure. Figure 2.8 shows a computer generated schematic of the virus structure. The yellow dots represent the cysteine residues added to the coat protein. It can be seen that the residues on the upper rings are not exposed to the outside of the virus particle. The only ones exposed to the outside of the virus are along the end of the rod. Therefore, the majority of the cysteine functional groups are not exposed to the gold surfaces used for self-

assembly in these experiments and previous studies. Utilizing a virus as a template for biosensor patterning is beneficial because of its monodispersity and its ability to be chemically modified.

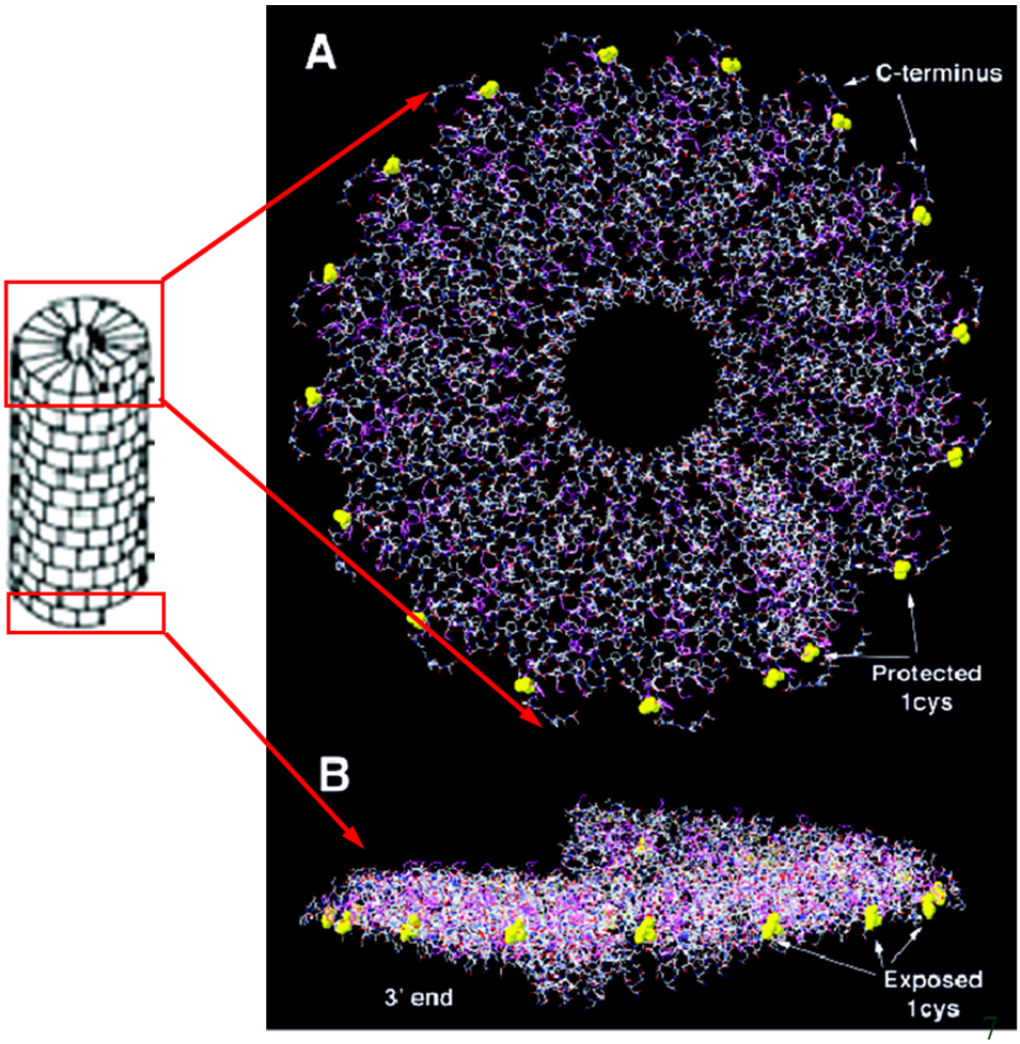


Figure 2.8: Computer model of TMV1cys virus structure showing exposed vs. protected cysteine residues

### 2.3.3 Polymer Selection

The polymer utilized in these experiments was a poly(styrene)-b-poly(2-vinylpyridine) block copolymer.

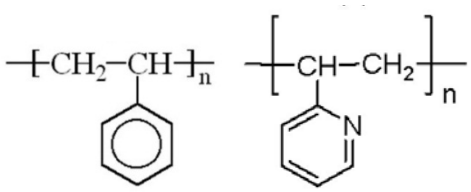

Figure 2.9: Chemical structure of poly(styrene) and poly(2-vinylpyridine) polymers

Previous studies have well characterized the structure of this polymer in films at different molecular weight ratios [35-37]. The structure of PS-P2VP is such that when doped with gold nanoparticles, they are only attracted to the poly(2-vinylpyridine) block of the copolymer due to its amine group. Several research groups have studied the doping of this block copolymer with metal nanoparticles.

### 2.3.4 Research Design and Methods

Poly(styrene-b-2-vinylpyridine) polymers with molecular weight ratio of 57,000:57,000 g/mol were purchased from Polymer Source (Quebec, Canada). Samples in a 50:50 dioxane:chloroform solution were spin cast onto 1 inch square glass slides by using 200 µL of 3% polymer solution. The solution was then annealed in chloroform vapor at 50ºC for 48 hours to ensure microphase separation of the two blocks.

The samples were treated with a 1% solution of the gold precursor, Chloroauric acid ($HAuCl_4$), in ethanol for 30 minutes and then rinsed with deionized water several times. This was followed by three treatments of 30 seconds each in the reducing solution of 1% sodium borohydride ($NaBH_4$). After drying, the samples were removed from the slides with hydrofluoric acid (HF), embedded in epoxy, and microtomed for TEM viewing.

The cysteine modified tobacco mosaic virus particles were genetically modified and harvested in similar fashion to as previously described [1, 34]. A 0.01 mg/mL virus solution was placed on the nanopatterned polymer samples, followed by a 2% TWEEN wash to prevent non-specific binding. Uranyl acetate was used for negative virus staining. 5 mL of 2% solution was placed on the TEM grids and wicked away with filter paper after 1 minute. Transmission electron microscopy was used to verify attachment of the virus to the substrate with a JEM 2100 $LaB_6$ at 100 keV electron beam strength.

### 2.3.5 Results and Discussion

Microphase separation of the block copolymer and attraction of gold nanoparticles to one particular block was evident from the TEM pictures. In Figure 2.10, there are areas of lamellar morphology shown from the doping of the P4VP block doped with gold nanoparticles. EDS results showed that gold is present in the sample. There were also high concentrations of copper and carbon, likely due to the TEM grids on which the polymer film is tested, and chlorine, from the precursor $HAuCl_4$. Low resolution images are shown in Figure 2.11. From these images, it appears that there is a small area that is strongly doped with gold nanoparticles surrounded by an area with less doping within the epoxy sandwich. The vertical lines are marks from the diamond knife as the sample was cut parallel to the direction in which the sample lay in the epoxy. There is no evidence other than the TEM image that the gold nanoparticles are sufficiently exposed for interaction with the TMV 1cys rods. However, since the samples are cut in a direction perpendicular to the film's surface, it is inferred that there are some nanoparticles exposed on the surface of the film.

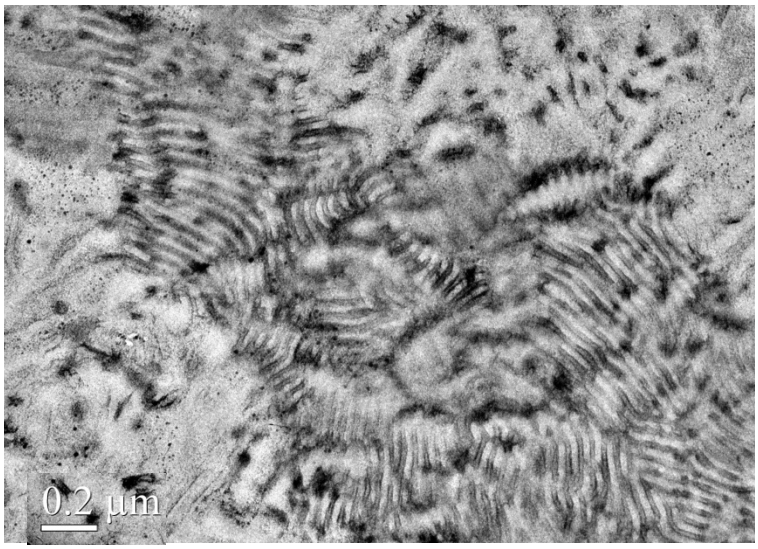


Figure 2.10: Block copolymer microphase separation with gold nanoparticles embedded in the P2VP block

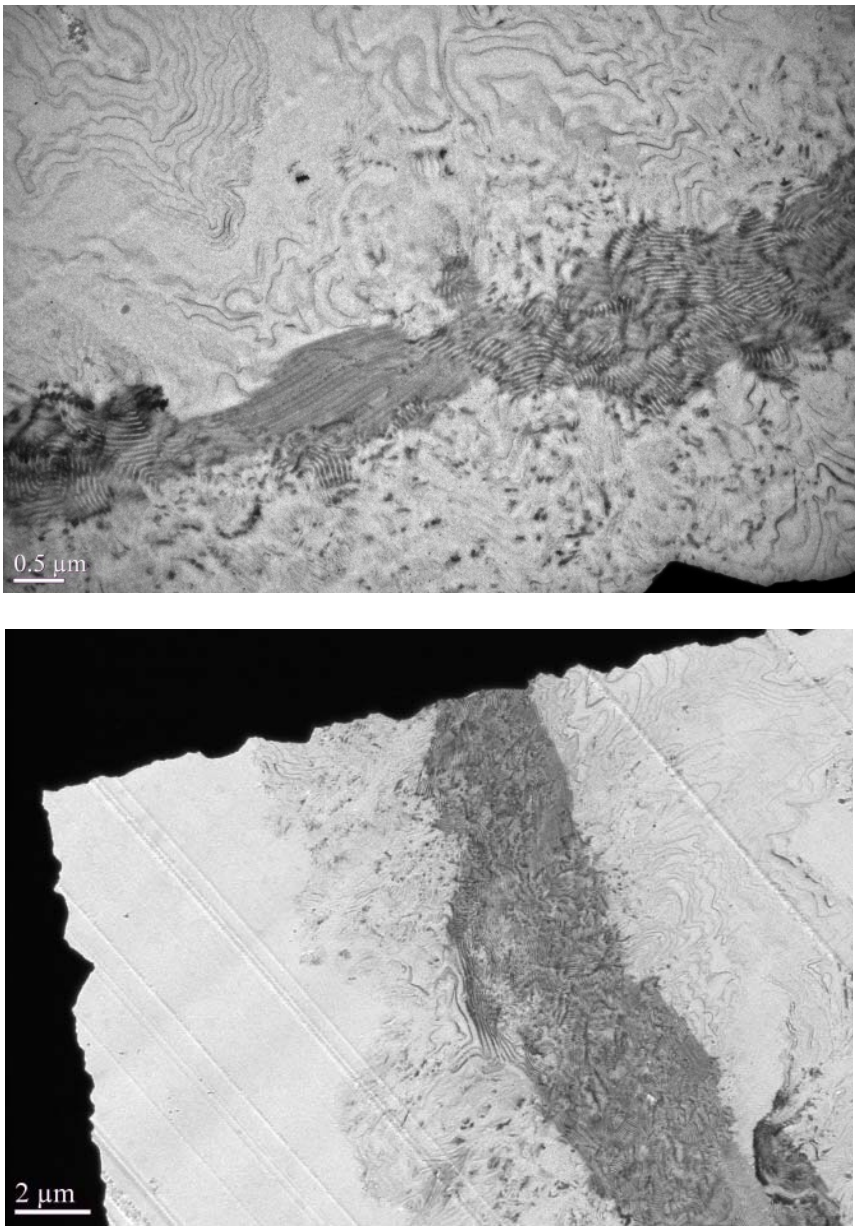


Figure 2.11: Low resolution images of the block copolymer film embedded in epoxy

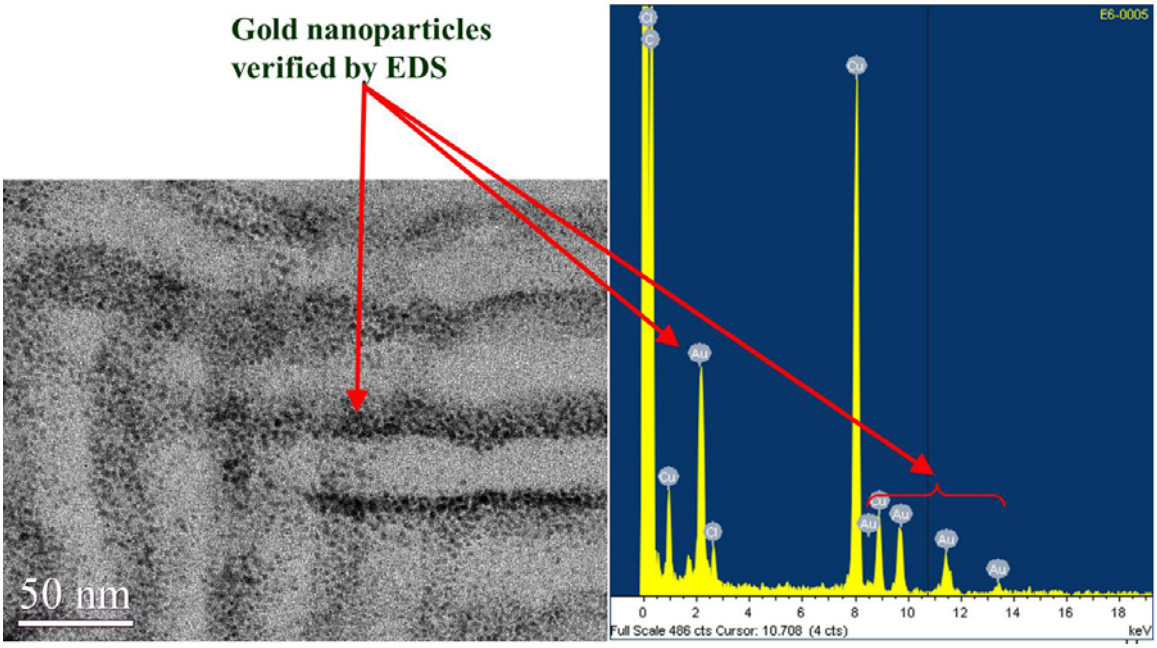


Figure 2.12: EDS spectrum of gold nanoparticles

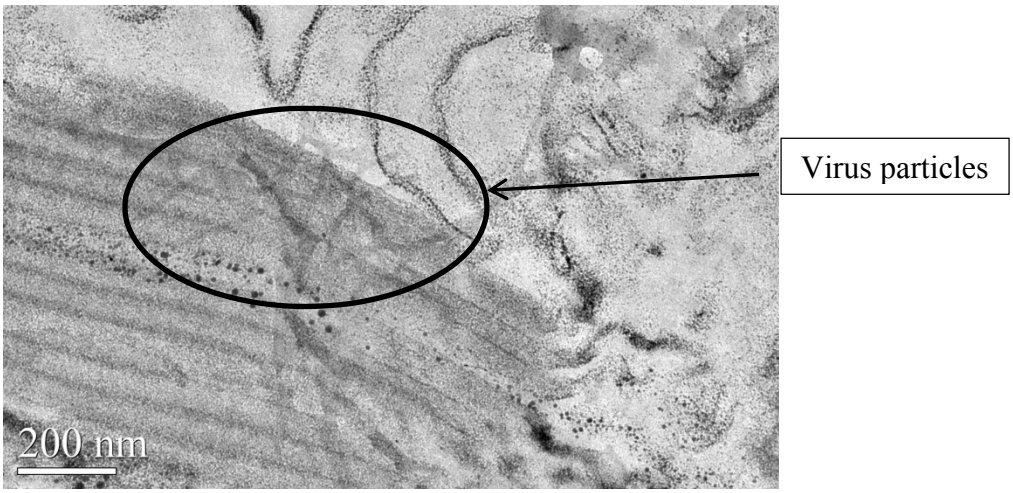


Figure 2.13: TMV particles stained with uranyl acetate

Figure 2.12 is a high resolution TEM image of the virus particles attached to the PS-P4VP polymer film. Although areas of dense gold concentration seemed to contain larger number of viruses (Figure 2.13), specificity of the virus to a particular block could

not be determined because the virus particles lay across multiple phases of the block copolymer. The virus particles are seen aggregating in both side-to-side and head-to-tail formations due to the affinity to each other. It is believed that the visible virus particles are on the top surface of the block copolymer due to the procedures in preparing the samples. The viruses were applied in a drop on the TEM grid, and then rinsed with a TWEEN solution to prevent non-specific binding. Staining was performed by drop casting onto the top of the TEM grid, then wicking away with filter paper and rinsing the grid with water in the same manner. Future work should be to study a procedure that would allow individual virus particles to be assembled on the surface without aggregation. This method of patterning with a block copolymer may also be more applicable for self-assembly of smaller biological agents such as proteins, since the lamellae were too small for the virus particles. This method is easier than current lithography methods of substrate patterning because the samples do not have to be fabricated in a clean room, while still generating lamellae of the same size with each sample.

# Chapter 3: Molecular Imprinting for Detection

## 3.1 Introduction

### 3.1.1 Molecular Imprinting

Molecular imprinting is a technology which allows for synthesis of materials that possess binding sites specific to a target molecule. Through this process, three-dimensional cavities are formed within a polymeric matrix or on a film's surface matching the size, shape, and functional group orientation of the target molecule.

Molecularly imprinted polymers (MIPs) can mimic the function of some enzymes by creating cavities of a specific size and shape complementing that of the target molecule for recognition of bioactive compounds [4]. MIPs have been the focus of previous investigations for several reasons. They have high affinity and selectivity similar to natural receptors and possess stability superior to that of natural biomolecules. MIPs can also be easily adapted to different applications, and are known to be resistant to chemically harsh environments [5]. Applications for MIPs include catalysis, separation and purification, drug delivery, and detection technologies [38-43].

The virus imprinted MIP proposed in this research utilizes readily available shape-conforming polymers that can be applied to the development of a device for the detection and identification of viruses. The need is widespread in diverse sectors, including gene therapy, national security, human and animal health, and crop protection [4].

Molecular imprinting utilizes a readily available polymer in aqueous solutions rather than organic solvents has been presented in recent articles [44, 45]. This greatly

increases the use of MIPs and may bring the technology closer to application to biological systems. The development of general methods using MIPs capable of specific recognition of biological analytes would have an enormous value in medicine and bioanalytics. A detailed understanding of the parameters influencing surface imprinting and association of a virus with an imprinted polymer surface are needed before commercial manufacturers can create a reproducible device on a batch-to-batch basis. Such a device would have widespread applications for detection of pathogenic viruses and perhaps in biodefense as a viral specific sensor for environmental samples.

Some advantages that MIPs have over their natural analogues (i.e. antibodies and enzymes) are:

1. MIPs are stable in a wide range of conditions (i.e. different solvents, high temperatures, various pHs), and can be stored for long periods of time in their dry state while maintaining performance. Biomolecules require storage in certain controlled and sometimes costly environments in order to remain effective.
2. Synthesis of MIPs is simple relative to biomolecule production. For example, materials needed for MIP s can be obtained by purchase from chemical vendors and the synthesis can be completed within 24 hours, while antibody or enzyme harvesting and purification can take longer and be more labor intensive.
3. MIPs can be reused many times as long as the target molecule is removed between cycles, while biomolecules can be used a limited number of times before decreased performance is observed.

### 3.1.2 Mechanism of Molecular Imprinting

Molecular imprinting exploits the simple, but elegant, principle of using elements of the target molecule to create its own recognition site. This is achieved by forming a highly crosslinked polymeric matrix around a template, which can be the target molecule itself or a close structural analogue. The template molecule serves two functions. The first is as a space-filling object around which a complementary polymer cavity can be formed. The second is to organize complementary interactions between groups on the template and functional monomers during polymerization. The templated molecules are subsequently extracted from the polymer. Left in the polymer matrix are three-dimensional cavities, "molecular imprints", that are complementary in shape to the templated molecule with desired functionality in a specific arrangement (Figure 2.1). The highly cross-linked polymers prepared this way can selectively recognize and rebind the template molecules.

Molecular imprinting's earliest beginnings can be traced to Linus Pauling's work in the late 1930's and early 1940's [46, 47]. Pauling, in an attempt to explain antibody formation, suggested that antibodies may form as a result of an immunoglobin folding around an antigen. This idea suggests that the antigen acts as a template by which the immunoglobin could become a specific antibody.

While this is not how the formation of antibodies proceeds, an important idea was founded on this flawed theory. Frank Dickey, a student of Pauling's, synthesized silica gels in the presence of various dyes and observed a preference in the silica gels for rebinding the imprinted dye. Since this initial discovery, there has been a variety of work aimed at the development and refinement of molecular imprinting procedures.

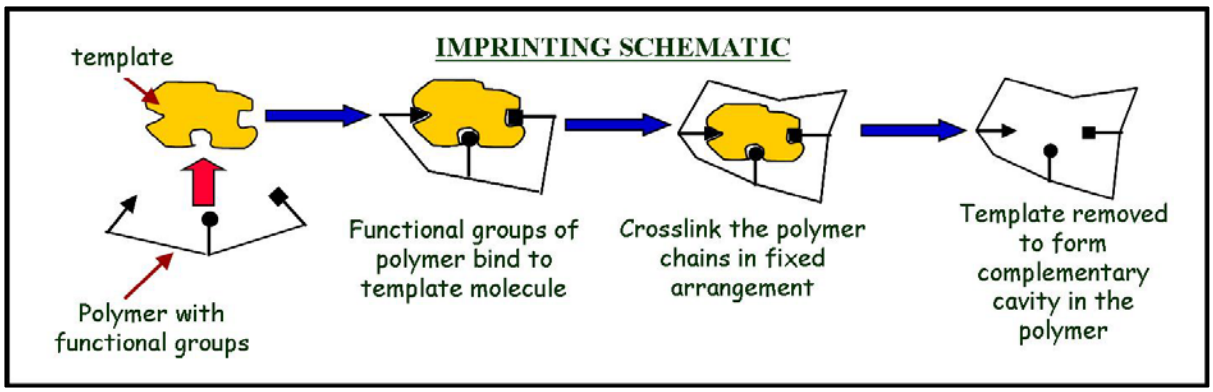


Figure 3.1: Schematic of molecular imprinting

Many bioactive molecules have complex shapes and/or a low degree of symmetry with regard to shape and functionality. In order to create the complex, irregular cavities necessary to accommodate these molecules, one must use a matrix flexible enough to conform to the imprint molecule's shape. At the same time the matrix must have sufficient mechanical strength to maintain the shape and integrity of the cavities during synthesis procedures and in applications such as chromatographic supports and sensor elements. Because of their ability to conform to complex shapes and achieve sufficient structural integrity, some polymers are excellent candidates for molecular imprinting. Polymers and silica matrices are the only regularly employed materials in this field [45, 48-55].

While methods of template fixation vary among research groups, the large majority of molecular imprinting studies have concentrated on synthesizing imprinted polymers in organic solvents. Polymerizable, functional monomers, capable of non-covalent interactions with the template molecule, are mixed in organic solutions with the template and allowed to associate. Problems may arise when working with organic solvents if the templates are naturally found in aqueous solutions because the template

needs to dissolve in the solvent used for imprinting (i.e. the biological molecule may become denatured).

Currently, most of the synthetic methods for developing MIPs use functional methacrylate monomers as the starting material [50, 52, 53]. Monomer units bind to both the template and to other monomers by their functional groups. A crosslinker is added to hold the template in place. Upon removal of the template, a three-dimensional polymeric matrix is left with cavities which are complementary to the template with respect to size and functional group orientation. Further work has been done by Li et. al. [49] where the monomer used acts also as the crosslinker, which simplifies the process.

Another way to synthesize an MIP is to crosslink an already formed polymer in the presence of the template molecule to form the matrix [45]. After the template associates with the polymer chains by its functional groups, a crosslinker is added to covalently connect the polymer chains together using any remaining functional groups. The result is still a three-dimensional polymeric matrix with cavities complementary to the template molecule.

Different methods have been used to synthesize MIPs, but can typically be classified as either covalent or non-covalent molecular imprinting. Both methods have been successfully employed in the creation of MIPs. The different bonding types refer to the chemical bond formed between the template and the polymer or polymerizable entity prior to crosslinking or polymerization. In the covalent technique, the functional groups of the monomer and template are covalently linked [54, 55]. After crosslinking, the template is removed from the matrix by breaking this bond. The template is covalently linked again to the binding sites during rebinding. An advantage of using this technique is

that the functional groups in the matrix will be limited to within the cavities and will be arranged in a nearly perfect fashion around the template upon removal. However, only a small number of distinct template-monomer complexes can be created, limiting the number of molecules that can be targeted by MIPs.

Alternatively, the non-covalent imprinting approach holds more potential with respect to the number of compounds able to be imprinted [48, 51, 52]. The increased potential is due to the vast number of compounds, including biological compounds, which are capable of non-covalent interactions with polymerizable monomers. Non-covalent interactions include ionic interactions, hydrogen bonding, pi − pi interactions, and hydrophobic interactions. Another advantage of the noncovalent approach to molecular imprinting is the fact that non-covalent interactions are more easily reversed. This is important because it is necessary to reverse the template-polymer interaction once the imprinted matrix is formed in order to remove the template to form the MIP. Reversal of the template-polymer interaction for non-covalent interactions is usually accomplished by a wash in aqueous solution of an acid, base or methanol. One disadvantage of the noncovalent technique is that the functional groups in the matrix are not all located within the created cavities, which leads to more non-specific binding.

One of the difficult tasks in molecular imprinting is finding the balance between flexibility and rigidity of the polymer matrix which will yield the optimum binding of the target molecule. Mechanical properties are controlled by varying the amounts of the materials used during synthesis, such as polymer and crosslinker. The MIP needs to have enough flexibility to conform to the template's shape, while also having the rigidity to maintain the shape of the cavity when the template is removed.

### 3.1.3 3-Dimensional Imprinting

An important consideration with 3-dimensional (3-D) imprinting is the control of porosity and pore size of the polymer matrix. During the rebinding process, the target molecule will need to move freely within the matrix to be reintroduced to the imprinted site. Several groups have recently studied the use of polymers for 3-D imprinting of hydrogels, sol-gels, and acrylates [38, 56-63].

Hydrogels are a class of polymers which can undergo reversible volume transitions between the swollen and collapsed phases. These changes can be triggered by stimuli such as temperature, solvent, and pH. Kofinas et al. [44, 45] has synthesized a glucose phosphate imprinted hydrogel made of poly(allylamine hydrochloride) capable of quantitative isomer specific glucose recognition. This complex of ionic interactions is crosslinked with epichlorohydrin and is selective in rebinding glucose over fructose.

Sol-gel imprinting has been applied to the encapsulation of proteins and has recently been adapted to protein imprinting because sol-gels can be synthesized in conditions close to those favorable to proteins (pH, ionic strength, aqueous solutions) [58, 59].

Several groups have prepared protein MIPs using water soluble acrylic monomers, due to the insolubility of acrylate polymers in aqueous solutions. Vaidya et al. demonstrated that in a trypsin imprinted poly(acrylamide) gel, the target molecule binding was favored when in a mixture of chymotrypsin [60]. Also, the Hjerten group created a column consisting of poly(acrylamide) and N,N'- methylenebisacrylamide) that selectively adsorbed a specific protein [61].

### 3.1.4 2-Dimensional Imprinting

2-dimensional (surface) imprinting is a method for imprinting larger target molecules that may not be able to locate binding sites within a 3-dimensional bulk polymer matrix. The binding sites on these MIPs are limited to the surface of a thin film, providing additional support to the film by a fixed surface, which creates increased durability to the system and allows for the development in MIP-based biosensors.

The majority of surface imprinting has been performed using either stamping or self-assembled monolayers. Stamping involves organizing the template on a glass slide or other surface and applying it to a polymer film during crosslinking [39, 64]. Dickert et al. [39] has utilized this method to create a tobacco mosaic virus (TMV) templated MIP for virus sensing with quartz crystal microbalance (QCM). Balci et al. utilized an oxidized PDMS substrate as the imprinted material for TMV stamps [65]. Whitesides et al. [66] has used poly(dimethylsiloxane) (PDMS) stamps to print patterns of bacteria on agar plates. These stamps are easily adaptable to different sizes and patterns and can regenerate to be used for up to a month if culture media is included with the bacteria. A disadvantage of stamping is that it cannot be used for templates with a fragile surface, because the templates may deform during the imprinting process, yielding inaccurately sized cavities.

Self-assembled monolayers (SAMs) have been employed to address this complication. One method that has been used is to submerse a substrate in a mixture of the template and polymer [67-69]. If both possess an affinity toward the surface, it allows self-assembly of the polymer and template onto the substrate in a single layer. A second technique to create a SAM is to apply the template to the substrate prior to

exposure to the polymer solution [69]. This allows the template and polymer to evenly disperse on the substrate and prevents competition between the polymer and template for binding to the substrate.

### 3.2 Project Objectives

The goal of these experiments was to create imprint sites on a polymer surface via a modified stamping method for virus detection. A poly(allylamine hydrochloride) hydrogel was synthesized for surface imprinting with a template, the tobacco mosaic virus. The template, or stamp for the imprint was a surface consisting of metal coated cysteine-modified virus particles.

### 3.3 Research Design and Methods

Current techniques apply the template to the imprinted polymer during crosslinking. This becomes problematic if imprinting with a fragile template and also risks deformation of the imprint site due to pressure from the stamp. Instead of creating a stamp with a virus on a glass slide, the virus was arranged on a surface, while another polymer was placed on top of it during crosslinking. This insured the cavity size and template shape would not be affected by pressure from the stamp. A schematic of the stamping procedure is shown in Figure 3.2.

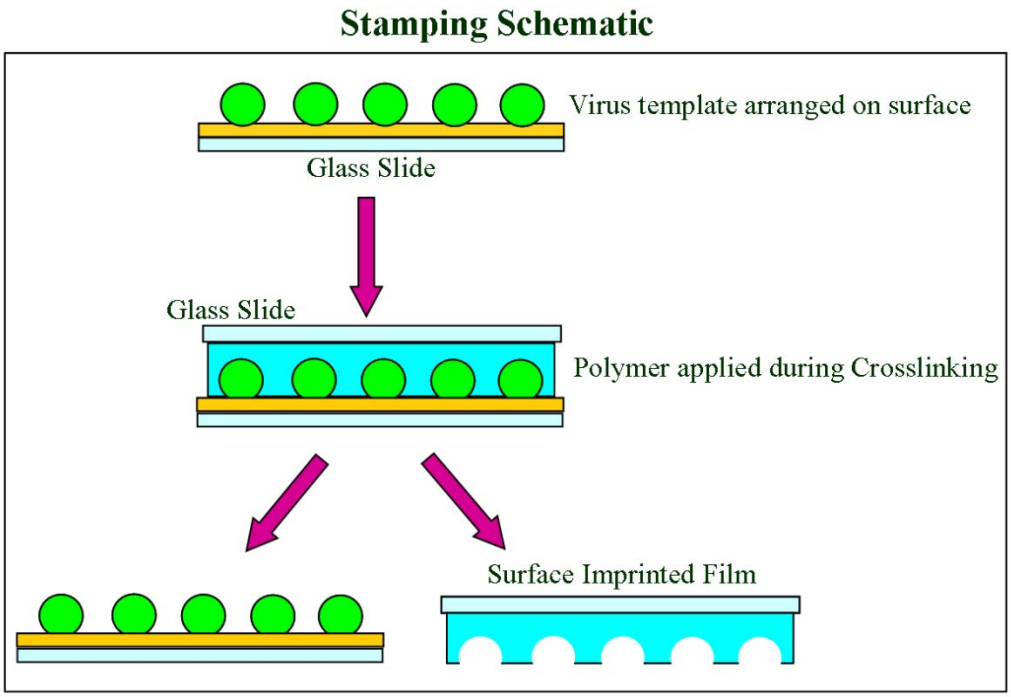


Figure 3.2: Procedure for stamping experiments

The template or stamp for the imprint utilized metal coated cysteine-modified virus particles on gold surfaces as described by Royston et al. [2]. The TMV1cys encodes a cysteine codon at the N-terminus of the coat protein open reading frame, which creates virus particles that form strong gold-thiol interactions. The virus templates were assembled onto gold-coated silicon chips. To create the gold surface, a thin layer of chrome was deposited on a silicon wafer surface, acting as an adhesion layer for the gold. This was followed by gold sputtering. Once the gold was deposited, a thin layer of photoresist was spun onto the wafer and scored into 0.25 $cm^2$ squares. The chips were sonicated in acetone, methanol, and isopropanol for 30 minutes each to remove the photoresist layer. Immediately prior to use, the chips were sonicated in acetone for 30 minutes, and then rinsed in ethanol and water to remove any organic contaminants, which

would interfere with virus attachment. The chips were placed in a 0.2 g/L virus in 0.1 M phosphate buffer (pH 7) solution overnight.

Platinum metal nanoparticles were applied to the virus assembled on the gold chip using an electroless plating method. Metal plating on the virus particles was performed by placing the chip in 300 µL of 3-(N-morpholino)propanesulfonic acid (MOPS) solution, and alternating the addition of platinum ions ($K_2PtCl_4$, 99.9+%, Aldrich) and dimethylaminoborane (DMAB, $((CH_3)_2NHBH_3$, Aldrich, 97%)) reducing agent at 5 minute increments. Two different protocols were utilized for the experiments. A detailed description of the platinum plating can be found in the Appendix.

| Protocol #1 | Protocol #2 |
|---|---|
| 300 µL MOPS | 300 µL MOPS |
| 10 µL $K_2PtCl_4$ } x 10 | 10 µL $K_2PtCl_4$ } x 10 |
| 1 µL DMAB | 1 µL DMAB |
| 100 µL $K_2PtCl_4$ | New solution (300 µL MOPS): |
| 10 µL DMAB | 100 µL $K_2PtCl_4$; 10 µL DMAB |

In both protocols, the platinum plated virus coated chips were removed from the final solution 10 minutes after the last DMAB addition. A Hitachi SU-70 field emission scanning electron microscope (FE-SEM) was used to visually determine which protocol produced the most homogeneous metal plating, which was ideal for imprinting. Element analysis was performed by a Bruker energy-dispersive x-ray spectrometer (EDS) at 5keV electron beam strength to verify the presence of the platinum layer.

A solution of poly(allylamine hydrochloride) (PAA HCl) (MW 60k Da, Polysciences, Warrington, PA in water was applied to the surface during crosslinking. This mixture was prepared with 50% PAA-HCl in water and 50% of crosslinker ethylene glycol diglycidyl ether (Sigma-Aldrich, St. Louis, MO). Various volume ratios (60-90% polymer solution) were tested to optimize the properties of the film. The solution was pipetted onto the virus template surface after 20 minutes of crosslinking. The PAA-HCl was left overnight to insure completion of the reaction, then removed from the block copolymer slide. The PAA-HCl film was washed with NaOH to remove any template remaining in the MIP.

### 3.4 Results and Discussion

SEM images are shown in Figures 3.3 and 3.4. Protocol #2 yielded more homogeneous plating of the metal onto the viruses. Protocol #1 showed higher aggregation of the metal nanoparticles which covered areas of the virus making imprinting of the rods difficult.

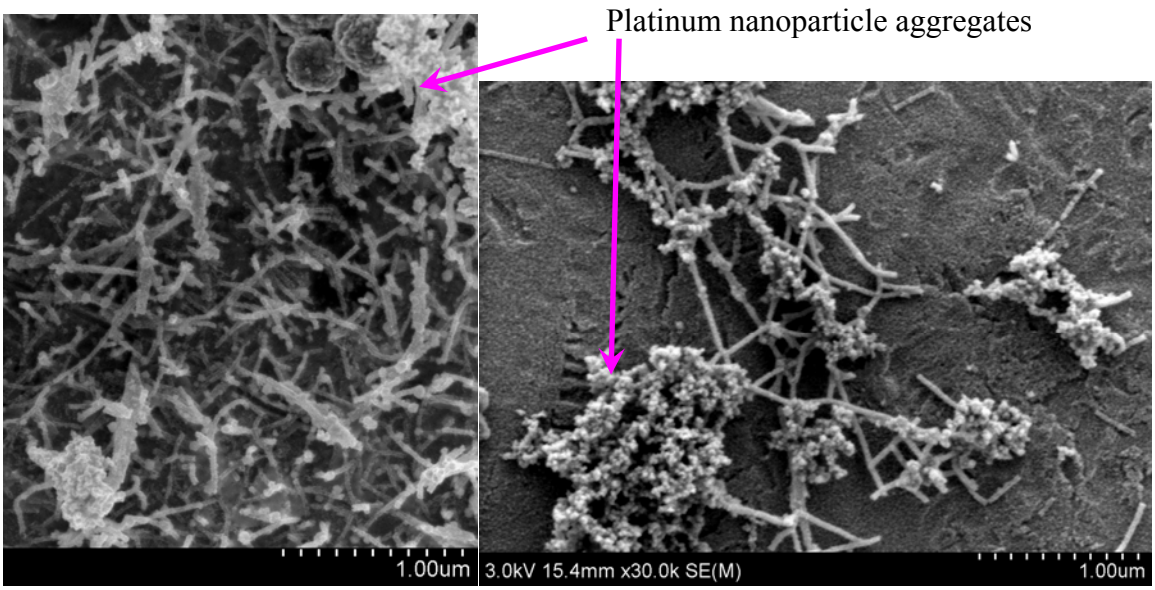


Figure 3.3: SEM image of platinum plating protocol #1 (30k magnification)

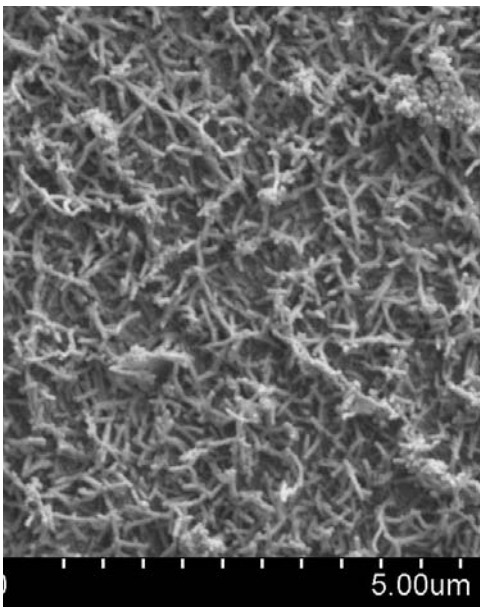


Figure 3.4: SEM image of platinum plating protocol #2 (10k magnification)

The homogeneous coverage of metal nanoparticles could have been due to the placement of the chip in a new vial of MOPS buffer without the previous additions of metal and DMAB. The new solution prevents excess metal nanoparticles from attaching to the chip. Even though protocol #2 produced the more desirable metal nanoparticle coverage, imprinting the viruses would still pose a problem due to the virus particles overlapping on one another. It would be ideal to find a procedure that would allow virus density on the surface to vary for different applications.

The EDS results shown in Figure 3.5 were analyzed in the areas of high virus density. The peaks at keV 0.1, 2, and 9.5 are indicative of platinum presence on the sample.

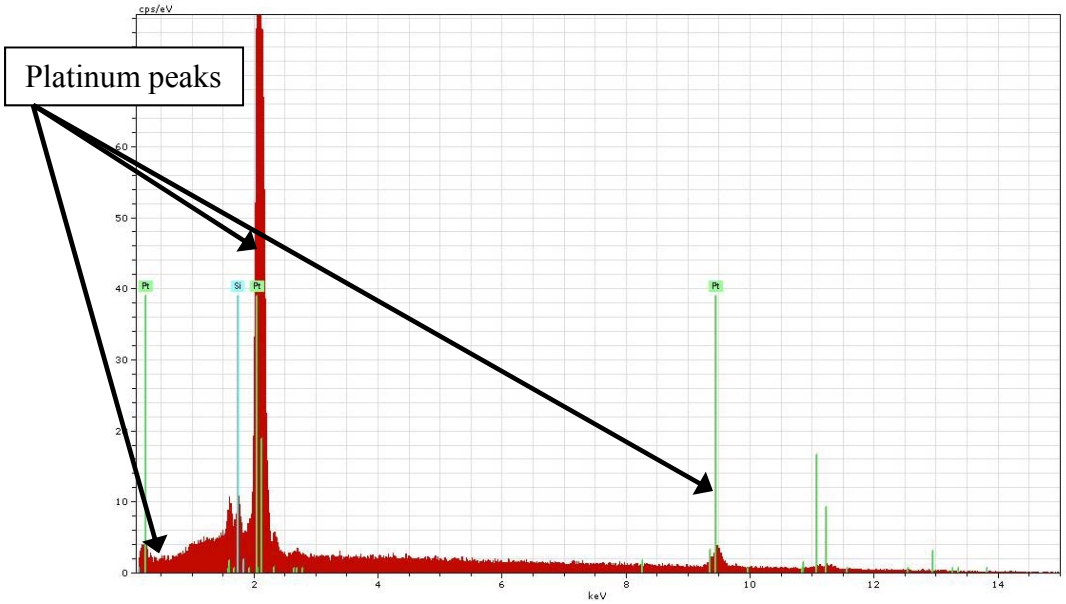


Figure 3.5: EDS spectrum for platinum plating

Hydrogel films for stamping were tested at various crosslinker concentrations. The ideal results would be those that yield a film that could easily be removed from the "stamp" surface while maintaining its structure. The lower crosslinker percentages produced hydrogels that peeled away from the imprint stamp; however, the volume changes during the washes due to expansion and contraction of the gel caused it to break apart. The higher crosslinker percentage produced a gel that was too brittle to peel away from the imprint without breaking into small pieces. Figure 3.6 shows a digital photograph of two of the lower concentration crosslinker (60%/70%). On sample #1, the black circle drawn around the imprint stamp area was still visible, but the gel was too deformed to characterize the imprint sites. We were unable to obtain a clear picture of the higher concentration gels due to poor lighting conditions and limitations of the camera in the laboratory. The gel had the appearance of sand granules after it fell apart.


Figure 3.6: Digital picture of 60% and 70% crosslinker in PAA hydrogel

The platinum plating method #2 allowed for individual virus particles to be visible on the surface. The difference between results the two plating methods is likely from adding the platinum ions multiple times. When the ions and DMAB are added all at the same time, there is an excess of nanoparticles that aggregate within the solution, and attach to the substrate. The PAA hydrogel, however, did not form an imprinted film that could be used for the detection of virus particles. Future studies should include utilizing different films with higher elasticity.

# Chapter 4: Controlled Virus Assembly on Surfaces

## 4.1 Introduction

The spacial control and arrangement of biomimetic nanostructured materials have attracted interest for its potential in research applications in electronic and photonic devices, ranging from molecular nanoelectronics to biological sensing devices. Biological molecules such as DNA, plant viruses [65, 70], bacteria, protein tubes, and protein fibers have been used in studies of the assembly of nanoscale biomolecular arrays for these devices, as functional units or templates.

Balci et al. showed that the selective adsorption and alignment of TMV on siloxane stamps resulted in extended, printable nanostructures [65]. This research group oxidized a PDMS surface with oxygen plasma to create a hydrophilic surface to assist in the alignment of TMV particles on the stamp surface. Suh et al. adhered anitbodies to substrates patterned with poly(ethylene glycol (PEG) nanowells for use in *E. coli* detection using host-parasite and virus-antibody interactions [71]. The same group also patterned the M13 bacteriophage by confining the particles into wells fabricated by nanomolding a PEG based random copolymer [72]. The Arter research group grafted the M13 bacteriophage into an array of poly(3,4-ethylenedioxythiophene) (PEDOT) nanowires to generate hybrids of conducting polymers and viruses. This resulted in real-time, reagent-free electrochemical biosensing of analytes [73].

There have also been several studies researching polymers that are used to assist in virus patterning. The self-assembly of tobacco mosaic virus (TMV) assisted by the polymerization of aniline creates one dimensional nanofibers with high aspect ratio. The

electrostatic interaction between the negatively charged virus and positively charged amine group on the polymer induces head-to-tail assembly of the virus [70]. There have also been studies where electrostatic assemblies of M13 viruses were patterned onto a polyelectrolyte multilayer. Solvent-assisted capillary molding of the polymer layers was employed to form micrometer-scaled dense patterns of viruses and the ability to modify the surface with biological ligands was examined for applications in biological detection [74].

### 4.2 Project Objectives

The goal of these experiments was to study the effects of a surfactant on the assembly of a cysteine modified tobacco mosaic virus onto a gold surface. Metal plating on the virus particles was performed with platinum and gold nanoparticles. Control experiments were also performed to verify the necessity for the cysteine modified particles.

### 4.3 Research Design and Methods

Gold chips were prepared as previously described in section 3.3. Triton was chosen as the surfactant to add to the virus solution at different ratios. The chips were left in the virus/triton solution overnight. Triton-to-virus ratios (Molar:Molar) used for platinum plating were 0% triton in solution, 62:1, 124:1, and 186:1. After the virus attachment onto the chip, the surface was plated with the metal nanoparticles. Platinum plating was applied using the procedure described in Section 3.3.

Triton-to-virus ratios for gold plating were determined from the results obtained in the platinum plating experiments. Gold nanoparticles were applied by a three step process using a hypophosphite bath originally used by Swan & Goslin [75]. First,

palladium ions were attached to the virus particles to activate the TMV surface and catalyze the electroless plating reaction. This was completed by adding 7 mg/mL palladium solution (0.01g/1.5mL $Na_2PdCl_4$) for every 100 mL virus solution. Nickel plating was performed by using a standard electroless nickel plating solution at pH 7 containing 0.1 M nickel chloride ($NiCl_2$), 0.15 M sodium tetraborate ($Na_2B_4O_7$), and 0.25 M glycine, with 0.5 M dimethylamine borane (DMAB) ($(CH_3)_2NHBH_3$)) for the reducing agent. A detailed description of the nickel plating protocol can be found in the Appendix (page 91). The plating solution was diluted with deionized water with a 1:1 ratio and the gold chip was placed in the solution until it darkened uniformly (approximately 5-10 minutes). After the nickel layer was complete, the chip was rinsed thoroughly with water and gold plating was performed by incubating the chips in approximately 300 µL of a solution of potassium aurocyanide ($KAu(CN)_2$), ammonium chloride ($NH_4Cl$), sodium citrate, and sodium hypophosphite ($NaH_2PO_2$) at 90 °C until gold coverage on the chip was complete. The gold plating components and detailed procedure are shown Table 1 in the Appendix, and a schematic of the plating is shown in Figure 4.1. Initial molarities added were chosen in order for the final volume to equal 1 mL, and the molarity of each component in that solution to equal that of the last column.

Figure 4.1. Computer schematic showing (1) virus assembly on chip, (2) virus particles after nickel coating, and (3) virus particles after gold coating

The thickness of the plating at two different time points was also investigated. These tests were performed with higher concentrations of triton in order to provide more separation of the virus particles. Scanning electron microscopy was used to quantify arrangement and density of virus particles on the chip.

The structure of the virus particles at different triton concentrations (used in the surfactant experiments) was studied. 5 μL aliquots of wild-type virus solution were dropped onto formvar coated carbon TEM grids, and then wicked away with filter paper for 1 minute. The grids were rinsed with water followed by an application of saturated uranyl acetate solution to achieve negative staining of the virus particles. TEM was performed using 100 keV electron beam strength on a JEOL JEM Lab6 device.

Control experiments were performed to investigate the assembly of wild-type tobacco mosaic virus and 1cys TMV particles during binding to the gold surface and after metal plating of the virus (with and without surfactant present). Surfactant studies were performed at 0.05% triton concentration after determining the level at which the highest SERS signal was received from experiments in Chapter 5. SEM images were taken after each step in the metal plating process, (a) initial virus assembly, (b) nickel plating, (c) gold plating. EDS was performed on each sample to verify metal plating on the virus particles. The virus assembly of wild type and TMV1cys was also tested on a plain silicon wafer, without the gold coating.

Experiments similar to those on gold coated wafers were performed using uncoated silicon wafers as the binding surface for the wildtype and TMV1cys virus particles with and without surfactant. The same methods as those used in the previous paragraph were employed for these studies.

### 4.4 Results and Discussion

Platinum Plating

The chips were removed from the second plating solution after 10 minutes. They had visibly changed color from gold to dark silver/black. SEM images show the different densities relating to each virus:triton concentration. The sample with 0% triton concentration shows the results similar to those obtained in Section 3.4. The subsequent samples show that with an increasing triton concentration, the virus density decreases. In the 0.1% sample, the virus rods aligned next to each other in side to side and head to tail manner. The size of the rods in the image indicates that there is more than one virus present underneath the plating.

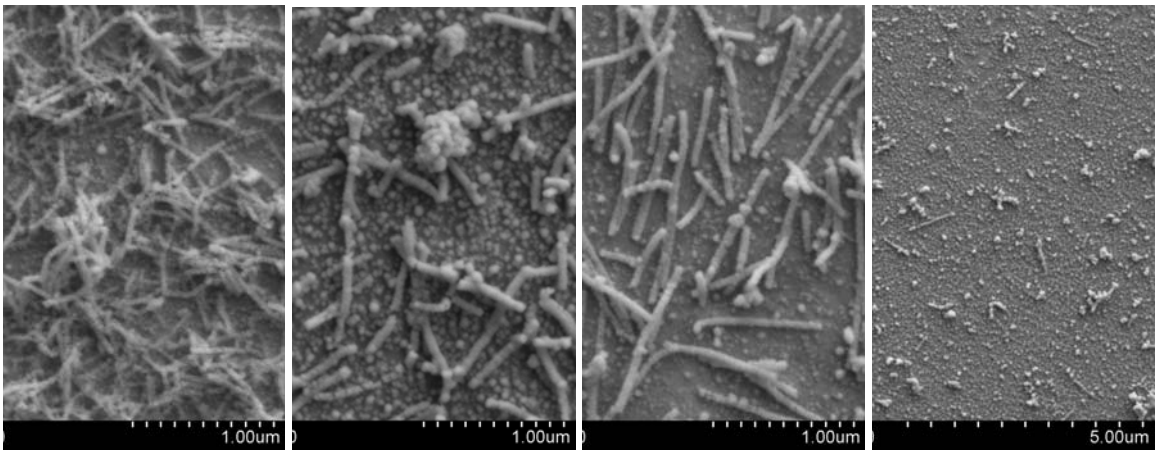


(a) (b) (c) (d)

Figure 4.2: SEM images (10k magnification) of platinum plated virus particles at (a) 0% triton concentration, (b) 0.075% (93:1 triton:virus), (c) 0.01% (124:1 triton:virus), and (d) 0.15% (186:1 triton:virus)

The platinum plating results show that in order for the virus particles spread apart and not overlapping each other, the triton concentration should be higher than 0.05%. The number of rods per micrometer squared ($\mu m^2$) were manually counted and graphed as a function of triton concentration (Figure 4.3). This was performed by choosing a random area on the SEM images for each sample and counting the number of rods seen within that space. The triton to virus ratios chosen for gold plating were 62:1 (0.05%), 93:1 (0.075%), 124:1 (0.1%), and 186:1 (0.15%).

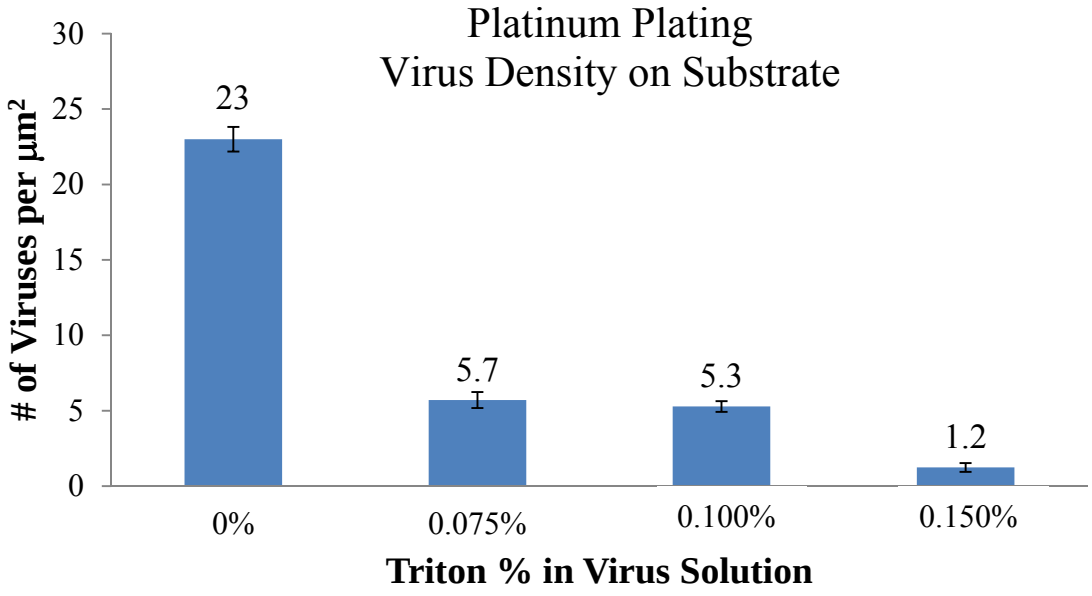


Figure 4.3: Platinum plating virus density as a function of triton concentration

Gold Plating

The chips visibly changed color from shiny gold to a dark brown/black during the nickel plating. Once the chips were completely covered in the dark color, about 5-10 minutes after placing them in the solution, they were transferred to the gold plating

solution. The chips were checked after 10 minutes and every 5 minutes afterward in order to verify when the gold plating was complete. For the time trials, chips were removed from the gold plating solution at the 15 minute time period and 30 minute time period. EDS was used to determine gold presence on the virus (Figure 4.4). The peaks at energy values 0.25 and 2.0 keV show the presence of gold in the sample. Figure 4.5 shows that the gold coated virus particles gain approximately 100nm extra in diameter with 30 minutes in solution versus the 15 minutes (170-190nm for 15 min; 245-345nm for 30 min).

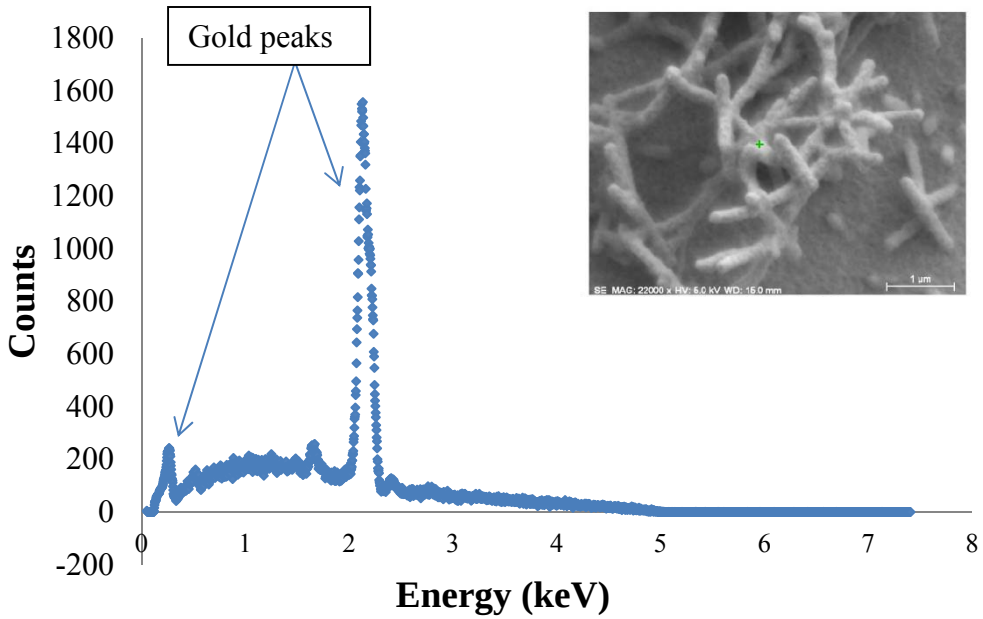


Figure 4.4: EDS spectrum of gold plated virus particles shown in SEM picture above. The green cross shows the area tested.

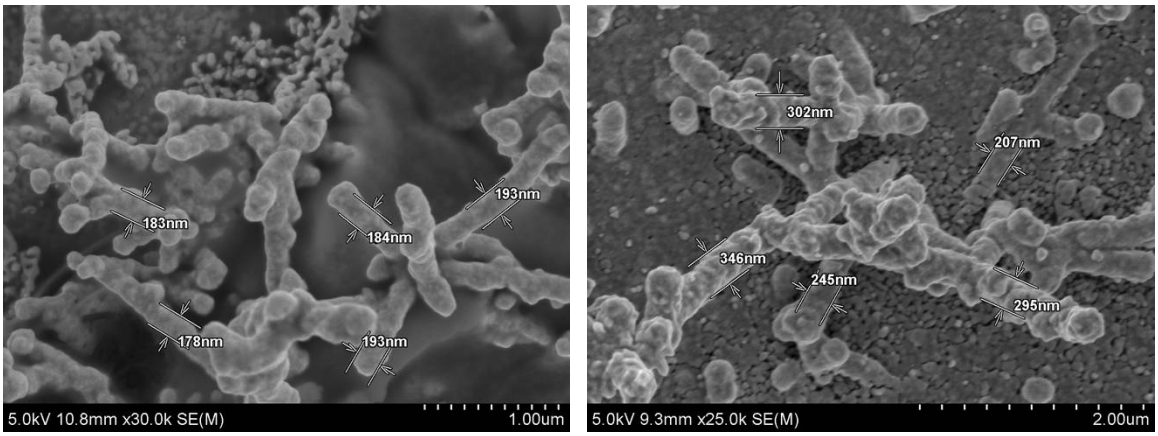


(a) (b)

Figure 4.5: SEM images (25k magnification) of time trials in gold plating experiments (a) 15 minutes and (b) 30 minutes in plating solution

The SEM images of the different triton:virus ratios are shown in Figure 4.6. The pictures show that as the triton concentration increases, the virus density decreases. The lowest triton concentration (62:1 ratio) shows very dense virus assembly with no clear virus particle rods visible. The highest triton concentration (186:1) shows very few virus particles with much empty space around each rod.

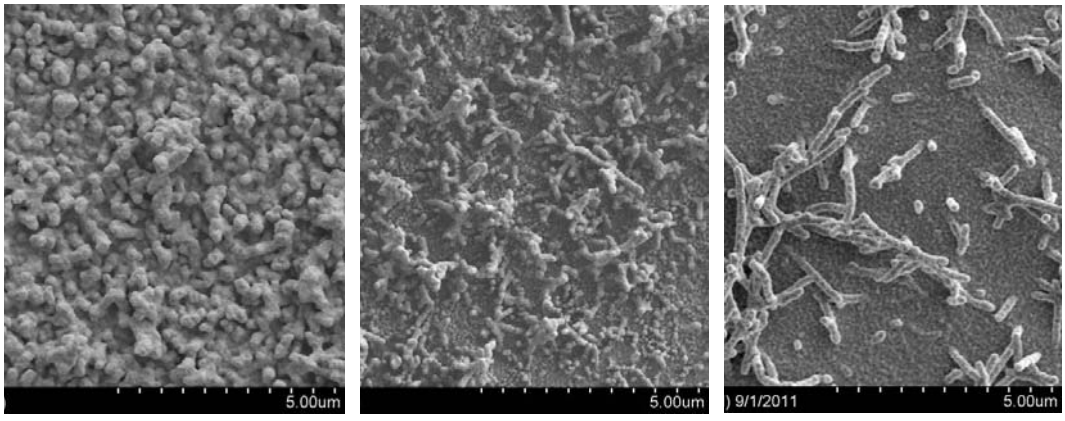


(a) (b) (c)

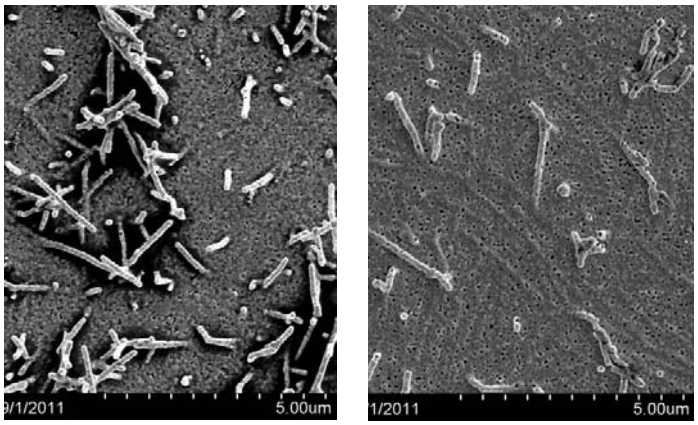


(d) (e)

Figure 4.6: SEM images of gold plated virus samples at triton concentrations (a-e) 0% (0:1 triton:virus), 0.05% (62:1), 0.075% (93:1), 0.1% (124:1), and 0.15% (186:1).

The number of rods per micrometer squared ($\mu m^2$) were manually counted and graphed as a function of triton concentration. This was performed by choosing four random areas on the SEM images for each sample, counting the number of rods seen within that space, and averaging the values. The samples were similar in its densities on larger scales of the chip as seen in Figure 4.7.

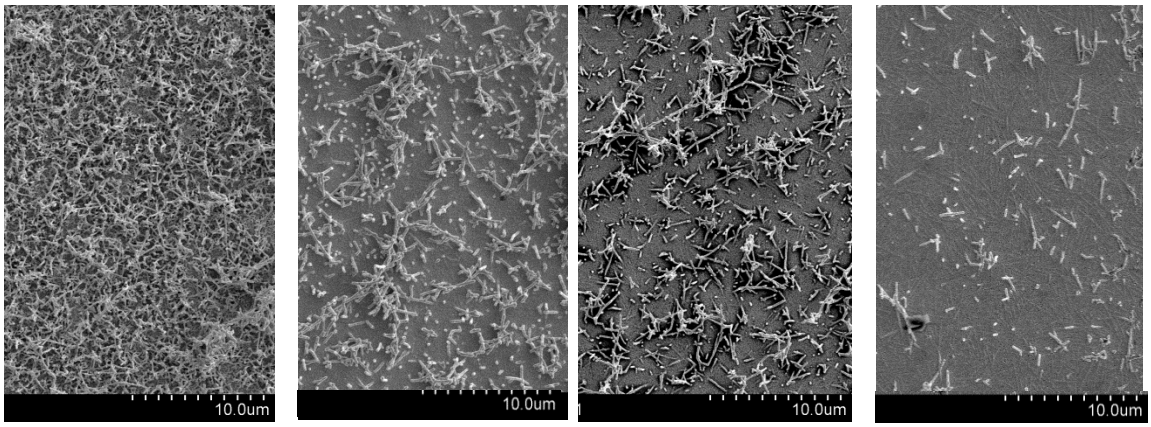


(a) (b) (c) (d)

Figure 4.7: Low magnification images of gold plating at triton concentrations (a) 0.05%, (b) 0.075%, (c) 0.1%, and (d) 0.15%

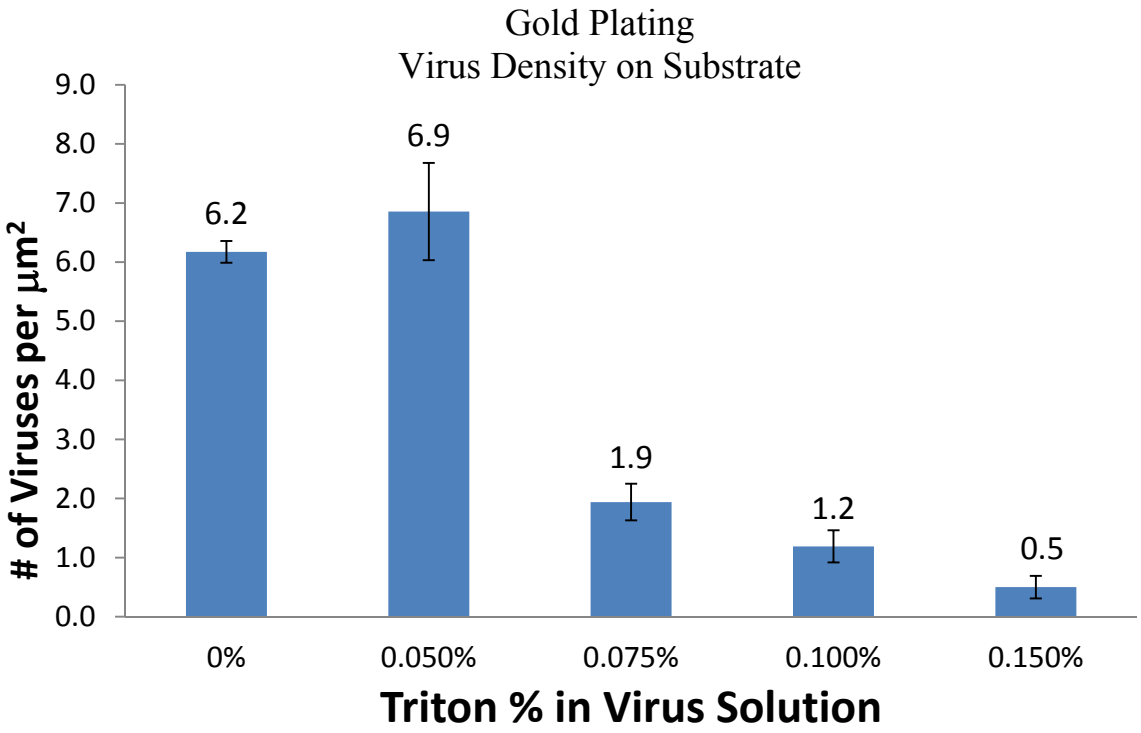


Figure 4.8: Gold plating virus density as a function of triton percentage

The results show that the surfactant addition was successful in decreasing the virus density on the gold surface. As seen in Figure 4.8, the number of viruses per $\mu m^2$ in the gold plating experiments drastically decreases (approximately 75% less virus particles) between 0.05% and 0.075%. These results also showed fewer number of virus particles at the 0% triton concentration versus the 0.05% concentration. Given the size of the plated particles on the 0% substrate, there may be more than one virus particle underneath each counted particle. This would increase the number of virus particles for that surface. The addition of a surfactant interferes with both the assembly of the virus on the chip as well as virus aggregation. These gold surfaces would be ideal substrates for Surface Enhanced Raman Spectroscopy applications due to the differences in roughness caused by the metal coated virus particles.

Virus structure with surfactant in solution

The structure of the virus particles was studied as a function of triton concentrations used in the surfactant experiments. 5 μL samples of the virus solution were dropped onto formvar coated carbon TEM grids, and then wicked away with filter paper for 1 minute. The grids were rinsed with water followed by an application of saturated uranyl acetate solution to achieve negative staining of the virus particles. TEM images show that the concentration of triton is not significant enough to denature the wild type tobacco mosaic virus particles (0.025%-0.15% triton in solution/virus coat protein to triton ratio). In Figure 4.9, the stained wild type virus particles remained intact with few virus particles less than 300 nm in length.

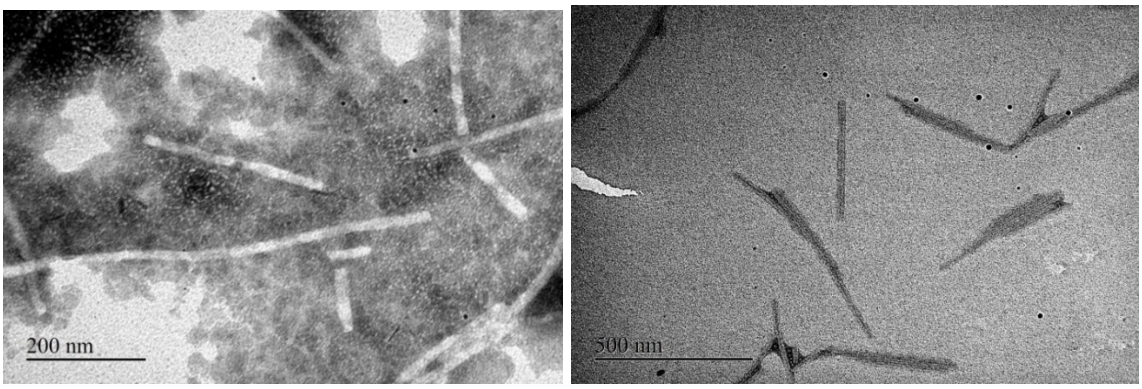


(a) (b)

Figure 4.9: TEM images of TMV with (a) 0.025% and (b) 0.15% triton added to solution

Control experiments with wild type TMV

SEM images were taken after each step in the metal plating process; (a) after initial virus assembly, (b) after nickel plating, and (c) after gold plating. Figure 4.10 shows the virus assembly on the chip and plating with nickel and gold for wild-type virus. There are no visible virus particles deposited onto the surface of the gold coated silicon wafers with

the wild-type TMV particles, which indicates that there is no affinity of the wildtype TMV to the gold coated wafer. EDS of the nickel plated samples yielded minimal nickel peaks, suggesting that most of the nickel nanoparticles do not adhere to the surface during metal plating. It is inferred that since no cysteine residues are present along the virus rod, that there are no nucleation points for the metal plating to occur. Even if some metal plating occurred, the gold peaks shown in (e) are most likely due to the gold coating on the silicon wafer, and not from metal plating.

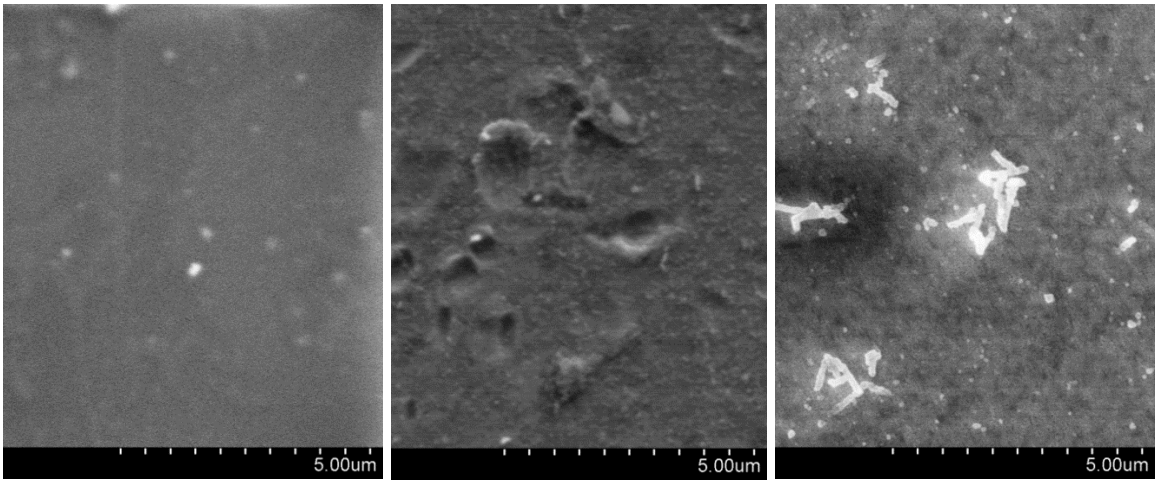


(a) (b) (c)

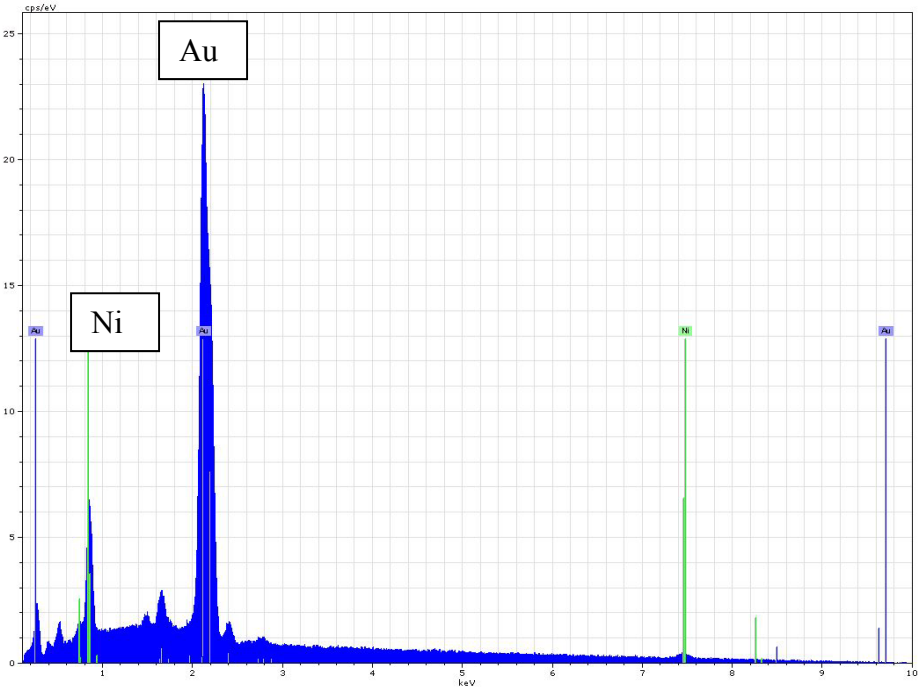


(d)

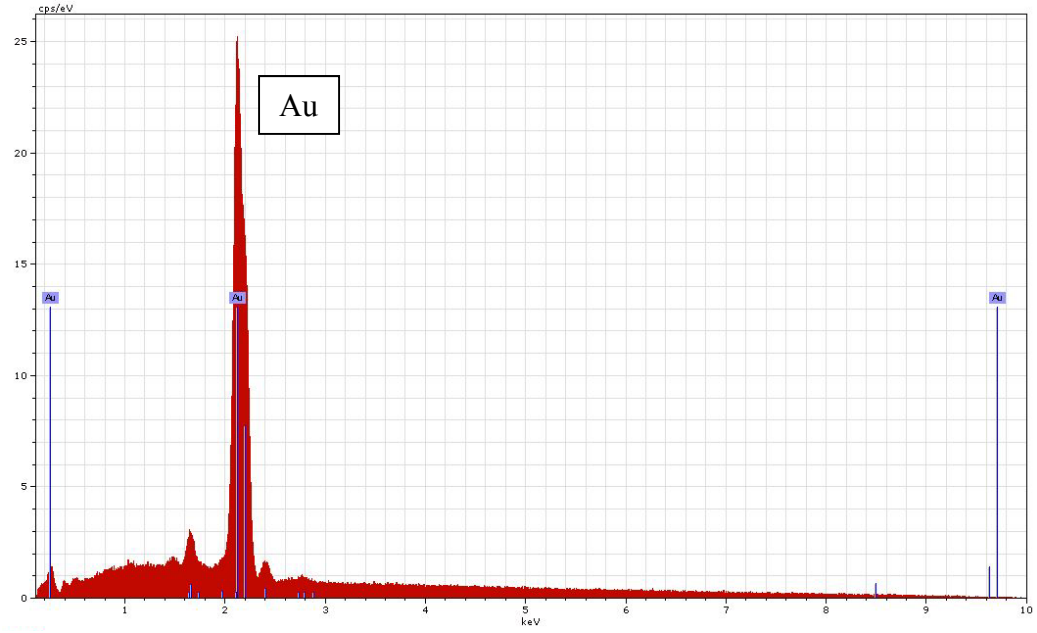


(e)

Figure 4.10: SEM images of wild-type TMV on gold coated silicon wafers (a) after virus assembly on the chip, (b) after nickel plating, and (c) after gold plating; EDS spectra of (d) nickel plated samples and (e) gold plated samples

The TMV1cys particles without surfactant in Figure 4.11 showed the presence of virus rods on the gold coated silicon wafer, as thin dark rods in the SEM image. Some of the rods were greater than 300 nm in length, suggesting that the viruses align in a head to tail fashion when on the surface. After each metal plaing application, the rod thickness increases to ~200 nm after nickel plating and ~500 nm after gold plating. After the last round of plating, the individual virus rods are not discernible because of the high density of the viruses. EDS spectra verifies the nickel and gold plating on the virus surface. The nickel plating image is similar to that obtained in previous results by Royston et al [2].

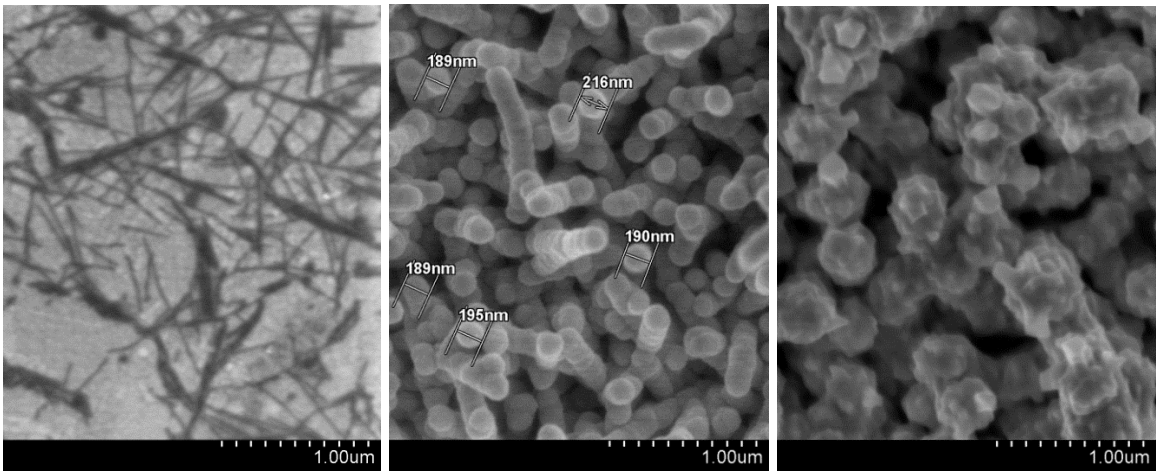


(a) (b) (c)

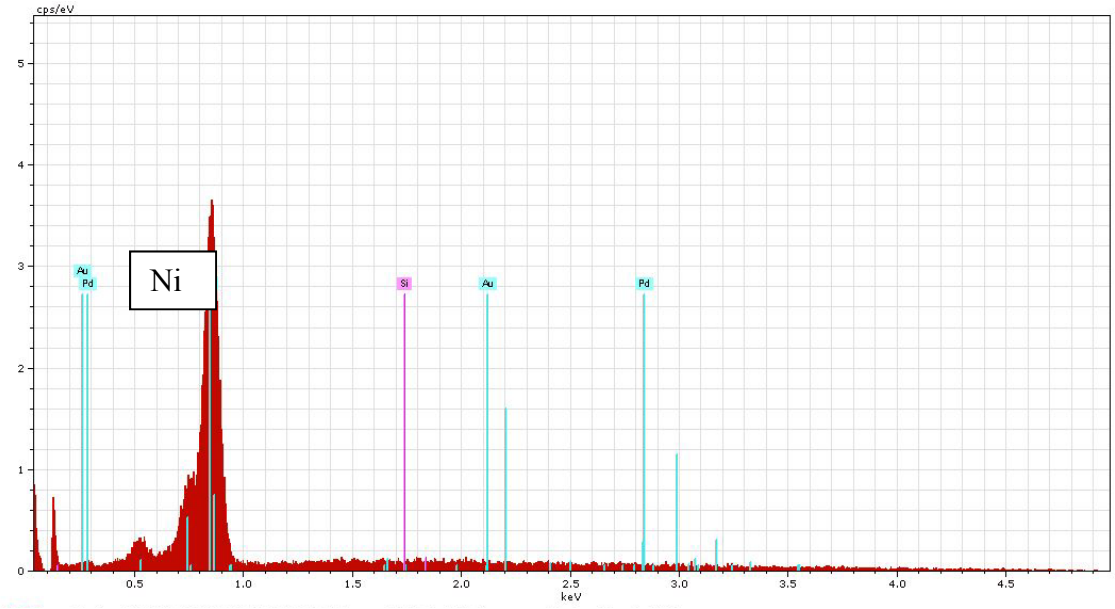


(d)

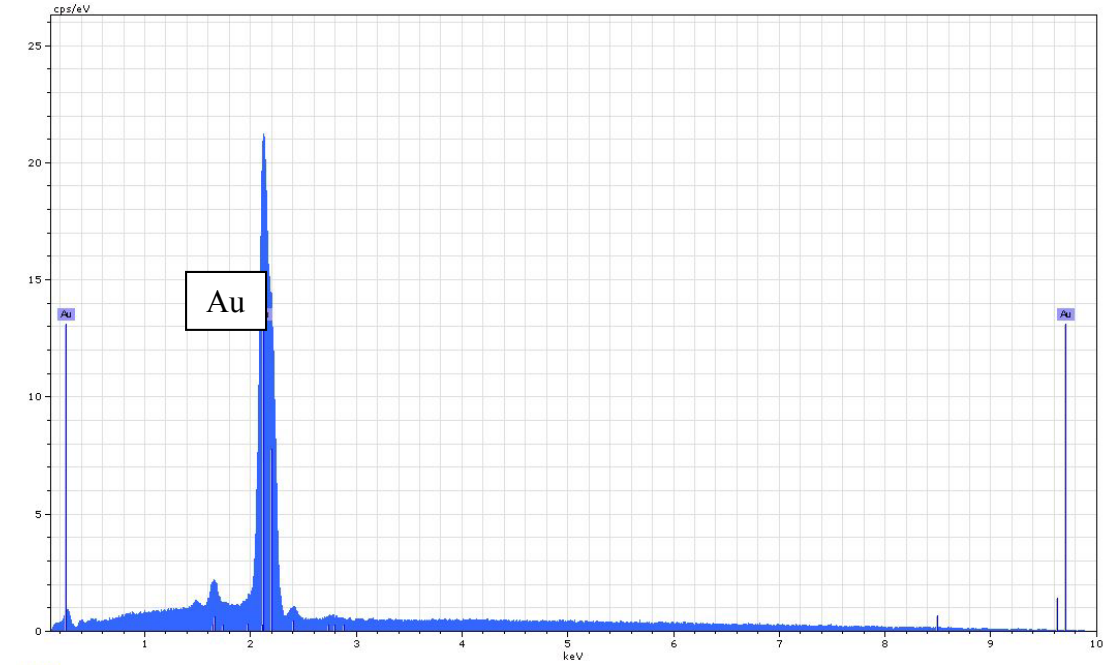


(e)

Figure 4.11: SEM images of TMV1cys particles on gold coated silicon wafers (a) after virus assembly on the chip, (b) after nickel plating, and (c) after gold plating; EDS spectra of (d) nickel plated samples and (e) gold plated samples

Figure 4.12 shows SEM images of the silicon wafer studies with wild-type virus and 0.05% triton solution. There were no virus particles visible after leaving the wafer in the solution overnight. The nickel plating yielded spherical nanoparticle aggregates between 200-300nm diameter which became larger after the gold plating step. EDS showed that nickel was present in Figure 4.12(b) and gold in Figure 4.12(c). This indicates that nickel and gold nanoparticles adhere to the surface of the virus, but do not attach specifically to virus particles. This implies that there may be an interaction between the metal plating solution and the triton or Pd molecules left on the chip from the initial virus solution. Since the chip is not washed after submersion in the virus/triton solution, there will be molecules still left on the chip during metal plating.

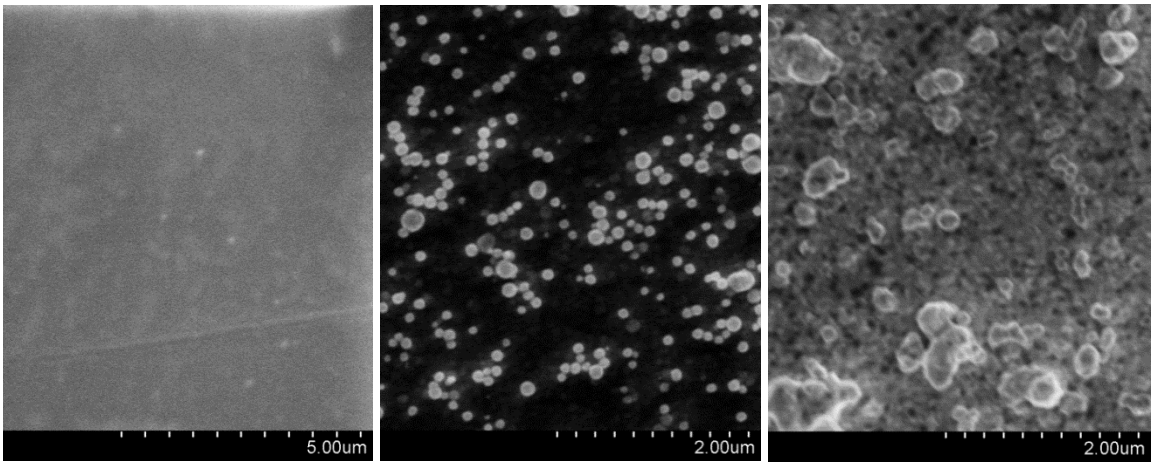


(a) (b) (c)

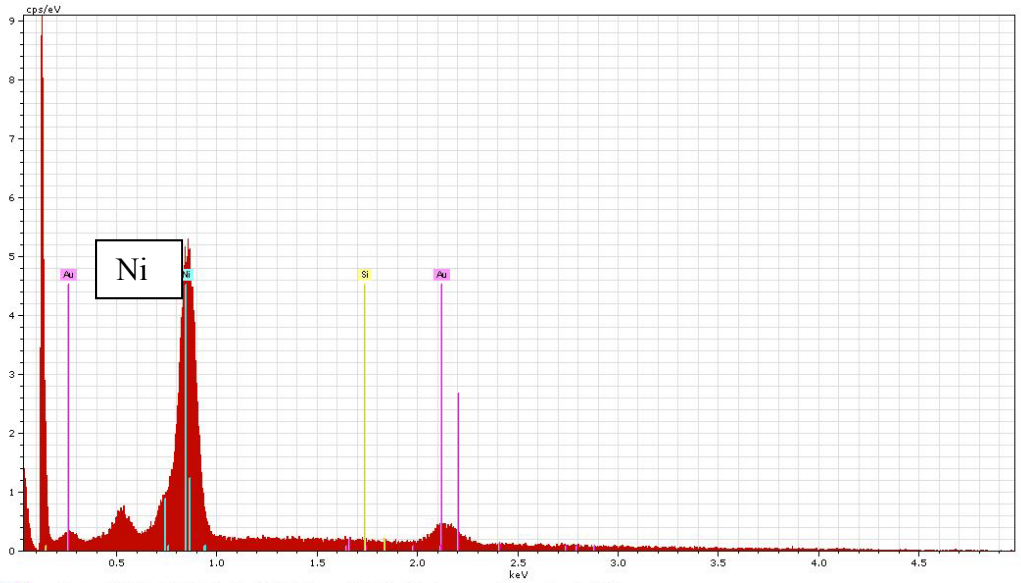


(d)

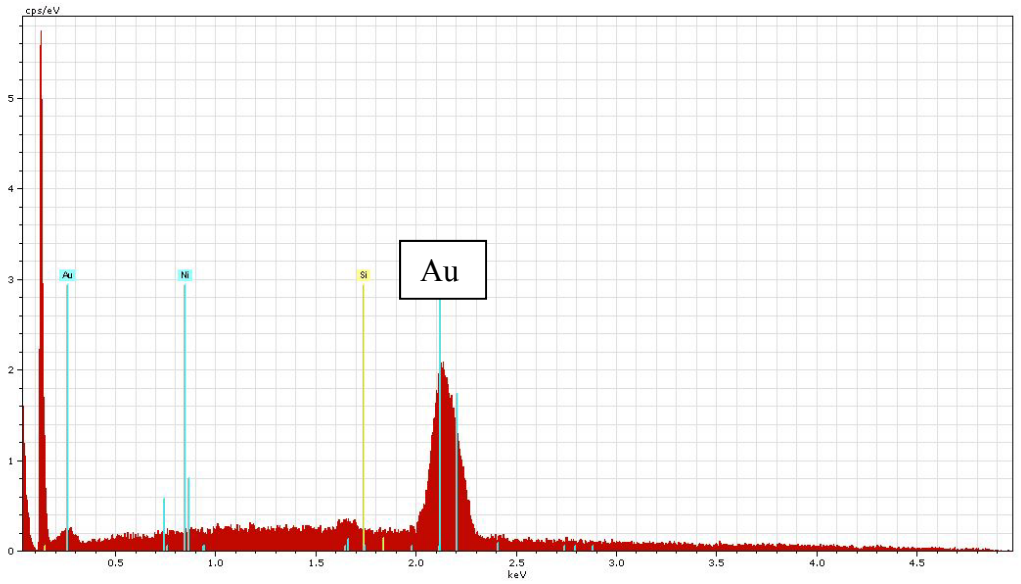


(e)

Figure 4.12: SEM images of wild-type TMV particles with 0.5% triton concentration on gold coated silicon wafers (a) after virus assembly on the chip, (b) after nickel plating, and (c) after gold plating; EDS spectra of (d) nickel plated samples and (e) gold plated samples

SEM images of virus assembly and plating for TMV1cys with triton surfactant are shown in Figure 4.13. Virus rods are visible on the gold surface prior to metal plating and are less dense than those shown in Figure 4.11. Nickel and gold plating images are similar to those shown in Figure 4.6 at the same concentration. The diameter of the nickel plated rods are approximately 130 nm, slightly less than that those in Figure 4.11. The addition of triton to the virus solution causes the viruses to spread apart, showing individual rods on the surface after gold plating.

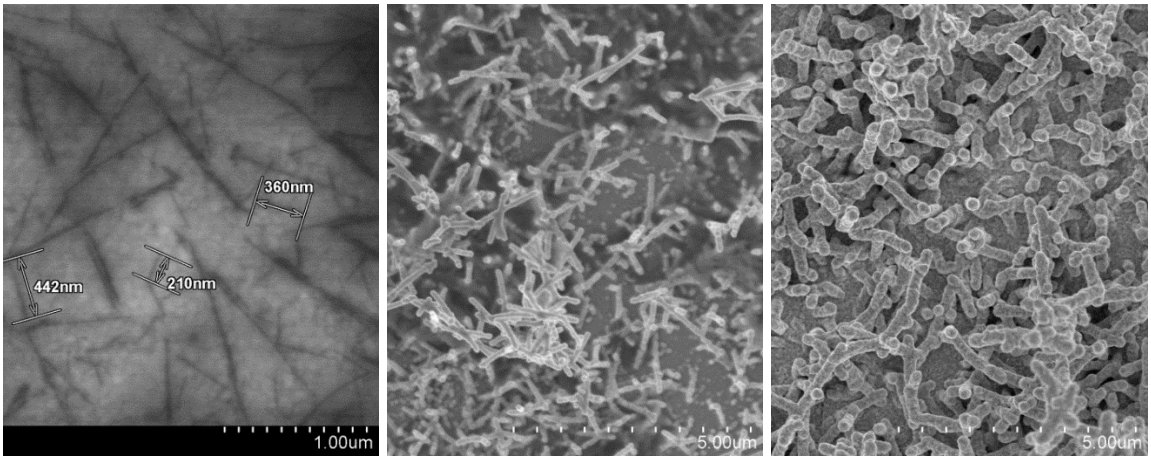


(a) (b) (c)

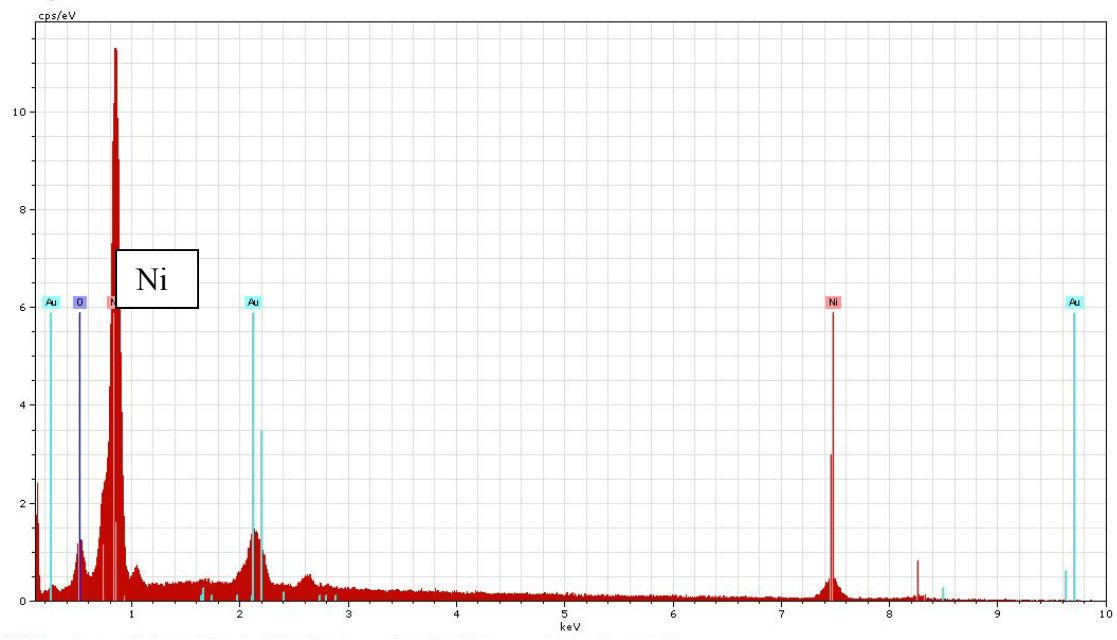


(d)

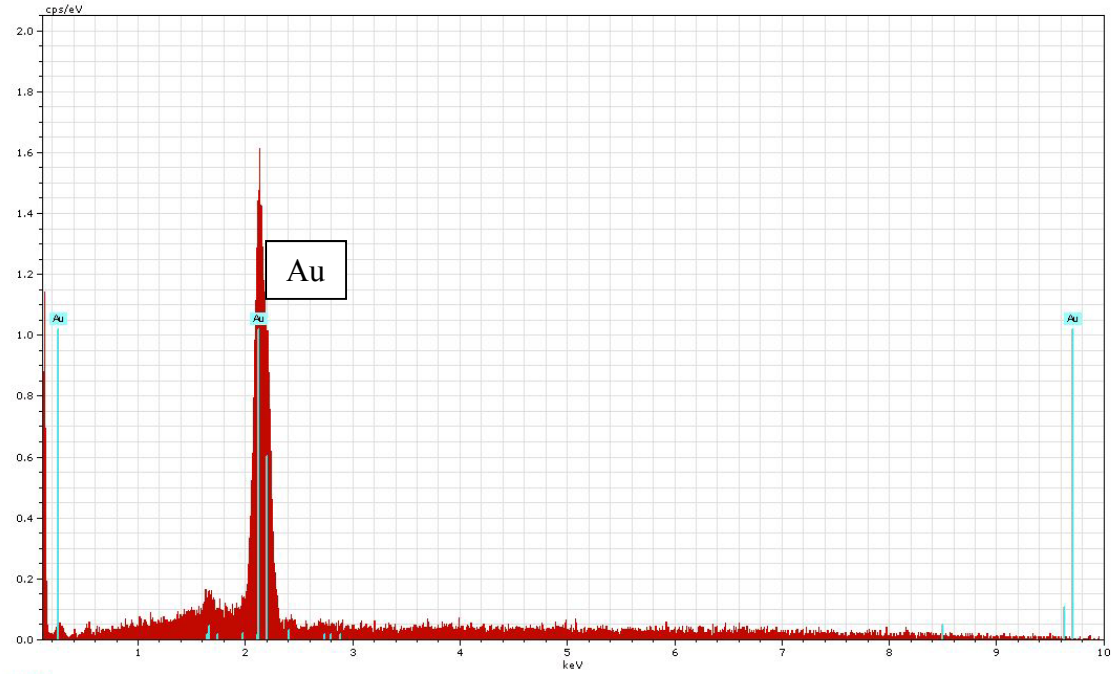


(e)

Figure 4.13: SEM images of TMV1cys particles with 0.5% triton concentration on gold coated silicon wafers (a) after virus assembly on the chip, (b) after nickel plating, and (c) after gold plating; EDS spectra of (d) nickel plated samples and (e) gold plated samples

Virus assembly and plating on silicon wafers

SEM images were taken after each step in the virus assembly and plating process using plain silicon wafers instead of gold coated chips, after (a) virus assembly, (b) nickel plating, and (c) gold plating. Figure 4.14 shows SEM results from wafers placed in wild-type TMV solution with no surfactant. Dark marks can be seen in the image after the wafer has been placed in the virus solution, however, after nickel plating, no virus rods remain on the chip. There appears to be metal nanoparticles and the EDS spectra of that sample show the peak for nickel.

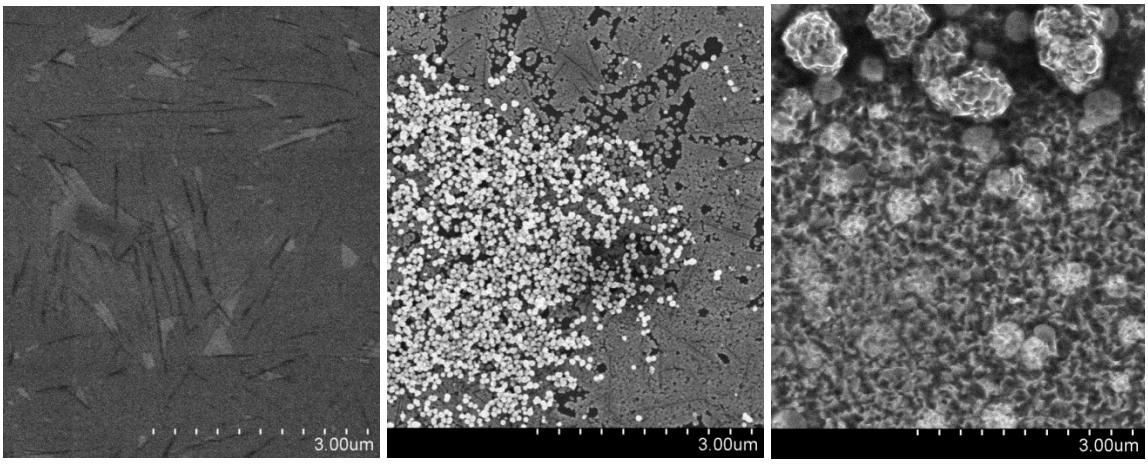


(a) (b) (c)

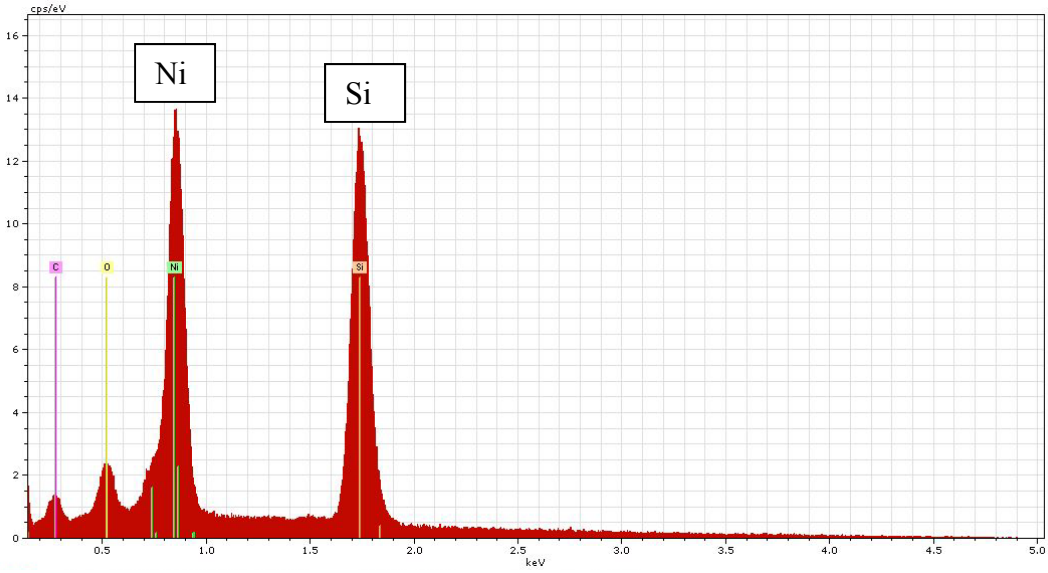


(d)

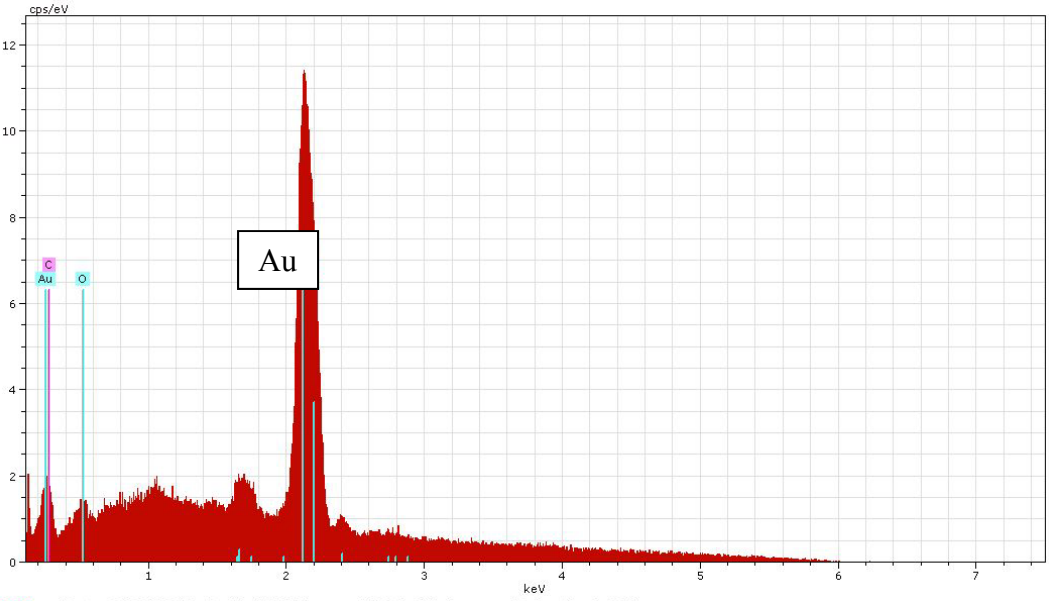


(e)

Figure 4.14: SEM images of wildtype TMV on plain silicon wafers (a) after virus assembly, (b) after nickel plating, and (c) after gold plating experiments; and EDS after (d) nickel and (e) gold plating

Virus assembly and plating of wildtype TMV with triton added to the virus solution are shown in Figure 4.15. These SEM images show no virus particles prior to the metal plating, as well as after these steps. There was also no visible color change to the chip, and EDS verified that no metal plating occurred by the nickel solution. After the gold plating process, small metal nanoparticles (between 15-50 nm diameters) appeared in areas along the edges of the chip, however large areas of the chip remained blank. Figure 4.16 is a high resolution SEM image showing the nanoparticles in greater detail.

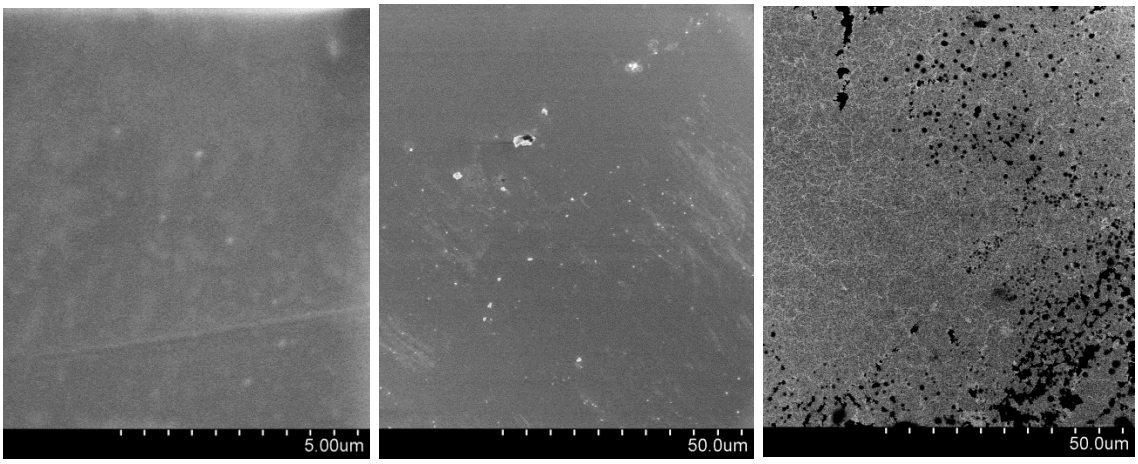


(a) (b) (c)

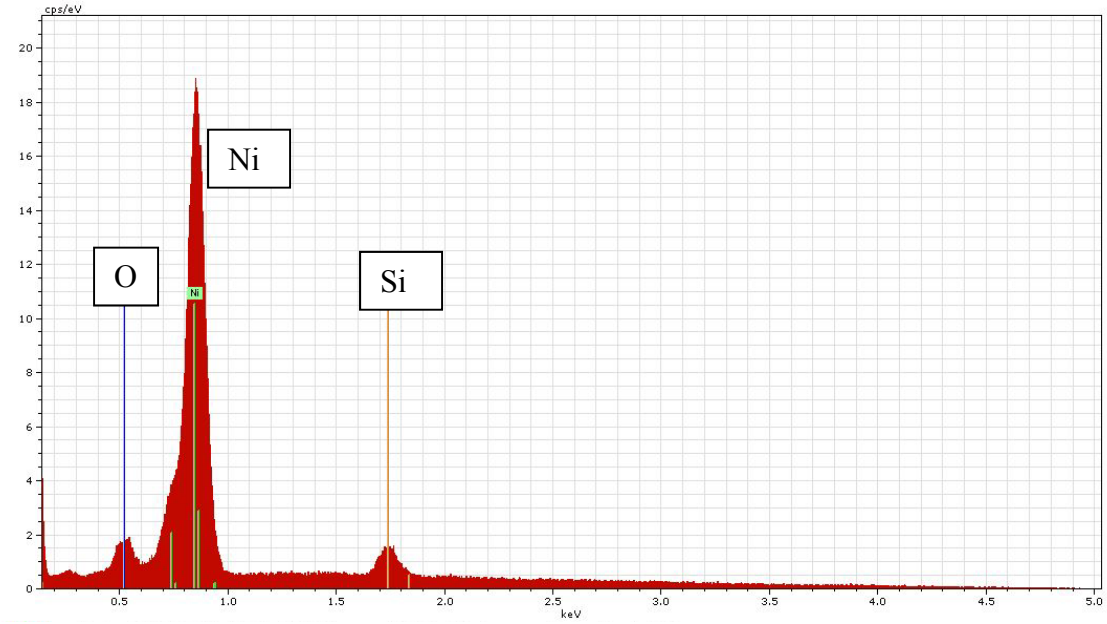


(d)

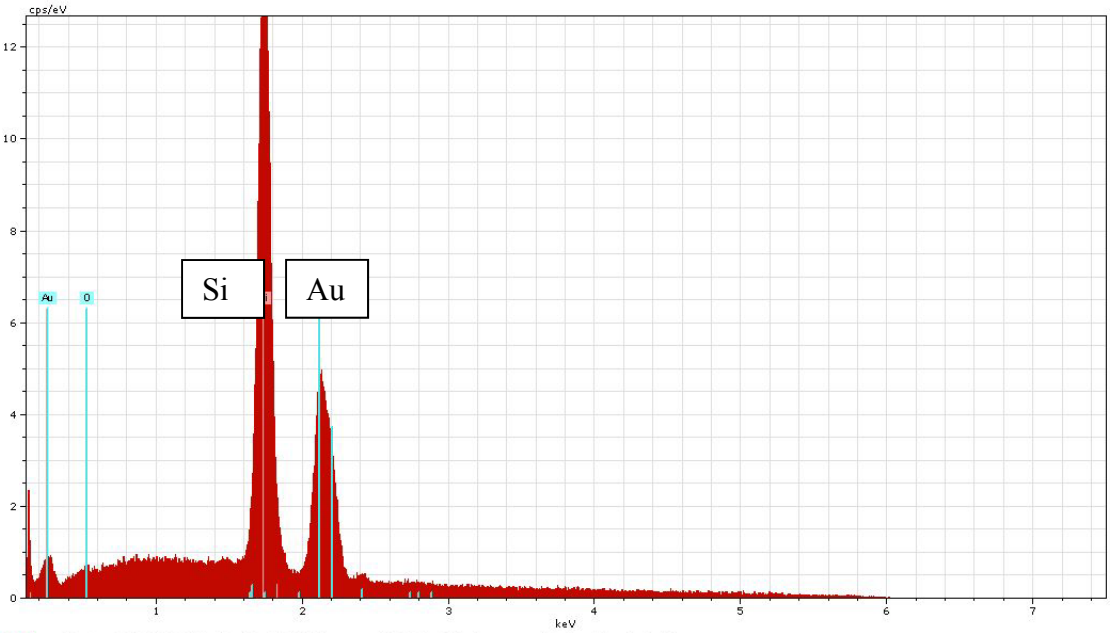


(e)

Figure 4.15: SEM images of wild-type TMV particles with triton on plain silicon wafers (a) after virus assembly, (b) after nickel plating, and (c) after gold plating; and EDS after (d) nickel and (e) gold plating

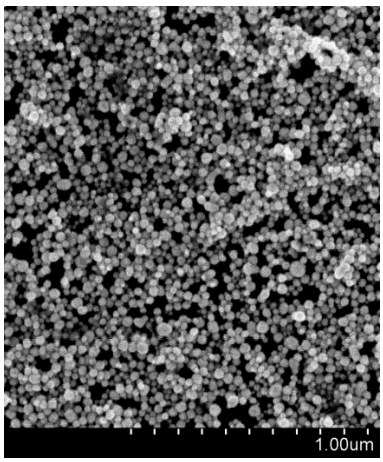


Figure 4.16: High resolution image of TMV1cys on a silicon wafer after gold plating

As seen in Figure 4.17, virus rods are very densely assembled on the silicon wafer surface. The rods also show localized alignment with the particles aligned in the same direction. After the nickel plating, the rods were packed with multiple layers, and yielded diameters of approximately 130 nm, similar to those seen in the TMV1cys with triton samples. The diameter after gold plating could not be assessed due to the entire surface being covered with gold nanoparticles, no longer showing individual rods. Since the virus particles are packed very close together after the assembly and nickel plating, it causes the gold to coat the top of the virus layers without attaching to individual rods. The virus attachment and plating are not uniform across the entire chip as shown in the comparison between silicon and gold in Figure 4.18.

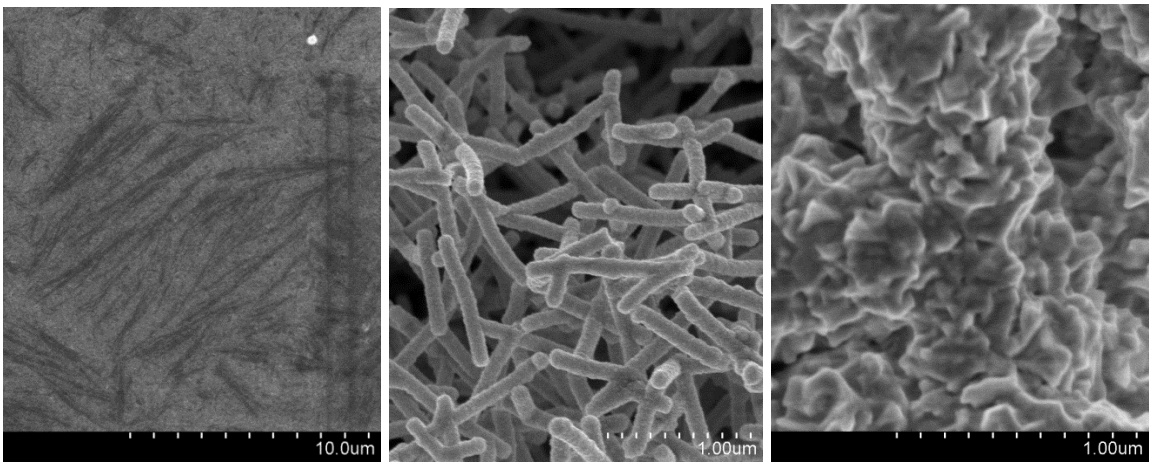


(a) (b) (c)

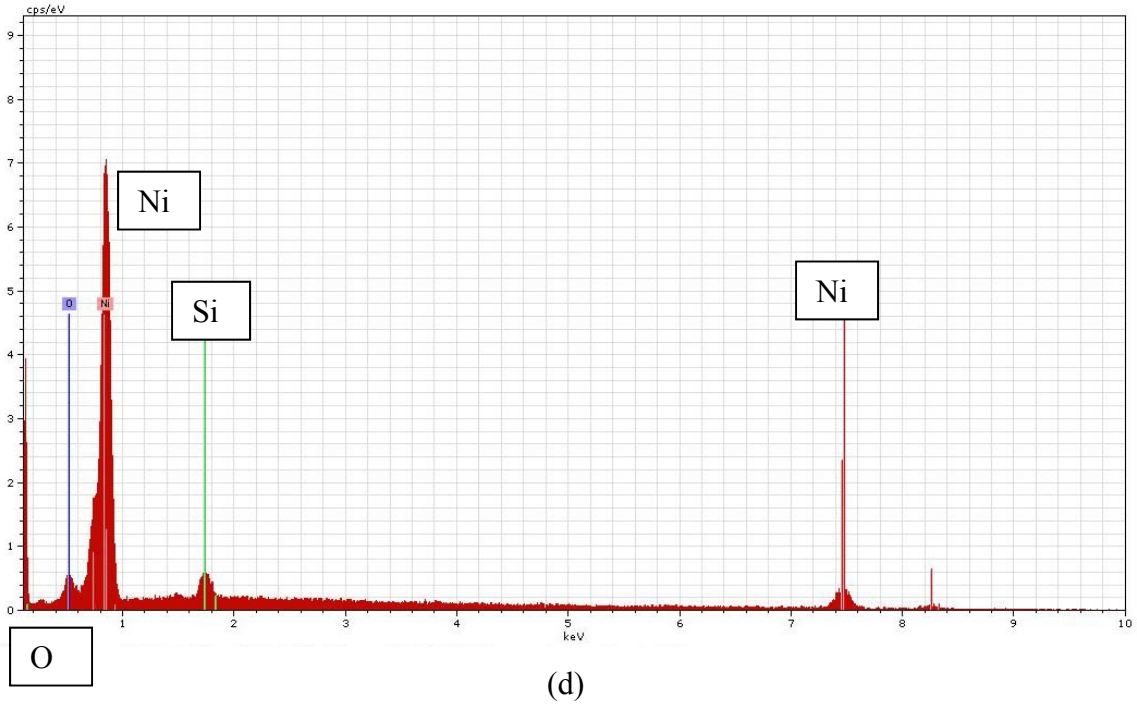


(d)

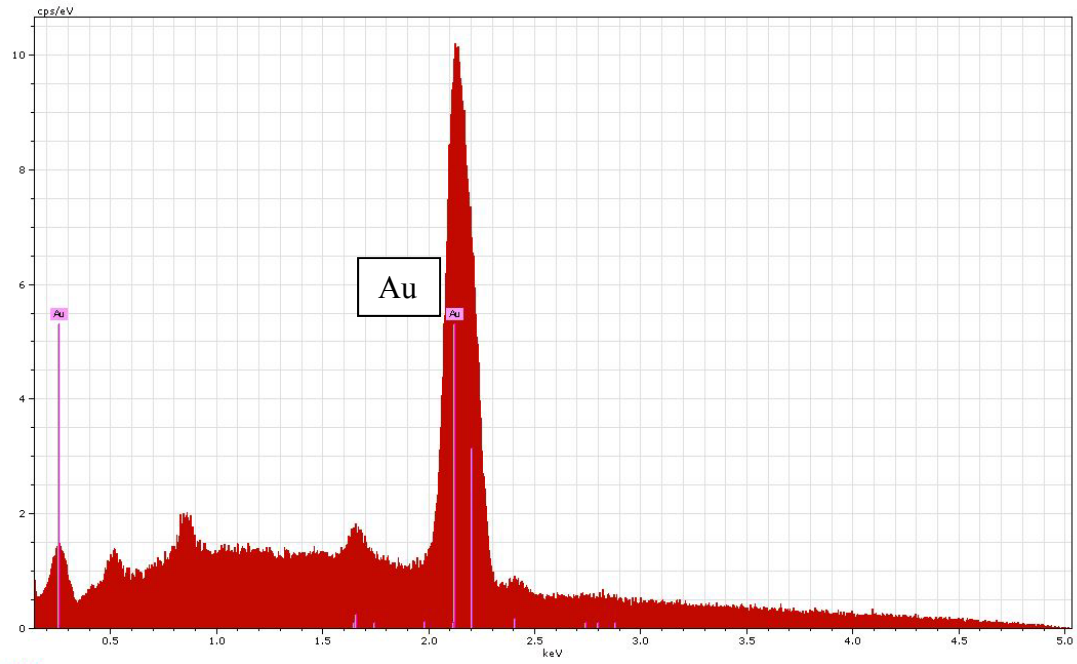


(e)

Figure 4.17: SEM images of TMV1cys on plain silicon wafers (a) after virus assembly, (b) after nickel plating, and (c) after gold plating; and EDS after (d) nickel plating and (e) gold plating

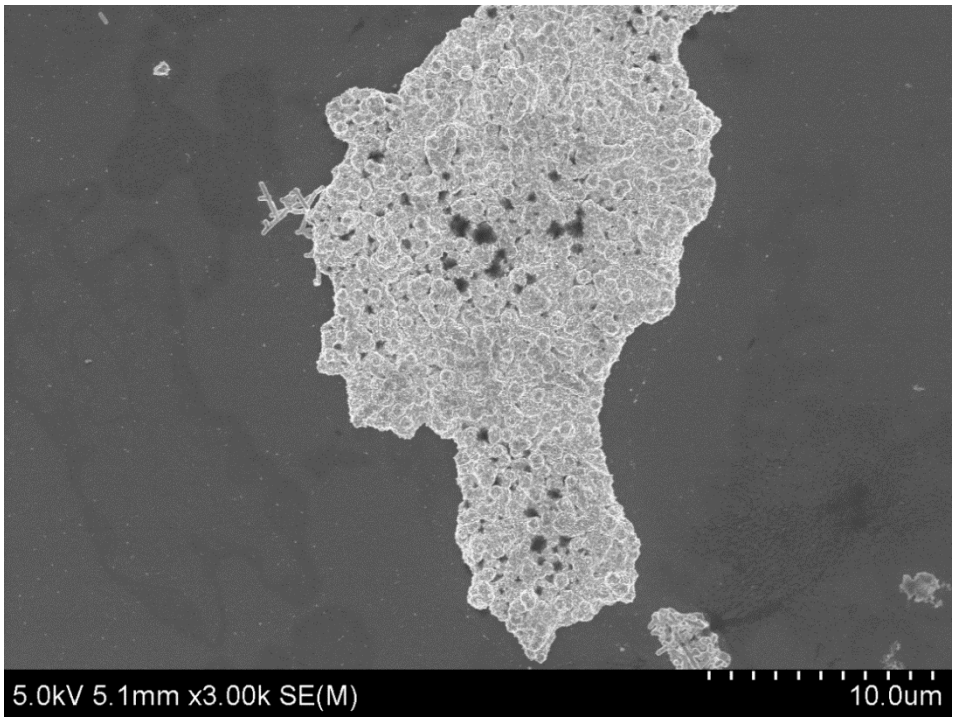


(a)

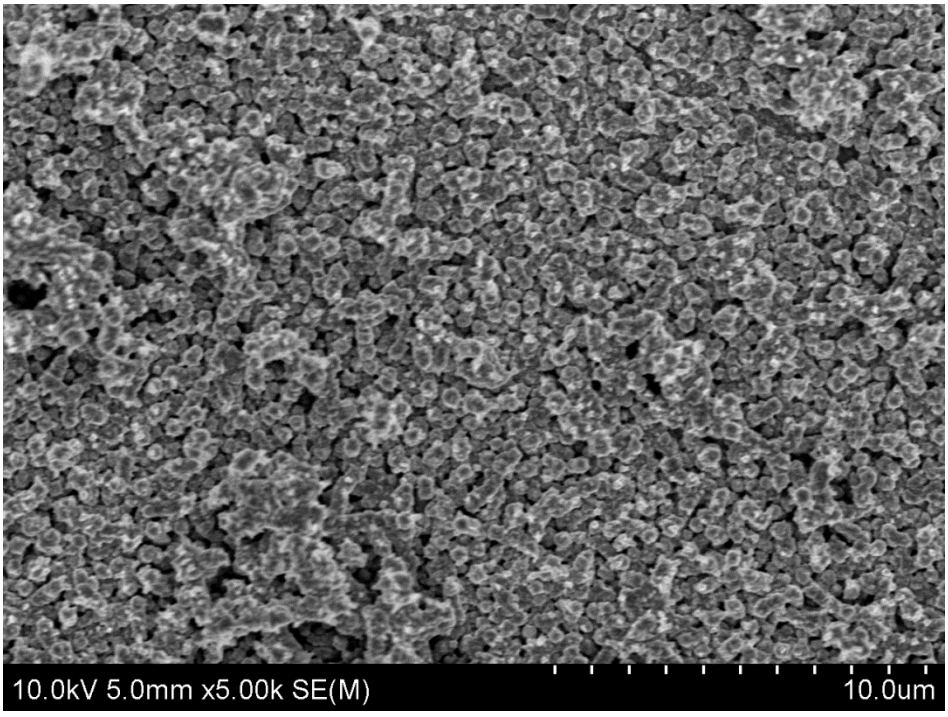


(b)

Figure 4.18: Low resolution images comparing gold plating uniformity of TMV1cys on a (a) silicon wafer and (b) gold chip

The experiments using TMV1cys with triton on plain silicon wafers (Figure 4.19) showed a virus assembly that was less dense than the solution without triton prior to metal plating. Some nickel plating occurred as seen in the SEM image and EDS results, but the virus rods (~130 nm after nickel plating and ~250 nm after gold plating) are laying down on the silicon wafer surface. The EDS composition showed less nickel in these samples than the previous ones without triton added. As in the samples on the gold coated silicon wafer, the triton seemed to interfere with the assembly of the virus particles onto the silicon wafer surface, but still allowed metal plating due to the cysteine modified viruses. However, the attachment of the viruses and metal plating is not uniform across the surface of the wafer (Figure 4.20).

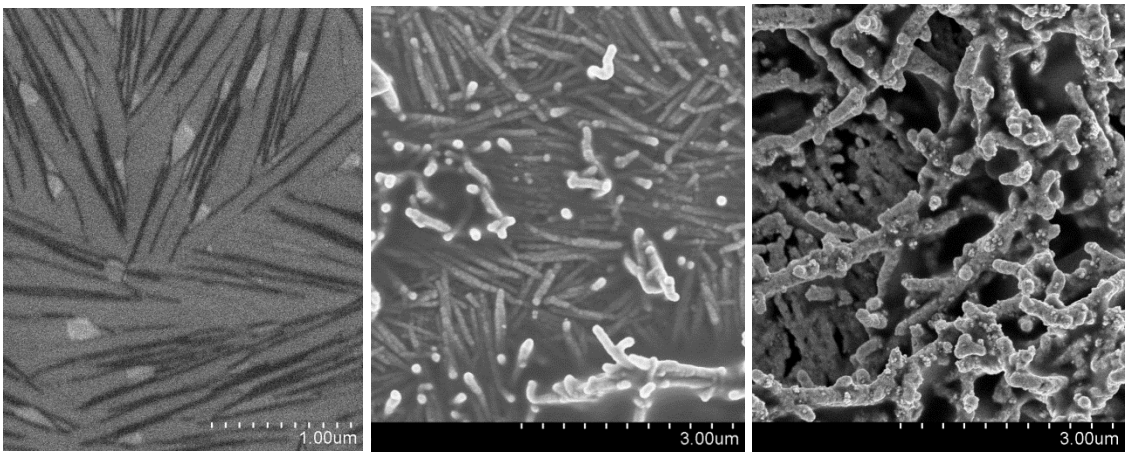


(a) (b) (c)

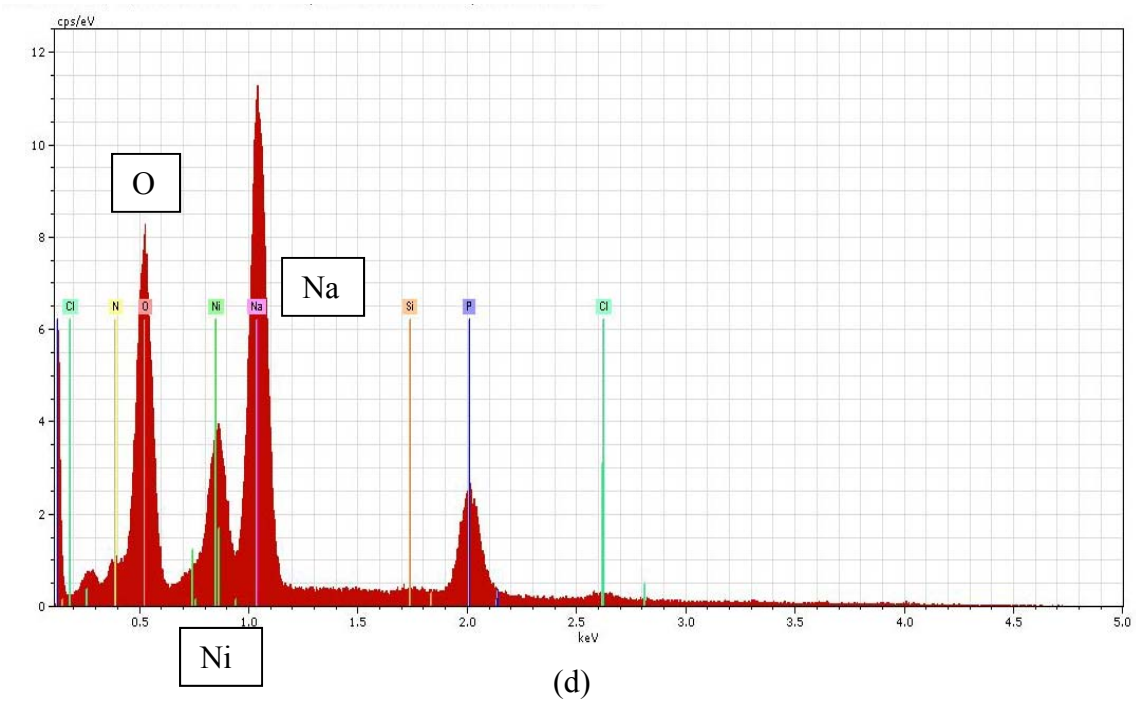


(d)

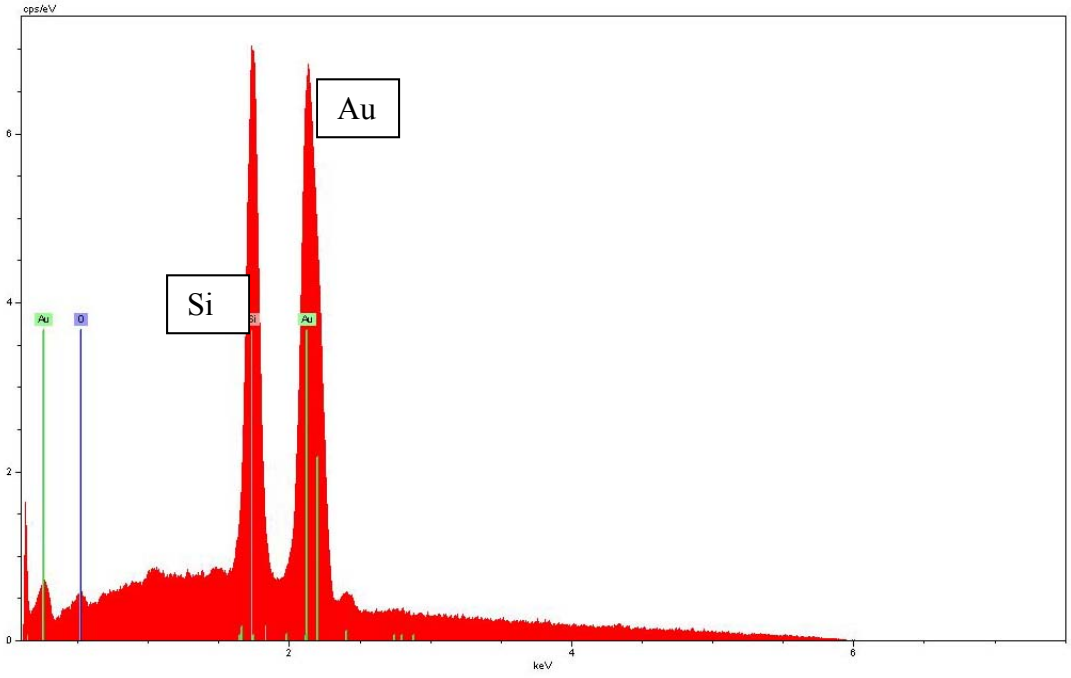


(e)

Figure 4.19: SEM images of TMV1cys with triton on plain silicon wafers (a) after virus assembly, (b) after nickel plating, and (c) after gold plating; and EDS after (d) nickel and (e) gold plating

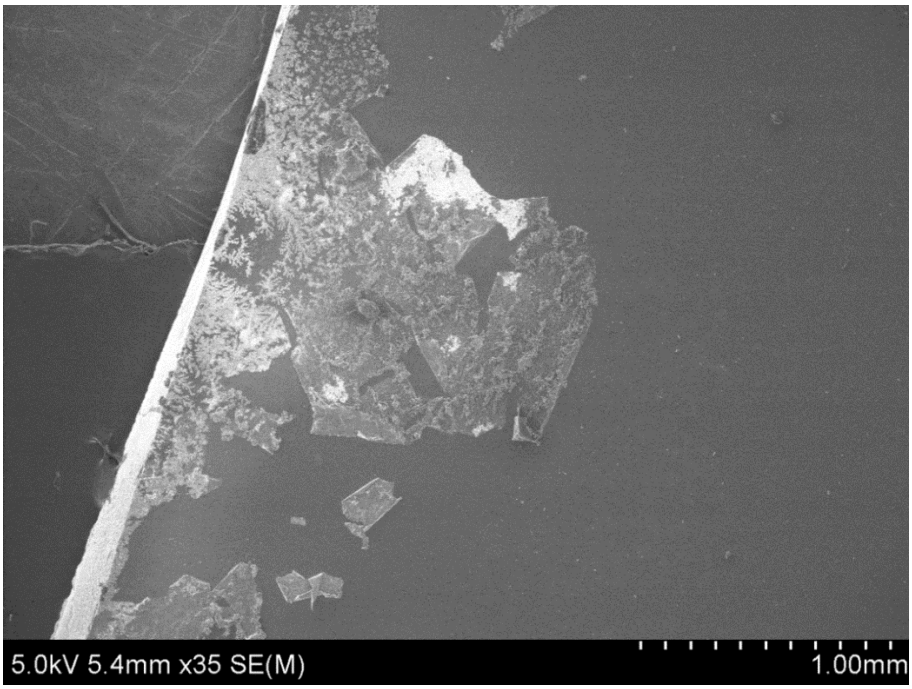


Figure 4.20: Low resolution image of TMV1cys with triton on a silicon wafer

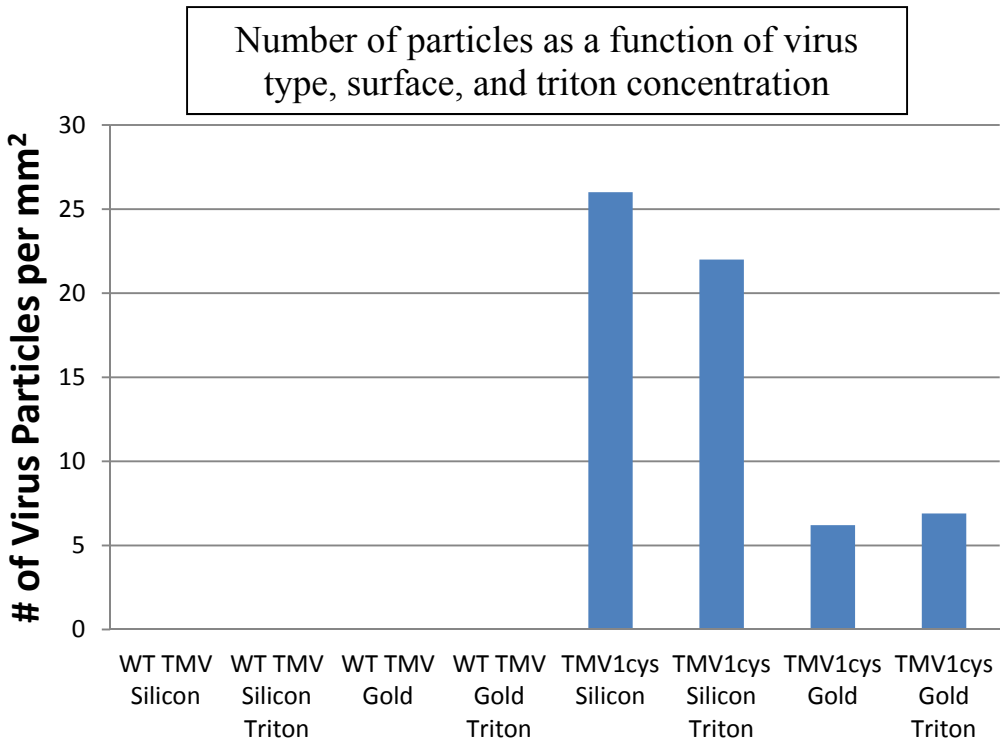


Figure 4.21: Number of particles as a function of virus type, surface, and triton concentration

The results from the control experiments show that while virus attachment is seen in some cases with wildtype TMV, there is no uniform metal plating that occurs, verifying that the cysteine virus is an important factor in the plating procedure. The nanoparticles that appeared in the wildtype images are most likely due to residual Pd from the initial virus solution. Although the highest number of virus particles were seen using TMV1cys on silicon wafers, there is no specificity of the cysteine residue to the surface, and the viruses lay in multiple layers on top of each other.

# Chapter 5: Virus Templated Substrates for Surface-Enhanced Raman Spectroscopy

## 5.1 Introduction

The development of a rapid and reliable detection method of biomolecules such as pharmaceuticals, amino acids, and proteins has been the focus of many researchers in recent years. Surface-enhanced Raman spectroscopy (SERS) has been investigated as a technique for these applications due to its relatively simple laboratory equipment, sample preparation and field-portable devices [76-79]. Surfaces coated with silver, gold, and copper have shown increased intensity in the signals due to the electromagnetic interaction around the target molecules. Studies have also shown that the use of patterned nanostructures (creating surface roughness) produce a stronger signal [6]. This research utilizes a virus template in order to create nanostructures at varying densities for use as a metal nanostructured surface, in order to increase the intensity in SERS detection methods.

There are several advantages to Raman Spectroscopy over current detection methods. It has a "fingerprinting" ability to produce distinct spectra from molecules similar in structure and function, which allows the same substrate to be used for the detection of multiple analytes. Also, it eliminates the use of expensive reagents or time-consuming sample preparation associated with current techniques such as polymerase chain reaction (PCR) or immunoassays. Finally, some Raman Spectroscopy devices are now portable and can be easily taken in the field.

The Raman effect was discovered in 1928 by Chandrasekhara Venkata Raman and Kariamanickam Srinivasa Krishnan while performing studies in light scattering [80]. Raman scattering is a process in which incident photons gain or lose energy due to the vibrational and rotational motion of the analyte molecule. The resulting spectrum is made up of bands (peaks) specific to the molecular structure of a certain analyte. When light is scattered from a molecule or atom, most photons are elastically scattered, because they have the same energy and wavelength as the incident photons (Rayleigh scattering). Approximately 1 out of $10^6 - 10^8$ photons are scattered at frequencies different from the incident photons (inelastic scattering), which is a process known as the Raman effect. The incident photons either lose (Stokes) or gain (anti-Stokes) energy on the vibrational-rotational or electronic level. When a photon (light) is scattered from a molecule in a ground vibrational state ($v = 0$), there is a momentary change in the energy state of the molecule corresponding to the virtual state designated as $j$. Molecules in the ground state can absorb a photon corresponding to an energy of $h\nu_{ex}$ and emit a photon with a change in energy represented by $h(\nu_{ex} - \nu_v)$, and is referred to as Stokes shift ($\nu_s$). Molecules that are already in an excited vibrational state ($v = 1$), will scatter and return to their ground state, producing a photon with energy corresponding to $h(\nu_{ex} + \nu_v)$. This effect is known as anti-Stokes shift [76, 81, 82].

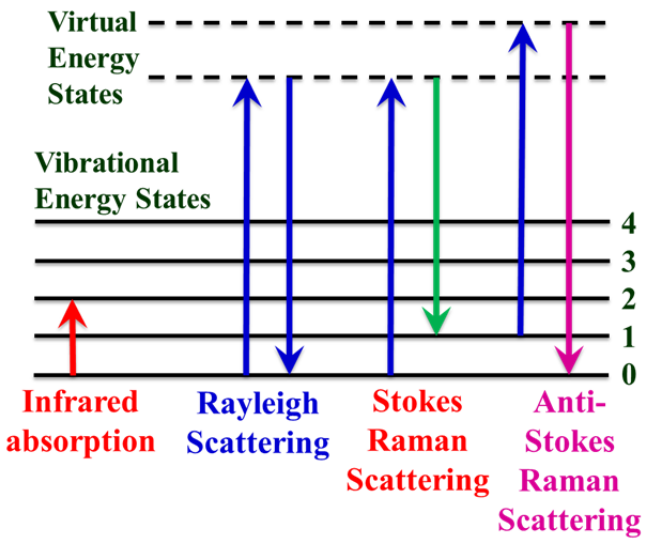


Figure 5.1: Schematic of energy states in Raleigh and Raman scattering

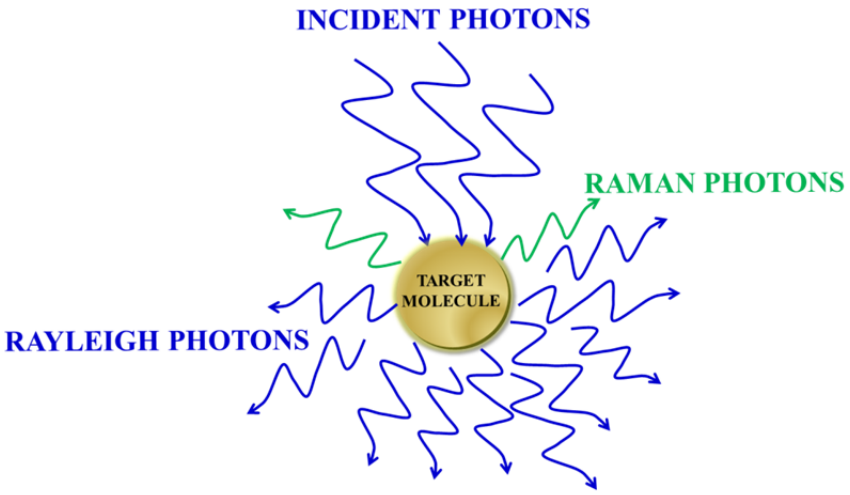


Figure 5.2: Schematic of photon scattering in Raman Spectroscopy

Raman spectrometers consist of a laser source, sample holder, and signal collection device. Some laser sources used are He-Ne, $Ar^{+}$, or $Kr^{+}$, each corresponding to different wavelengths. Some samples will absorb the incident or Raman scattered photons, while others will fluoresce. Also, photodecomposition of the sample can occur at lower

wavelengths. The incident wavelength is chosen in order to maximize the signal while minimizing photodecomposition, fluorescence, and absorbance.

A Raman signal can be obtained using gas, liquid, and solid samples. Aqueous samples are often used for both inorganic and biological samples since water has a weak Raman signal.

In the past, Raman spectrometers have used photomultiplier tubes as detectors. In order to improve the signal to noise ratios and reduce background noise, those systems have been replaced by photon counting systems [82]. More recently, linear diode arrays and CCD detectors have been used to produce Raman spectra.

History of Surface Enhanced Raman Spectroscopy

Fleischmann et. al first reported strong Raman signals (enhancement factors of $10^5$) from an interface of pyridine, sodium carbonate, formic acid, and potassium formate adsorbed to redox-cycled silver electrodes as well as pyridine adsorbed to copper electrodes in 1974 and 1975. The formation and reduction of silver chloride resulted in substantial etching of the silver surface, resulting in an estimated tenfold increase in surface area. They suggested that the high intensity of the signal was due to a large number of adsorption sites on the roughened surface [83]. However, Jeanmaire and Van Duyne examined factors such as surface features and potential of the electrode, solution analyte concentration, and electrolyte composition of the solution, which affect the intensity of the Raman bands of adsorbed molecules [84]. Albrecht and Creighton continued Fleishmann's studies in 1977, looking at the spectra acquired for pyridine adsorbed to a silver electrode before and after a single oxidation-reduction cycle. After a

cycle of a single voltage sweep, the spectral bands were almost five times greater compared to that of the sample before the sweep. Raman spectrum performed after removal of the electrode was missing the 1025 $cm^{-1}$ band, confirming that the increased signal was due to pyridine adsorbed at the electrode surface [85]. The conclusion from these experiments was that Fleishmann's initial explanations of increased surface area were incorrect. It was determined that localized plasmons that were resonant at the incoming wavelength were responsible for the enhanced signal.

SERS is a result of both an electromagnetic and a chemical effect. The electromagnetic enhancement arises from the excitation of the localized surface plasmon. An external electric field provides an excitation causing the conduction electrons to oscillate collectively, leading to a surface plasmon resonance [86].

The chemical mechanism contributes to the signal by allowing the electrons from the molecule to interact with those of the metal surface. Chemical enhancement requires the adsorbate to be chemisorbed directly to the surface. SERS measurements are possible on several metals (i.e. platinum, iron, cobalt, and nickel), but the achievable enhancement factors are significantly larger for molecules adsorbed on gold, silver and copper surfaces due to the electromagnetic enhancement mechanism from the interaction of the incident laser with the surface plasmon in these metals [86]. Simply stated, mobile electrons are required for enhancement, and since the other metals oxidize quickly, the electrons are not mobile.

SERS has attracted attention due to its high sensitivity and speed of detection. Since its discovery, it has been applied to a wide variety of biomedical and environmental analytical applications to molecules, pathogens, and cells [87-89].

Surface-Enhanced Raman Spectroscopy Substrates

Although the strongest SERS enhancements have been seen with silver, gold and copper substrates, the effect is expected to be seen with any metals with outer shells of $(n-1)d^{10}ns^1$ [84, 90-93]. In addition to the material, the substrate structure has been shown to play a role in the enhancement factor in SERS. It has been shown that the electromagnetic field is greater in regions with high curvature, resulting in a higher SERS signal [94]. Murphy et al. created silver and gold nanorods of various aspect ratios using a controlled growth environment of metal salts with a weak reducing agent [95].

During the 1980s, SERS was developed by depositing SERS-active metals onto non-SERS-active substrates, including coating SERS-active Ag or Au electrodes with ultrathin films of other metals such as Ni, Co and Fe. The weak SERS spectra of adsorbates on the transition metal overlayer could be obtained with the long-range effects of the electromagnetic (EM) enhancement of the SERS-active substrate underneath. The EM field decreases drastically though from the coated film, so studies showed that the layer applied must be ultrathin, around 3-10 atomic layers [96-102]. Because it was difficult to completely coat the roughened substrates with a thin layer of film, Weaver et al. developed methods to create a "pinhole-free" transition metal coating over the SERS-active Au surface using electrochemical atomic-layer epitaxy. This utilized constant-current deposition at a low current density or by redox replacement of underpotential-deposited metals on Au [103-107].

SERS detection does not require the adsorbate to be in direct contact with the metal surface; however, the enhancement decreases as the distance between the two increases [108-111]. Dieringer et al. investigated the distance dependence of SERS

signals using atomic layer deposition to fabricate alumina dielectric spacers. Their results showed that the signal decreases logarithmically between zero and 5 nm alumina thickness [109].

Silver and gold nanoparticles are the most frequently used substrates for SERS detection because of the ease in preparation and well characterized SERS properties [109, 112-118]. Kneipp et al. and Nie et al. reported enhancement factors of up to $10^{15}$ in the 1990s in clusters of silver nanoparticles, enabling single molecule spectroscopy [112, 118]. Metal nanoparticles are created by reduction of a metal salt (i.e. silver nitrate or chloroauric acid) by agents such as sodium citrate and EDTA. The size of the nanoparticles may be controlled based on the amount of reducing agent compared to the metal [119-121]. Intersection points between nanoparticles where electromagnetic fields may overlap generate large field enhancements and have allowed for single molecule detection. Much of the SERS detection has been performed in solution; however, Doering and Nie immobilized silver colloids on a glass surface inside a microfluidic device and obtained enhancement factors of $10^2 – 10^3$ for rhodamine 6G molecules adsorbed on the surface.

Another method that has been used for SERS detection was to assemble gold nanoparticles into structured porous films templated by colloidal crystals. The Kuncicky group found an enhancement factor of $10^3$ for the structured films versus the non-structured in the detection of cyanide [122]. Lu et al. utilized varying experimental conditions in order to control the structures of macroporous Au and Ag nanostructured films. They showed that these porous nanostructured films with large interconnected aggregates are desirable SERS substrates in terms of increased signal, stability and reproducibility [123].

SERS substrates have also been developed using lithography techniques. Jensen et al. studied the localized surface plasmon resonance (LSPR) of silver nanoparticle arrays

created by nanosphere lithography. By encapsulating the nanoparticles in $SiO_x$ and controlling nanoparticle size, height, and shape, they were able to systematically tune the LSPR from ~400-6000 nm [124]. The Im research group found that when controlling the size, position, shape and orientation of nanogap arrays using atomic layer deposition, there is an increasing SERS signal enhancement of up to $10^9$ as the gap size decreases to 5 nm [125]. Deng et al. fabricated gold nanograting on silicon wafers consisting of 120 nm gold cladding on top of parallel silica nanowires with gaps <10 nm at the narrowest point. The SERS signal produced was uniform and reproducible.

Other groups have also used SERS for targeting molecules such as proteins, DNA and RNA [87-89]. Negri et al. developed a SERS-active silver surface with aligned nanorods using oblique-angle vapor deposition (OAD), which successfully detected an anti-influenza aptamer [87]. Another group utilized SERS to characterize yeast cell walls by detection of alkali sensitive proteins. They were able to correlate expression of the proteins generating SERS activity and cell division, demonstrating a convenient and sensitive method for cell wall analysis [88].

Some recent work has included the development of novel substrates such as a paper-based inkjet-printed surface by White et al. [126, 127]. This research group modified the surface chemistry of cellulose paper on which they patterned nanoparticle sensing arrays for the detection of R6G dye and achieved an enhancement factor of 2 x $10^5$. Singamaneni et al. utilized filter paper adsorbed with plasmonic nanostructures (gold nanorods) and obtained SERS detection of 0.5 nM *trans*-1,2-bis(4-pyridyl)ethane [128].

Current issues with SERS substrates are reproducibility, degradation of substrates over time, and particular conditions required to create the nanoparticle colloid hotspots.

Hotspots also require testing to occur in those areas where the nanoparticle aggregates occur. With the metal coated virus surface developed in this research, homogeneous assembly of the virus is shown on the entire chip.

SERS and R6G

Rhodamine 6G (R6G) is a chemical compound and a dye. It is often used in biotechnology applications such as fluorescence, microscopy, flow cytometry, and spectroscopy.

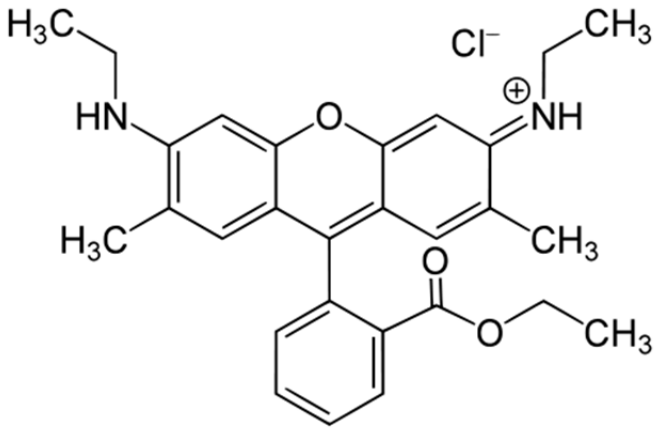


Figure 5.3. Chemical structure of R6G dye

This compound was chosen for these experiments because SERS detection of R6G dye has been previously characterized by many groups using silver for enhancement [118, 129-133]. In 1997, Nie and Emory reported the observation of spectra from single R6G molecules adsorbed on citrate-reduced Ag nanoparticles electrostatically immobilized on glass [118]. R6G yields a net positive charge in water, while metal contains a net negative charge allowing it to interact well electrostatically with the metal nanoparticles.

This dye has a very strong Raman signal and groups study new substrates with it in order to compare their results to previous studies.

SERS and TNT

Detection of explosives has been of interest to homeland security. 2,4,6-Trinitrotoluene (TNT) is one of the most common explosives used for military and terrorist activities. One of the major concerns of TNT is the contamination of soil and groundwater due to its toxicity and mutagenicity. It can also absorb through the skin and is shown to cause anemia and abnormal liver function if exposure occurs for a prolonged period of time. There are also global security concerns for detecting hidden explosive devices in war zones and transportation hubs. Previous technologies for TNT detection, such as fluorescent polymers, microcantilevers, ion mobility spectrometry, and raman spectroscopy, are time consuming, do not produce the sensitivity level desired, and do not allow for on-site detection.

Several groups have investigated the detection of TNT using surface enhanced raman spectroscopy. Dasary et al. utilized a cysteine modified gold nanoparticle based surface for TNT recognition with SERS. The formation of the Meisenheimer complex between TNT and cysteine allowed aggregation of the nanoparticles forming several hot spots which provide significant enhancement of the Raman signal intensity by 9 orders of magnitude [134]. Jiang et al. employed the Meisenheimer complex with 3-D porous anodic alumina (PAA) membranes. The vertical pores in the membranes were filled with cysteine-modified gold nanoparticles to create hot spots for TNT detection [135]. Xu et al. studied the detection of 2,4-dinitroanisole (DNAN) in tap water as a TNT replacement

using L-cysteine modified Ag nanoparticles [136], however, the deposition of the metal particles onto the surface was not consistent. The main problem with creating hotspots for these SERS surfaces is that the laser must be targeting certain areas on the surface. It would be ideal for the signal to be consistent throughout the entire substrate. Holthoff et al. has developed a molecularly imprinted polymer system for TNT detection. TNT imprinted micron thick films of sol-gel-derived xerogels were deposited onto SERS active substrates as the sensing layer [137]. A disadvantage of the imprinted gels is that residual TNT remains in the gels after the wash; therefore, this remaining signal must be subtracted from any spectrum when testing for the presence of TNT.

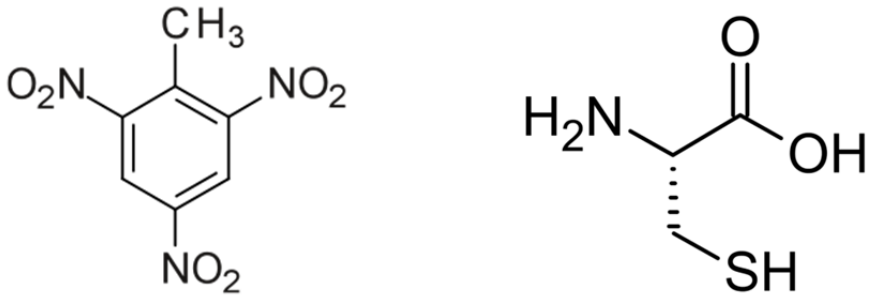


Figure 5.4: Chemical structures of TNT and cysteine

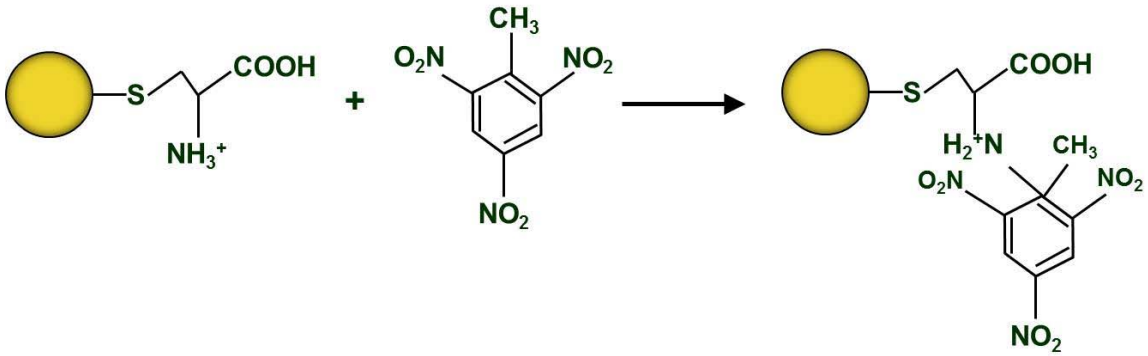


Figure 5.5: Mechanism of Meisenheimer complex between TNT and cysteine. The circles represent gold nanoparticles to which the cysteine binds.

SERS and Melamine

Melamine (1,3,5-triazine-2,4,6-triamine) is a nitrogen-rich molecule commonly used in the manufacturing of plastics, such as whiteboards, kitchenware, and commercial filters. The ingestion of melamine can cause severe renal failure from absorption into the gastrointestinal tract and precipitation in the kidney in the form of crystals.

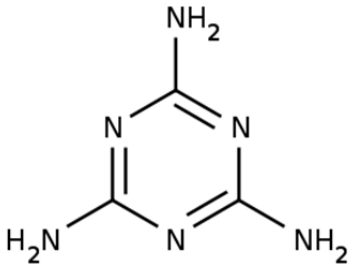


Figure 5.6: Chemical structure of melamine

In 2008, the illnesses and deaths of babies in China were linked to melamine-tainted formula. It was also discovered in eggs during October 2008 and pet food in 2007. It was illegally added to food in order to increase the protein readings of these products. The acceptable concentration for melamine in food products set by the Food and Drug Administration (FDA) is 1 ppm [138].

A number of groups have studied melamine detection using SERS in the past few years [139-142]. Lin et al. utilized Klarite SERS active substrates to detect melamine in gluten, chicken feed, and processed foods. The level of detection obtained with these samples was 33 ppb (0.033 μg/mL) [139]. The Ren and Dong research groups both applied melamine screening to portable devices, which is ideal for rapid detection in the field [140, 141]. Ren tested the level of detection of melamine in sucrose, urea, and arginine and found the limit at 0.5 ppm [141]. Lou et al. developed a substrate with 4-

mercaptopyridine (MPY)-modified gold nanoparticles for this application. The SERS measurement of melamine on this substrate relied on the "hotspot" effect in which gold nanoparticles aggregated upon addition of melamine to the solution. Detection limits as low as 0.1 ppb were observed in these experiments [142].

### 5.2 Project Objectives

The goal of this project was to investigate the effect that metal coated virus patterning had on the signal enhancement in SERS. This was achieved by completing the following tasks:

- Determine which gold coated virus density from Chapter 4 (various virus:triton ratios) yields the highest signal with R6G dye.
- Use sample with highest signal for targets such as melamine for biosensing applications.

The substrates in these experiments are a more robust alternative to current techniques.

### 5.3 Research Design and Methods – R6G

Substrates from Section 4.4 (gold coated virus particles on silicon wafers) with varying triton concentration were evaluated for SERS signals using Rhodamine 6G (R6G) dye. A 785 nm laser diode and a portable Ocean Optics spectrometer (QE65000) were used to obtain Raman signals from the substrate (Figure 5.6).

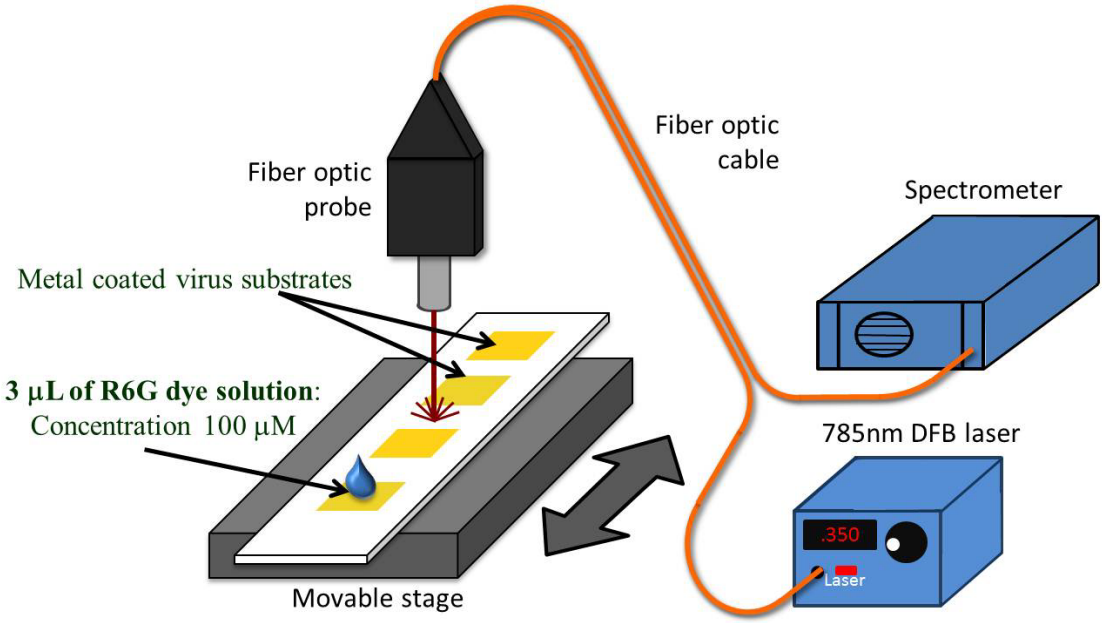


Figure 5.7: Schematic diagram of SERS setup

3 µL of 100 µM R6G dye was drop cast onto the 0.5 $cm^2$ wafers with the gold plated viruses. Data was collected at 1 second intervals at setting level 0.4, which corresponds to a power of 17.5 mW. A total of ten scans were taken for each sample and averaged to minimize background noise. Readings were done immediately after applying the dye as well as after drying for 15 minutes to determine if the signal was higher.

### 5.4 Results – R6G

Figure 5.8 shows the SERS spectra for the different triton concentrations. The sample that showed the highest signal was 0.05%. The spectral peaks at wave numbers of approximately 600, 760, 1200, 1310, and 1510 $cm^{-1}$ are the well-known Raman peaks for R6G. The wave number is the inverse of frequency values read by the CCD camera in the spectrometer. The intensity is the number of photons counted at each frequency

(wave number). The control sample, which is a gold-coated silicon wafer without virus assembly and metal plating, showed no discernible SERS signal at the 100 μM concentration.

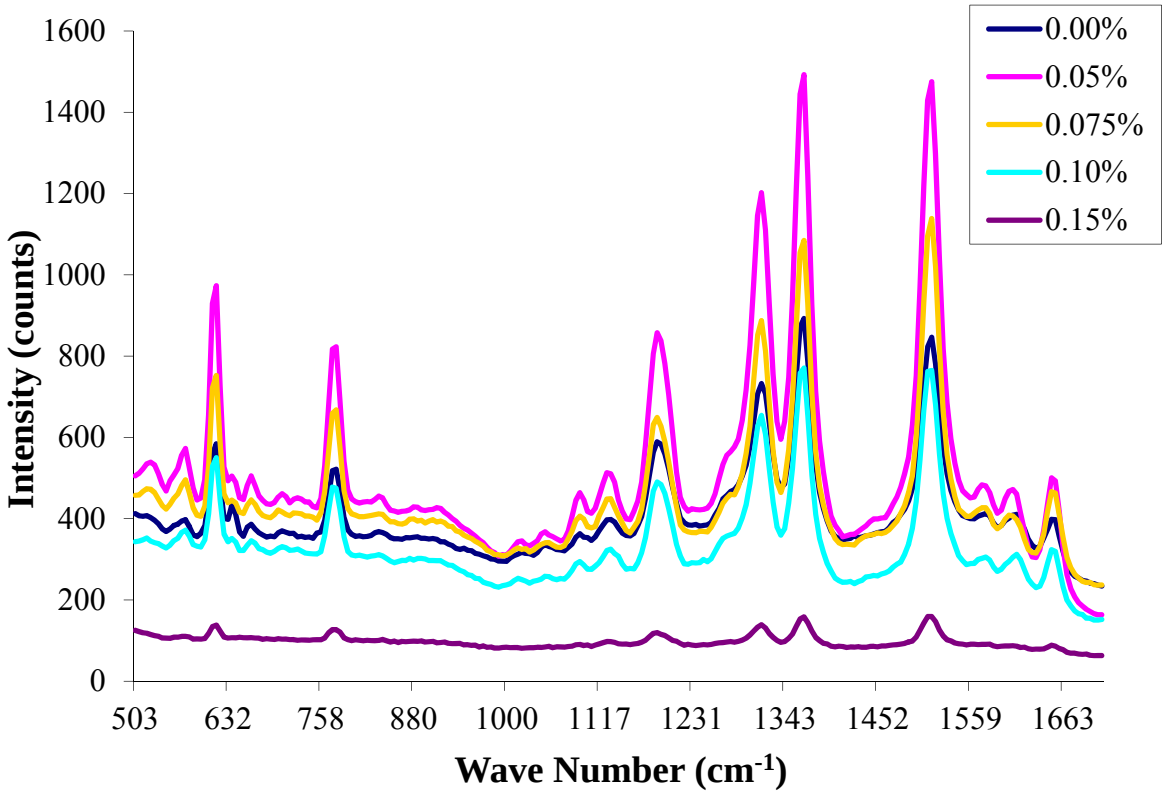


Figure 5.8: SERS spectra of R6G dye on gold plated virus surfaces

The averages of the spectra for wet and dry samples were graphed in Figure 5.9. These results showed that there was a distinct difference in the SERS signals after the evaporation of the water in the R6G sample. This is most likely due to the concentration of the dye particles onto the gold surface and the proximity of the particles to the surface.

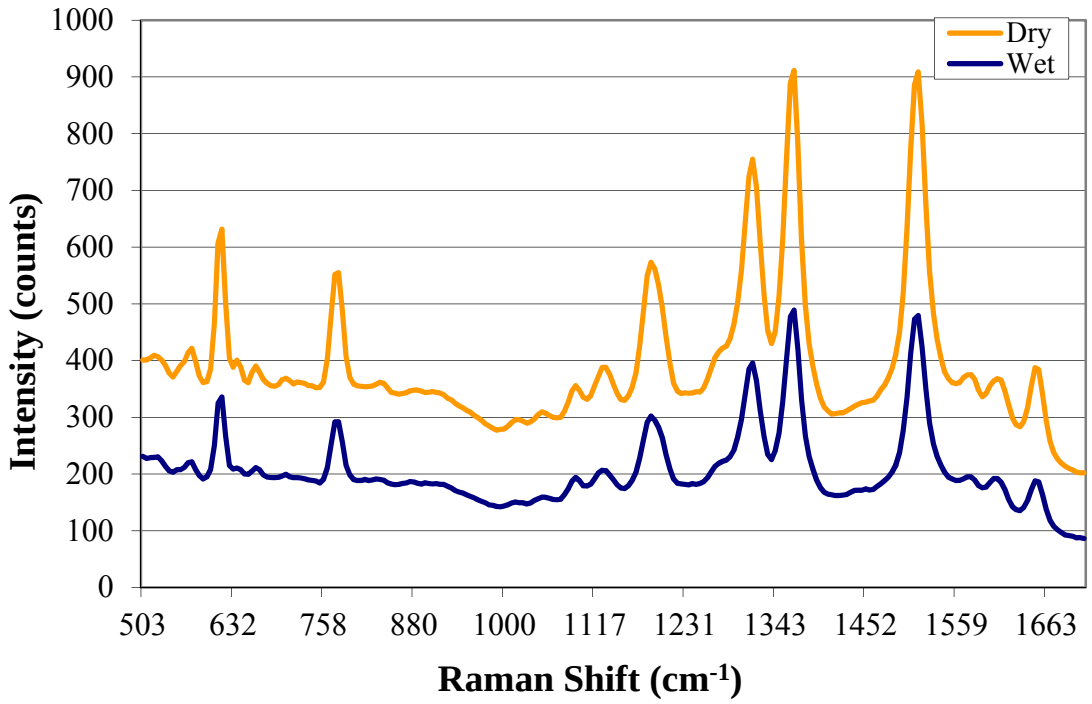


Figure 5.9: SERS spectra averages of R6G dye on gold plated virus surfaces before and after drying

Since the gold chip with no virus showed no SERS signal, it was used for the enhancement factor tests. The raman spectroscopy signal was read using a high concentration of R6G. The enhancement factor for the SERS samples was calculated using the following equation:

$$Enhancement\ factor = \frac{non\ SERS\ molarity}{SERS\ molarity} \times \frac{SERS\ signal\ height}{non\ SERS\ signal\ height}$$

Where the non-SERS molarity was the R6G concentration used on the plain gold chip (10 mM), and the SERS molarity was 100 µM. The SERS signal height was the highest value for the intensity readings obtained with the 0.05% triton concentration samples and the non-SERS signal height was 13. The enhancement factor calculated for these

experiments was $10^4$ with similar values seen across different areas of the chip. This is at the lower level of EF from other research groups who have reported values of $10^4 - 10^8$, but could be increased with future studies optimizing the testing conditions as described in the discussion in Section 5.7. The enhancement factors for each peak at that triton concentration as well as the 1510 $cm^{-1}$ peak for all concentrations were calculated and shown in Table 1. The results show that the enhancement factors are similar across different peaks in the spectrum, which is expected for R6G dye. The enhancement factors for the different triton concentrations range from 10-$10^4$. The lowest corresponds to the sample with the least number of viruses present on the surface,

Table 1. Enhancement factors for R6G on metal plated virus substrate

| | **Wavenumber** | | | | |
|---|---|---|---|---|---|
| **Triton Concentration** | 1510 | 1310 | 1200 | 760 | 600 |
| 0% | $10^2$ | | | | |
| 0.05% | $10^4$ | $10^4$ | $10^4$ | $10^4$ | $10^4$ |
| 0.075% | $10^4$ | | | | |
| 0.10% | $10^2$ | | | | |
| 0.15% | 10 | | | | |

Experiments were also performed to demonstrate homogeneity of the metal coated virus surface. Low resolution SEM images were taken at three separate points around the surface of the 0.5 $cm^2$ chip (at least 2 mm apart from each other) and are shown in Figure 5.10. Although some agglomeration of the virus particles is shown in the image, the overall density remains consistent throughout the chip. SERS results show that the signal also remains consistent throughout the different areas of the chip. The

average number of virus particles for each image is 6.2, 6.2, and 6.9 per $\mu m^2$. The SERS signals also showed similar intensities at different points on the sample (Figure 5.11).

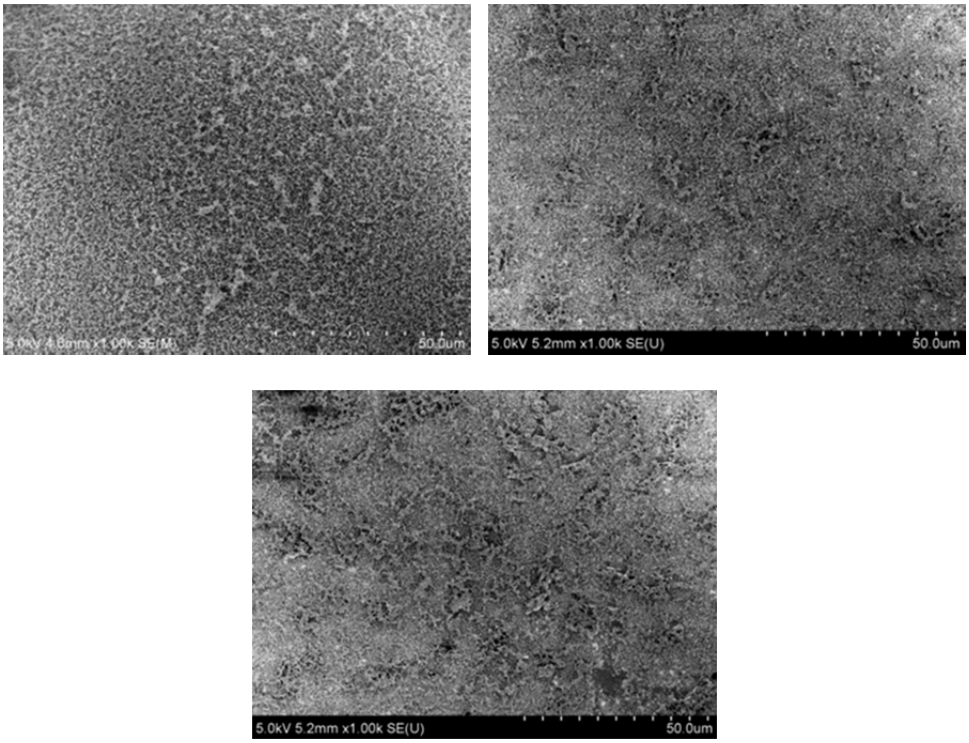


Figure 5.10: Low resolution SEM images of metal plated virus substrate used for SERS at different points on the 0.5 $cm^2$ surface showing homogeneity of the virus assembly

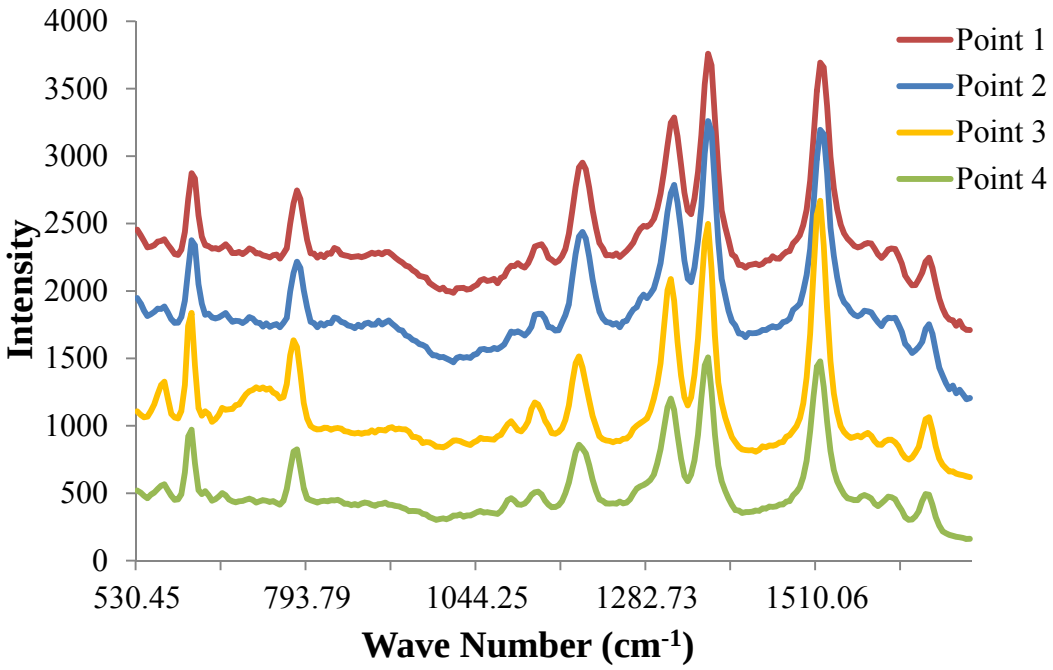


Figure 5.11: SERS signal at different points around the metal plated virus surface

### 5.5 Research and Design Methods – Melamine

The gold plated virus surface with the highest SERS signal, 0.05% triton concentration, was also used in experiments with Melamine as the analyte. For these experiments, melamine was tested at concentrations of 50 µM, 500 µM, and 5 mM. 1.5 µL of each solution was placed on the chips and allowed to dry prior to SERS testing.

### 5.6 Results – Melamine

Figure 5.12 shows the SERS spectra obtained from samples of melamine. Distinct peaks can be seen at approximately wave number 700 $cm^{-1}$ at all three concentrations. The enhancement factor calculated for melamine on the SERS substrates was $10^3$, showing a SERS peak at concentrations as low as 50 mM. This EF is not as high as other studies

using melamine as an analyte; however, it can be increased if the laser wavelength is matched with the surface resonance frequency.

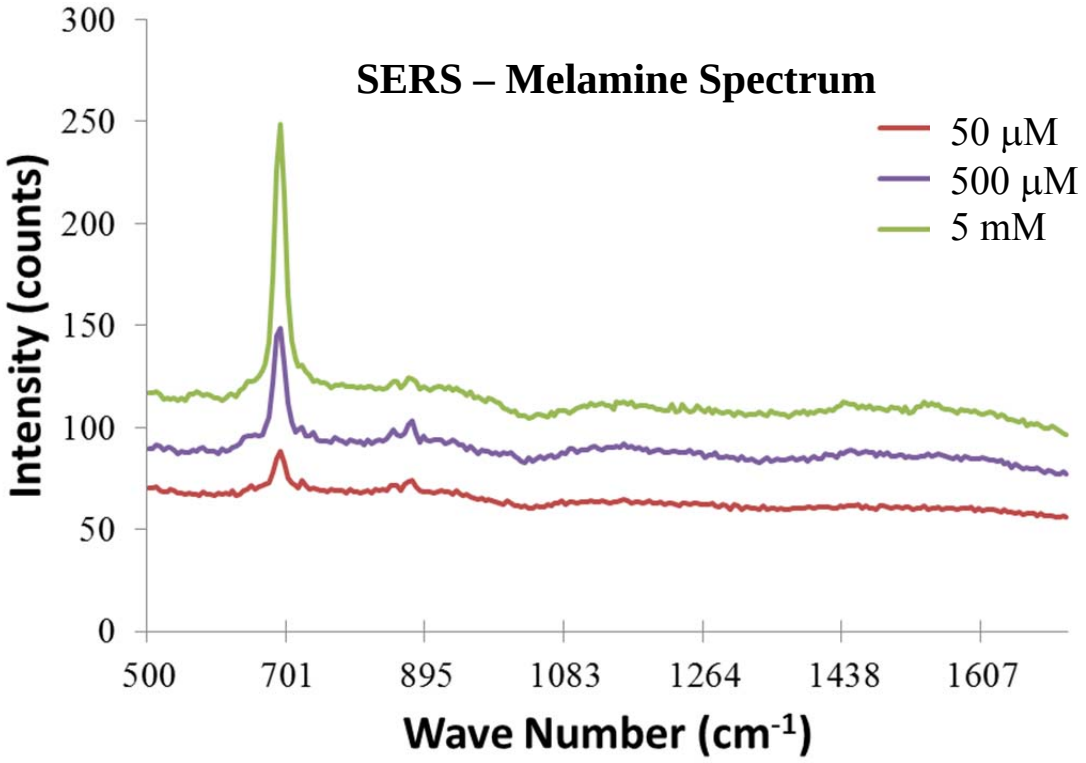


Figure 5.12: SERS spectra for Melamine on gold plated virus surfaces

### 5.7 Discussion

The gold plated virus surfaces exhibited qualities of a SERS active substrate. To our knowledge, these studies are the first time gold coated virus particles have been used for SERS detection of chemical agents. We were successful in experimentally identifying the fabrication protocol (surfactant concentration) that yielded the highest SERS signal. Distinct peaks for R6G dye were seen at 3 picomoles on the 0.5 $cm^2$ chips, with the highest at 0.05% triton concentration. These results are consistent with what is expected

for SERS surfaces due to the increase in photon activity that would occur at the points where the virus rods intersect each other. This surface was also applied to melamine detection as low as 50 μM, which corresponds to molecule number of 1.5 picomoles and 6 ppm. These surfaces are an improvement on previous SERS substrates because of their uniform enhancement factor over large areas of the sample, due to the virus density remaining consistent across the chip, rather than hotspots from colloid aggregation. The level of detection of the metal coated virus substrates is low compared to others in the literature; however the samples developed in these experiments are stable and do not require a clean room for synthesis. Future studies should focus on investigating the wavelength range for optimal excitation of these surfaces and applying the testing to other targets. Since SERS enhancement is based on the resonance between the excitation light and nanoparticle geometry, and the virus aggregates present a complicated geometry, the resonance that best matches the surface should be used for the experiments.

## Conclusions

Through this research, it has been shown that virus particles can act as a template for nanoscale patterning. The first set of experiments was developed to investigate the assembly of a cysteine-modified tobacco virus onto a gold-doped polymer. The microphase separation of the block copolymer and gold doping were evident in TEM images; however, the virus lay across multiple blocks of the polymer and aggregated in head-to-tail and side-by-side arrangements. Patterning could not be achieved using this method since the size of the viruses was much greater than that of the length scale of lamellar. The 2-dimensional molecular imprinting of virus particles onto the surface of a hydrogel film was unsuccessful due to the brittle nature of the polymer gel when formed into a thin film. Future studies could employ a polymer material that remains intact during the thin film polymerization process.

The use of a surfactant during the virus assembly onto gold chips assisted the patterning by creating various virus densities on the substrates. The increasing surfactant levels showed decreasing number of virus particles on the chip surface. It was deduced that this is due to the triton interfering with the assembly of the virus particles onto the chip and with each other. The control experiments, which were performed using wildtype virus on gold chips and silicon wafers, verified the need for the cysteine modified virus and gold surface for virus attachment and metal plating. The TMV1cys showed attachment to the silicon wafer after the metal plating; however, there were multiple layers of virus (seen on the SEM image) which was likely the result of the virus

interaction with other virus particles, and not the interaction with the surface. There seemed to be no specificity of the virus rod ends to the silicon surface.

These surfaces could be used for biosensor, battery, and other nano applications. One of the biosensor applications of these surfaces is SERS, which requires a substrate with a roughened gold, silver, or copper surface in order for the highest signal enhancement to occur. Our studies showed that the metal-coated virus substrates are SERS active, with the ability to detect R6G and melamine at less than 100 μM concentration. The substrate that corresponds to the highest signal possesses the most number of intersection points between metal coated virus particles and the surface, allowing high electromagnetic activity near the sample. The lowest signals were seen in the two extremes of density values (highest and lowest) because the surfaces do not have a roughness ideal for electron activity. The 0% triton level shows the viruses so densely packed that the surface is nearly flat, and the 0.15% triton sample shows few viruses with very low surface roughness. In order to obtain a lower detection level, the optimal wavelength for plasmon resonance can be investigated for the samples with 0.05% triton. This method can be a competitive alternative to current detection techniques due to its durability, speed, and simplicity.

# Appendix

**Pt-coating of TMV1cys Protocol (with viruses attached to gold surface)**

Solutions: 0.1M MOPS

0.05M $K_2PtCl_4$

0.01M DMAB

1. Submerge a (cleaned) gold-plated surface in a solution of .1 mg/mL 1Cys TMV overnight.
2. Remove surface from solution and place immediately, without rinsing, in 300µL MOPS buffer on ice.
3. Add 10µL $K_2PtCl_4$ and mix thoroughly and gently by pipetting. Let sit on ice for 5 minutes.
4. Add 1µL DMAB and mix thoroughly and gently by pipetting. Let sit on ice for 5 minutes.
5. Repeat steps 3 and 4 to a total of 10 times.
6. Add 10µL DMAB and mix thoroughly and gently by pipetting. Let sit on ice for 5 minutes.
7. Add 100µL $K_2PtCl_4$ and mix thoroughly and gently by pipetting. Let sit on ice for 5 minutes.
8. Add 100µL DMAB and mix very gently by pipetting. Let sit on ice for about 10 minutes.
9. Move surface to a new tube containing 300µL MOPS and 100µL $K_2PtCl_4$.
10. Add 50µL DMAB and mix very gently by pipetting. Let sit on ice for about 10 minutes.

11. Remove surface from solution and rinse with H20. Let dry.

Ni Plating Solution (2x):

Mix the following in a glass beaker (final concentrations: 0.1M metal salt and 0.5M DMAB):

- 0.6g $NiCl_2$ (Nickel (II) chloride) hexahydrate 99.9%, Sigma Aldrich
- 0.45g Glycine, tissue culture grade, Fisher Scientific
- 1.5g Sodium tetraborate, 99%, Sigma Aldrich
- 0.77g Dimethylamine borane (DMAB), 97%, Sigma Aldrich (add under fume hood)
- 25mL $H_2O$ (added last)

1) Place solution mixture with a stir bar on a stirplate, covered with parafilm.
2) Periodically check pH and stop mixing with pH paper indicates the solution has reached pH 7 (color will change from green to blue).
3) Remove supernatant, divide into microcentrifuge tubes and freeze at -20°C for storage.

Pd solution:

0.01g $Na_2PdCl_4$

1.5mL Methanol

Plating procedure for surface-attached TMV:

1) Submerge a (cleaned) gold-plated surface in a solution of .1 mg/mL 1Cys TMV overnight at 4°C.
2) Add 7μL Pd solution per 100μL TMV solution and mix well.
3) Let sit for at least 30 minutes.
4) In a fresh tube mix 1 part Ni plating solution with 1 part water.
5) Transfer gold surface without rinsing or drying quickly to the plating solution.
6) The surface should begin darkening after about 4 or 5 minutes. Once the surface is uniformly darkened, allow the plating reaction to continue for another 4-5 minutes.
7) Remove the surface from the plating solution and rinse thoroughly by submersion in water.*
8) Remove and let dry.

*The plating quality can be verified by submersion into ethanol instead of water. If coating is thin and/or noncontinuous, the surface will appear to lighten and mottle as the ethanol destroys the exposed virus and dislodges the metal coating, exposing the gold underneath.

**Au (gold) Plating Protocol** - *Au is deposited onto Ni-coated 1Cys TMV.

Au Plating Bath (pH adjusted to 7.0-7.5):

| | |
|---|---|
| 0.007M | $KAu(CN)_2$ |
| 1.4M | $NH_4Cl$ |
| 0.2M | Sodium citrate |
| 1M | $NaH_2PO_2$ |

Due to a lack of $NH_4Cl$, sodium citrate, and sodium hypophosphite the more specific protocol was followed.

Table 2. Gold plating protocol

| | Molarity added | Volume added | Final Molarity |
|---|---|---|---|
| **$KAu(CN)_2$** | 0.1 M | 70 µL | 0.007 M |
| **$NH_4Cl$:** | | | |
| - $NH_4OH$ | ~ 8.5 M | ~164 µL | ~1.4 M |
| - HCl | ~12 M | ~116 µL | ~1.4 M |
| **Sodium Citrate:** | | | |
| - NaOH | 2 M | 100 µL | 0.2 M |
| - Citric acid | 2 M | 100 µL | 0.2 M |
| **$NaH_2PO_2$:** | | | |
| - $H_3PO_2$ | 10 M | 100 µL | 1 M |
| - NaOH | 10 M | 100 µL | 1 M |
| **Water** | | 250 µL | |
| | | **~1 mL Final Volume** | |

*Volumes of $NH_4OH$ and HCl are approximate as slightly more or less was used to bring the final pH of the solution to 7.0-7.5.

## References


1. Yi, H., et al., *Patterned assembly of genetically modified viral nanotemplates via nucleic acid hybridization.* Nano Lett, 2005. **5**(10): p. 1931-6.
2. Royston, E., et al., *Self-assembly of virus-structured high surface area nanomaterials and their application as battery electrodes.* Langmuir, 2008. **24**(3): p. 906-12.
3. Cresce, A.V., et al., *Nanopatterning of recombinant proteins using block copolymer templates.* Macromolecules, 2006. **39**(17): p. 5826-5829.
4. Wulff, G., *Enzyme-like catalysis by molecularly imprinted polymers.* Chemical Reviews, 2002. **102**(1): p. 1-27.
5. Piletsky, S.A., S. Alcock, and A.P.F. Turner, *Molecular imprinting: at the edge of the third millennium.* Trends in Biotechnology, 2001. **19**(1): p. 9-12.
6. Brown, R.J.C. and M.J.T. Milton, *Nanostructures and nanostructured substrates for surface-enhanced Raman scattering (SERS).* Journal of Raman Spectroscopy, 2008. **39**(10): p. 1313-1326.
7. Yoo, P.J., et al., *Spontaneous assembly of viruses on multilayered polymer surfaces.* Nature Materials, 2006. **5**(3): p. 234-240.
8. Goodman, I., *Developments in Block Copolymers - 1*1982, New York: Elsevier Science Publishing Co., Inc.
9. Hadjichristidis, N., S. Pispas, and G. Floudas, *Block copolymers : synthetic strategies, physical properties, and applications*2003, Hoboken, N.J.: Wiley-Interscience. xx, 419 p.
10. Cresce, A.V., et al., *Block copolymer nanotemplating of tobacco mosaic and tobacco necrosis viruses.* Acta Biomater, 2008.
11. Sohn, B.H. and B.H. Seo, *Fabrication of the multilayered nanostructure of alternating polymers and gold nanoparticles with thin films of self-assembling diblock copolymers.* Chemistry of Materials, 2001. **13**(5): p. 1752-1757.
12. Lee, S.Y., et al. *Improved metal cluster deposition on a genetically engineered tobacco mosaic virus template*. 2005. Iop Publishing Ltd.
13. Herman, D.S., D.J. Kinning, and E.L. Thomas, *A compositional study of the morphology of 18-armed poly(styrene-isoprene) block copolymers.* Macromolecules, 1987. **20**: p. 2940-2942.
14. Kellogg, G.J., et al., *Observed surface energy effects in confined diblock copolymers.* Physical Review Letters, 1996. **76**(14): p. 2503-2506.
15. Li, M.Q. and C.K. Ober, *Block copolymer patterns and templates.* Materials Today, 2006. **9**(9): p. 30-39.
16. Lin, Z.Q., et al., *A rapid route to arrays of nanostructures in thin films.* Advanced Materials, 2002. **14**(19): p. 1373-1376.
17. Rockford, L., S.G.J. Mochrie, and T.P. Russell, *Propagation of nanopatterned substrate templated ordering of block copolymers in thick films.* Macromolecules, 2001. **34**: p. 1487-1492.
18. Stocker, W., *Lamellar orientation at the surface of thin block copolymer films.* Macromolecules, 1998. **31**: p. 5536-5538.

19. Tokarev, I., et al., *Microphase separation in thin films of poly(styrene-block-4-vinylpyridine) copolymer-2-(4'- hydroxybenzeneazo)benzoic acid assembly.* Macromolecules, 2005. **38**: p. 507-516.
20. Yokoyama, H., T.E. Mates, and E.J. Kramer, *Structure of asymmetric diblock copolymers in thin films.* Macromolecules, 2000. **33**: p. 1888-1898.
21. Liu, Y., et al., *Surface-induced ordering in asymmetric block copolymers.* Macromolecules, 1994. **27**: p. 4000-4010.
22. Hashimoto, T., M. Shibayama, and H. Kawai, *Ordered structure in block polymer-solutions .4. Scaling rules on size of fluctuations with block molecular-weight, concentration, and temperature in segregation and homogeneous regimes.* Macromolecules, 1983. **16**(7): p. 1093-1101.
23. Kane, R.S., R.E. Cohen, and R. Silbey, *Synthesis of PbS nanoclusters within block copolymer nanoreactors.* Chemical Materials, 1996. **8**(8): p. 1919-1924.
24. Kane, R.S. and R.E. Cohen, *Synthesis of doped ZnS nanoclusters within block copolymer nanoreactors.* Chemical Materials, 1999. **11**(1): p. 90-93.
25. Abes, J.I., R.E. Cohen, and C.A. Ross, *Selective growth of cobalt nanoclusters in domains of block copolymer films.* Chemical Materials, 2003. **15**(5): p. 1125-1131.
26. Mattoussi, H., et al., *Composite thin films of CdSe nanocrystals and a surface passivating/electron transporting block copolymer: Correlations between film microstructure by transmission electron microscopy and electroluminescence.* Journal of Applied Physics, 1999. **86**(8): p. 4390-4399.
27. Bchen-Osmond, C., *The Universal Virus Database*. ICTVdB, ed. I. Management. Vol. version 4. New York, USA: Columbia University.
28. Meulewaeter, F., J. Seurinck, and J. Vanemmelo, *Genome structure of tobacco necrosis virus strain-A.* Virology, 1990. **177**(2): p. 699-709.
29. Culver, J.N., *Tobacco mosaic virus assemble and disassembly: Determinants in pathogenicity and resistance.* Annual Review of Phytopathology, 2002. **40**: p. 287-308.
30. Regenmortel, M. and H. Fraenkel-Conrat, eds. *The Rod-Shaped Plant Viruses*. The Plant Viruses: Volume 21985, Plenum Press: New York.
31. Durham, A.C.H. and A. Klug, *Polymerization of tobacco mosaic virus protein and its control.* Nature-New Biology, 1971. **229**(2): p. 42-&.
32. Vamvakaki, M., *Micellization in pH-sensitive amphiphilic block copolymers in aqueous media and the formation of metal nanoparticles.* The Royal Society of Chemistry, 2004. **128**: p. 1-19.
33. Sidorov, S.N., *Influence of metalation on the morphologies of poly(ethylene oxide)-block-poly(4-vinylpyridine) block copolymer micelles.* Langmuir, 2004. **20**: p. 3543-3550.
34. Gooding, G.V., Jr. and T.T. Hebert, *A simple technique for purification of tobacco mosaic virus in large quantities.* Phytopathology, 1967. **57**(11): p. 1285.
35. Haryono, A. and W.H. Binder, *Controlled arrangement of nanoparticle arrays in block-copolymer domains.* Small, 2006. **2**(5): p. 600-611.
36. Chiu, J.J., et al., *Distribution of nanoparticles in lamellar domains of block copolymers.* Macromolecules, 2007. **40**(9): p. 3361-3365.

37. Jang, S.G., et al., *Morphology Evolution of PS-b-P2VP Diblock Copolymers via Supramolecular Assembly of Hydroxylated Gold Nanoparticles.* Macromolecules, 2012. **45**(3): p. 1553-1561.
38. Bolisay, L.D., J.N. Culver, and P. Kofinas, *Molecularly imprinted polymers for tobacco mosaic virus recognition.* Biomaterials, 2006. **27**(22): p. 4165-4168.
39. Dickert, F.L., et al., *Bioimprinted QCM sensors for virus detection - screening of plant sap.* Analytical and Bioanalytical Chemistry, 2004. **378**(8): p. 1929-1934.
40. Greene, N.T. and K.D. Shimizu, *Colorimetric molecularly imprinted polymer sensor array using dye displacement.* J Am Chem Soc, 2005. **127**(15): p. 5695-5700.
41. Haginaka, J. and C. Kagawa, *Chiral resolution of derivatized amino acids using uniformly sized molecularly imprinted polymers in hydro-organic mobile phases.* Analytical and Bioanalytical Chemistry, 2004. **378**(8): p. 1907-1912.
42. Hiratani, H., et al., *Ocular release of timolol from molecularly imprinted soft contact lenses.* Biomaterials, 2005. **26**(11): p. 1293-1298.
43. Tai, D.F., et al., *Recognition of dengue virus protein using epitope-mediated molecularly imprinted film.* Analytical Chemistry, 2005. **77**(16): p. 5140-5143.
44. Parmpi, P. and P. Kofinas, *Biomimetic glucose recognition using molecularly imprinted polymer hydrogels.* Biomaterials, 2004. **25**(10): p. 1969-1973.
45. Wizeman, W.J. and P. Kofinas, *Molecularly imprinted polymer hydrogels displaying isomerically resolved glucose binding.* Biomaterials, 2001. **22**(12): p. 1485-1491.
46. Pauling, L., *A theory of the structure and process of formation of antibodies.* Journal of American Chemical Society, 1940. **62**: p. 2643-2657.
47. Pauling, L., *The manufacture of antibodies in vitro.* Journal of Experimental Medicine, 1942. **76**: p. 211-220.
48. Kempe, M. and K. Mosbach, *Binding-studies on substrate and enantio-selective molecularly imprinted polymers* Analytical Letters, 1991. **24**(7): p. 1137-1145.
49. Li, Z., et al., *Synthesis and characterization of functional methacrylate copolymers and their application in molecular imprinting.* Macromolecules, 2005. **38**(7): p. 2620-2625.
50. Lu, Y., et al., *Molecular recognition through the exact placement of functional groups on non-covalent molecularly imprinted polymers.* Journal of Chromatography A, 2002. **950**(1-2): p. 89-97.
51. Sellergren, B. and K.J. Shea, *Influence of polymer morphology on the ability of imprinted network polymers to resolve enantiomers.* Journal of Chromatography, 1993. **635**(1): p. 31-49.
52. Sellergren, B. and K.J. Shea, *Origin of peak asymmetry and the effect of temperature on solute retention in enantiomer separations on imprinted chiral stationary phases.* Journal of Chromatography A, 1995. **690**(1): p. 29-39.
53. Spivak, D. and K.J. Shea, *Molecular imprinting of carboxylic acids employing novel functional macroporous polymers.* Journal of Organic Chemistry, 1999. **64**(13): p. 4627-4634.
54. Wulff, G., et al., *Enzyme-analogue built polymers, 5. Specificity distribution of chiral cavities prepared in synthetic-polymers* Makromolekulare Chemie-Macromolecular Chemistry and Physics, 1977. **178**(10): p. 2817-2825.

55. Wulff, G., et al., *Enzyme-analogue built polymers, 4. Synthesis of polymers containing chiral cavities and their use for resolution of racemates.* Makromolekulare Chemie-Macromolecular Chemistry and Physics, 1977. **178**(10): p. 2799-2816.
56. Casey, B.J., et al., *Coagulation-inducing polymer hydrogel for hemostatic application.* Abstracts of Papers of the American Chemical Society, 2010. **240**.
57. Janiak, D.S., O.B. Ayyub, and P. Kofinas, *Effects of Charge Density on the Recognition Properties of Molecularly Imprinted Polymeric Hydrogels.* Macromolecules, 2009. **42**(5): p. 1703-1709.
58. Gill, I. and A. Ballesteros, *Bioencapsulation within synthetic polymers (Part 2): non-sol-gel protein-polymer biocomposites.* Trends in Biotechnology, 2000. **18**(11): p. 469-479.
59. Gill, I. and A. Ballesteros, *Bioencapsulation within synthetic polymers (Part 1): sol-gel encapsulated biologicals.* Trends in Biotechnology, 2000. **18**(7): p. 282-296.
60. Vaidya, A.A., et al., *Creating a macromolecular receptor by affinity imprinting.* Journal of Applied Polymer Science, 2001. **81**(5): p. 1075-1083.
61. Tong, D., et al., *Some studies of the chromatographic properties of gels ('artificial antibodies/receptors') for selective adsorption of proteins.* Chromatographia, 2001. **54**(1-2): p. 7-14.
62. Byrne, M.E., K. Park, and N.A. Peppas, *Molecular imprinting within hydrogels.* Advanced Drug Delivery Reviews, 2002. **54**(1): p. 149-161.
63. Byrne, M.E. and V. Salian, *Molecular imprinting within hydrogels II: Progress and analysis of the field.* International Journal of Pharmaceutics, 2008. **364**(2): p. 188-212.
64. Hayden, O., et al., *Surface imprinting strategies for the detection of trypsin.* Analyst, 2006. **131**(9): p. 1044-1050.
65. Balci, S., et al., *Printing and aligning mesoscale patterns of Tobacco mosaic virus on surfaces.* Advanced Materials, 2008. **20**(11): p. 2195-+.
66. Weibel, D.B., et al., *Bacterial printing press that regenerates its ink: Contact-printing bacteria using hydrogel stamps.* Langmuir, 2005. **21**(14): p. 6436-6442.
67. Lieberzeit, P.A., et al., *From nanopatterning to functionality - surface and bulk imprinting for analytical purposes.* Superlattices and Microstructures, 2004. **36**(1-3): p. 133-142.
68. Piletsky, S.A., et al., *Molecularly imprinted self-assembled films with specificity to cholesterol.* Sensors and Actuators B-Chemical, 1999. **60**(2-3): p. 216-220.
69. Li, X. and S.M. Husson, *Two-dimensional molecular imprinting approach to produce optical biosensor recognition elements.* Langmuir, 2006. **22**(23): p. 9658-9663.
70. Niu, Z.W., et al., *Study and characterization of tobacco mosaic virus head-to-tail assembly assisted by aniline polymerization.* Chemical Communications, 2006(28): p. 3019-3021.
71. Suh, K.Y., et al., *Patterning and separating infected bacteria using host-parasite and virus-antibody interactions.* Biomedical Microdevices, 2004. **6**(3): p. 223-229.

72. Suh, K.Y., et al., *Direct confinement of individual viruses within polyethylene glycol (PEG) nanowells.* Nano Lett, 2006. **6**(6): p. 1196-1201.
73. Arter, J.A., et al., *Virus-PEDOT Nanowires for Biosensing.* Nano Lett, 2010. **10**(12): p. 4858-4862.
74. Yoo, P.J., et al., *Solvent-assisted patterning of polyelectrolyte multilayers and selective deposition of virus assemblies.* Nano Lett, 2008. **8**(4): p. 1081-1089.
75. Mallory, G.O. and J.B. Hajou, *Electroless Plating*1990, Orlando, FL: American Electroplaters and Surface Finishers Society.
76. Petry, R., M. Schmitt, and J. Popp, *Raman Spectroscopy - A prospective tool in the life sciences.* Chemphyschem, 2003. **4**(1): p. 14-30.
77. Premasiri, W.R., et al., *Characterization of the surface enhanced Raman scattering (SERS) of bacteria.* Journal of Physical Chemistry B, 2005. **109**(1): p. 312-320.
78. Shanmukh, S., et al., *Rapid and sensitive detection of respiratory virus molecular signatures using a silver nanorod array SERS substrate.* Nano Lett, 2006. **6**(11): p. 2630-2636.
79. Wang, Y., et al., *SERS opens a new way in aptasensor for protein recognition with high sensitivity and selectivity.* Chemical Communications, 2007(48): p. 5220-5222.
80. *Nobel Lectures*. Physics: 1922-1941.1956, Amsterdam: Elsevier Publishing Company.
81. Popp, J. and W. Kiefer, *Encyclopedia of Analytical Chemistry*. Vol. 21. 2000, New York, NY: John Wiley & Sons.
82. Ingle, J.D. and S.R. Crouch, *Spectrochemical Analysis*1988, Englewood Cliffs, New Jersey: Prentice Hall.
83. Fleischmann M., P.J. Hendra, and McQuilla.Aj, *Raman-spectra of pyridine adsorbed at a silver electrode.* Chemical Physics Letters, 1974. **26**(2): p. 163-166.
84. Jeanmaire, D.L. and R.P. Vanduyne, *Surface raman spectroelectrochemistry. 1. Heterocyclic, aromatic, and aliphatic-amines adsorbed on anodized silver electrode.* Journal of Electroanalytical Chemistry, 1977. **84**(1): p. 1-20.
85. Albrecht, M.G. and J.A. Creighton, *Intense Raman-spectra of pyridine at a silver electrode.* Journal of American Chemical Society, 1977. **99**(15): p. 5215-5217.
86. Kudelski, A., *New trends in the surface-enhanced Raman spectroscopy. A short review.* Polish Journal of Chemistry, 2005. **79**(10): p. 1551-1563.
87. Negri, P., et al., *Direct Optical Detection of Viral Nucleoprotein Binding to an Anti-Influenza Aptamer.* Analytical Chemistry, 2012. **84**(13): p. 5501-5508.
88. Syamala, K.M., et al., *Inhibition Assay of Yeast Cell Walls by Plasmon Resonance Rayleigh Scattering and Surface-Enhanced Raman Scattering Imaging.* Langmuir, 2012. **28**(24): p. 8952-8958.
89. Zhang, X.F., et al., *Detection of melamine in liquid milk using surface-enhanced Raman scattering spectroscopy.* Journal of Raman Spectroscopy, 2010. **41**(12): p. 1655-1660.
90. Moskovits, M., *Surface-enhanced spectroscopy.* Reviews of Modern Physics, 1985. **57**(3): p. 783.
91. Angel, S., et al., *Near-infrared surface-enhanced Raman spectroscopy. Part I: Copper and gold electrodes.* Applied Spectroscopy, 1988. **42**(8): p. 1327-1331.

92. Otto, A., et al., *Surface-enhanced Raman scattering.* Journal of Physics: Condensed Matter, 1999. **4**(5): p. 1143.
93. Zhao, L., L. Jensen, and G.C. Schatz, *Pyridine-Ag20 cluster: a model system for studying surface-enhanced raman scattering.* J Am Chem Soc, 2006. **128**(9): p. 2911-2919.
94. Wang, D.S. and M. Kerker, *Enhanced Raman scattering by molecules adsorbed at the surface of colloidal spheroids.* Physical Review B, 1981. **24**(4): p. 1777.
95. Murphy, C.J., et al., *Anisotropic metal nanoparticles: synthesis, assembly, and optical applications.* The Journal of Physical Chemistry B, 2005. **109**(29): p. 13857-13870.
96. Fleischmann, M. and Z.Q. Tian, *The induction of SERS on smooth Ag by the deposition of Ni and Co.* Journal of Electroanalytical Chemistry, 1987. **217**(2): p. 411-416.
97. Fleischmann, M. and Z.Q. Tian, *The effects of the underpotential and overpotential deposition of lead and thallium on silver on the Raman-spectra of adsorbates.* Journal of Electroanalytical Chemistry, 1987. **217**(2): p. 385-395.
98. Fleischmann, M., Z.Q. Tian, and L.J. Li, *Raman-spectroscopy of adsorbates on thin-film electrodes deposited on silver substrates.* Journal of Electroanalytical Chemistry, 1987. **217**(2): p. 397-410.
99. Mengoli, G., et al., *Enhanced Raman-scattering from iron electrodes.* Electrochimica Acta, 1987. **32**(8): p. 1239-1245.
100. Leung, L.W.H. and M.J. Weaver, *Extending surface-enhanced Raman-spectroscopy to transition-metal surfaces - Carbon-monoxide adsorption and electrooxidation on platinum-coated and palladium-coated gold electrodes.* J Am Chem Soc, 1987. **109**(17): p. 5113-5119.
101. Leung, L.W.H. and M.J. Weaver, *Extending the metal interface generality of surface-enhanced Raman-spectroscopy - Underpotential deposited layers of mercury, thallium, and lead on gold electrodes* Journal of Electroanalytical Chemistry, 1987. **217**(2): p. 367-384.
102. Leung, L.W.H. and M.J. Weaver, *Adsorption and electrooxidation of carbon-monoxide on rhodium-coated and ruthenium-coated gold electrodes as probed by surface-enhanced Raman-spectroscopy* Langmuir, 1988. **4**(5): p. 1076-1083.
103. Zou, S.Z. and M.J. Weaver, *Surface-enhanced Raman scattering an uniform transition metal films: Toward a versatile adsorbate vibrational strategy for solid-nonvacuum interfaces?* Analytical Chemistry, 1998. **70**(11): p. 2387-2395.
104. Zou, S.Z., et al., *Probing molecular vibrations at catalytically significant interfaces: A new ubiquity of surface-enhanced Raman scattering.* J Am Chem Soc, 1998. **120**(15): p. 3811-3812.
105. Mrozek, M.F., H. Luo, and M.J. Weaver, *Formic acid electrooxidation on platinum-group metals: Is adsorbed carbon monoxide solely a catalytic poison?* Langmuir, 2000. **16**(22): p. 8463-8469.
106. Weaver, M.J., S.Z. Zou, and H.Y.H. Chan, *The new interfacial ubiquity of surface-enhanced Raman spectroscopy.* Analytical Chemistry, 2000. **72**(1): p. 38A-47A.
107. Mrozek, M.F., Y. Xie, and M.J. Weaver, *Surface-enhanced Raman scattering on uniform platinum-group overlayers: Preparation by redox replacement of*

*underpotential-deposited metals on gold.* Analytical Chemistry, 2001. **73**(24): p. 5953-5960.
108. Bantz, K.C., et al., *Recent progress in SERS biosensing.* Physical Chemistry Chemical Physics, 2011. **13**(24): p. 11551-11567.
109. Dieringer, J.A., et al., *Surface enhanced Raman spectroscopy: new materials, concepts, characterization tools, and applications.* Faraday Discussions, 2006. **132**: p. 9-26.
110. Kovacs, G.J., et al., *Distance dependence of SERS enhancement factor from Langmuir-Blodgett monolayers on metal island films - evidence for the electromagnetic mechanism.* Langmuir, 1986. **2**(6): p. 689-694.
111. Kennedy, B.J., et al., *Determination of the distance dependence and experimental effects for modified SERS substrates based on self-assembled monolayers formed using alkanethiols.* Journal of Physical Chemistry B, 1999. **103**(18): p. 3640-3646.
112. Kneipp, K., et al., *Single molecule detection using surface-enhanced Raman scattering (SERS).* Physical Review Letters, 1997. **78**(9): p. 1667-1670.
113. Campion, A. and P. Kambhampati, *Surface-enhanced Raman scattering.* Chem. Soc. Rev., 1998. **27**(4): p. 241-250.
114. Schatz, G.C., *Theoretical studies of surface enhanced Raman scattering.* Accounts of Chemical Research, 1984. **17**(10): p. 370-376.
115. Haynes, C.L., A.D. McFarland, and R.P.V. Duyne, *Surface-enhanced Raman spectroscopy.* Analytical Chemistry, 2005. **77**(17): p. 338-346.
116. Moskovits, M., *Surface-enhanced Raman spectroscopy: a brief retrospective.* Journal of Raman Spectroscopy, 2005. **36**(6-7): p. 485-496.
117. Aroca, R., et al., *Surface-enhanced Raman scattering on colloidal nanostructures.* Advances in colloid and interface science, 2005. **116**(1): p. 45-61.
118. Nie, S.M. and S.R. Emery, *Probing single molecules and single nanoparticles by surface-enhanced Raman scattering.* Science, 1997. **275**(5303): p. 1102-1106.
119. De Jesus, M., K. Giesfeldt, and M. Sepaniak, *Use of a sample translation technique to minimize adverse effects of laser irradiation in surface-enhanced Raman spectrometry.* Applied Spectroscopy, 2003. **57**(4): p. 428-438.
120. Munro, C., et al., *Characterization of the surface of a citrate-reduced colloid optimized for use as a substrate for surface-enhanced resonance Raman scattering.* Langmuir, 1995. **11**(10): p. 3712-3720.
121. Turkevich, J., P.C. Stevenson, and J. Hillier, *A study of the nucleation and growth processes in the synthesis of colloidal gold.* Discuss. Faraday Soc., 1951. **11**: p. 55-75.
122. Kuncicky, D.M., B.G. Prevo, and O.D. Velev, *Controlled assembly of SERS substrates templated by colloidal crystal films.* Journal of Materials Chemistry, 2006. **16**(13): p. 1207-1211.
123. Lu, L., et al., *Designed fabrication of ordered porous au/ag nanostructured films for surface-enhanced Raman scattering substrates.* Langmuir, 2006. **22**(6): p. 2605-2609.
124. Jensen, T.R., et al., *Nanosphere lithography: tunable localized surface plasmon resonance spectra of silver nanoparticles.* The Journal of Physical Chemistry B, 2000. **104**(45): p. 10549-10556.

125. Im, H., et al., *Vertically oriented sub-10-nm plasmonic nanogap arrays.* Nano Lett, 2010. **10**(6): p. 2231-2236.
126. Yu, W.W. and I.M. White, *Inkjet printed surface enhanced Raman spectroscopy array on cellulose paper.* Analytical Chemistry, 2010. **82**(23): p. 9626-9630.
127. Yu, W.W. and I.M. White, *A simple filter-based approach to surface enhanced Raman spectroscopy for trace chemical detection.* Analyst, 2012. **137**(5): p. 1168-1173.
128. Lee, C.H., et al., *Highly Sensitive Surface Enhanced Raman Scattering Substrates Based on Filter Paper Loaded with Plasmonic Nanostructures.* Analytical Chemistry, 2011. **83**(23): p. 8953-8958.
129. Hildebrandt, P. and M. Stockburger, *Surface-enhanced resonance Raman-spectroscopy of rhodamine-6G adsorbed on colloidal silver.* Journal of Physical Chemistry, 1984. **88**(24): p. 5935-5944.
130. Michaels, A.M., J. Jiang, and L. Brus, *Ag nanocrystal junctions as the site for surface-enhanced Raman scattering of single Rhodamine 6G molecules.* Journal of Physical Chemistry B, 2000. **104**(50): p. 11965-11971.
131. Michaels, A.M., M. Nirmal, and L.E. Brus, *Surface enhanced Raman spectroscopy of individual rhodamine 6G molecules on large Ag nanocrystals.* J Am Chem Soc, 1999. **121**(43): p. 9932-9939.
132. Schwartzberg, A.M., et al., *Unique gold nanoparticle aggregates as a highly active surface-enhanced Raman scattering substrate.* Journal of Physical Chemistry B, 2004. **108**(50): p. 19191-19197.
133. Jiang, J., et al., *Single molecule Raman spectroscopy at the junctions of large Ag nanocrystals.* Journal of Physical Chemistry B, 2003. **107**(37): p. 9964-9972.
134. Dasary, S.S.R., et al., *Gold Nanoparticle Based Label-Free SERS Probe for Ultrasensitive and Selective Detection of Trinitrotoluene.* J Am Chem Soc, 2009. **131**(38): p. 13806-13812.
135. Jiang, K., I. White, and D.L. DeVoe, *Detection of trace explosives by SERS using 3-D nanochannel arrays*, in *14th International Conference on Miniaturized Systems for Chemistry and Life Sciences*2010. p. 2005-2007.
136. Xu, Z.H., et al., *Surface-Enhanced Raman scattering spectroscopy of explosive 2,4-dinitroanisole using modified silver nanoparticles.* Langmuir, 2011. **27**(22): p. 13773-13779.
137. Holthoff, E.L., D.N. Stratis-Cullum, and M.E. Hankus, *A Nanosensor for TNT detection based on molecularly imprinted polymers and surface enhanced Raman scattering.* Sensors, 2011. **11**(3): p. 2700-2714.
138. Tyan, Y.C., et al., *Melamine contamination.* Analytical and Bioanalytical Chemistry, 2009. **395**(3): p. 729-735.
139. Lin, M., et al., *Detection of melamine in gluten, chicken feed, and processed foods using surface enhanced Raman spectroscopy and HPLC.* Journal of Food Science, 2008. **73**(8): p. T129-T134.
140. Cheng, Y. and Y.Y. Dong, *Screening melamine contaminant in eggs with portable surface-enhanced Raman Spectroscopy based on gold nanosubstrate.* Food Control, 2011. **22**(5): p. 685-689.
141. Wen, Z.Q., G.Y. Li, and D. Ren, *Detection of trace melamine in raw materials used for protein pharmaceutical manufacturing using surface-enhanced Raman*

*spectroscopy (SERS) with gold nanoparticles.* Applied Spectroscopy, 2011. **65**(5): p. 514-521.
142. Lou, T.T., et al., *Rapid detection of melamine with 4-mercaptopyridine-modified gold nanoparticles by surface-enhanced Raman scattering.* Analytical and Bioanalytical Chemistry, 2011. **401**(1): p. 333-338.